Title	Study on the effect of upstream water and sediment discharge conditions to the alternate bar dynamics in gravel-bed rivers
Author(s)	Dai, Huang
Degree Grantor	北海道大学
Degree Name	博士(工学)
Dissertation Number	甲第15232号
Issue Date	2022-12-26
DOI	https://doi.org/10.14943/doctoral.k15232
Doc URL	https://hdl.handle.net/2115/87743
Type	doctoral thesis
File Information	Huang_Dai.pdf

Study on the effect of upstream water and sediment discharge conditions to the alternate bar dynamics in gravel-bed rivers

by

Huang Dai

A thesis submitted in partial fulfillment of the requirements for the degree of Doctor of Engineering

Examination Committee: **Assoc. Prof. Toshiki IWASAKI (Chairman)**
Prof. Norihiro IZUMI
Prof. Yasunori WATANABE

Division of Environment Field Engineering
Graduate School of Engineering, Hokkaido University
November 2022

Table of Contents

List of Figures

List of Tables

Chapter 1

Introduction

1.1 Introduction

Alternate bars play an important role in the river morphology, causing the scouring of riverbeds and banks alternately and making a river channel unstable by forming a meandering pattern [1]. Such meandering patterns might cause a series of problems in navigation, flood prevention, and hydraulic construction [2,3,4]. Meanwhile, the regular alternating shapes and migration properties are also very interesting and highly discussed topics in river morphology. Researchers have studied the alternate bars' characteristics such as bar height, wavelength, migration, etc. from many aspects such as flow conditions, sediment supply, bank vegetation, channel properties, etc. [5-18]. These studies have provided us with much new knowledge and viewpoints, however, due to the limitations of the research conditions, the studies are often accompanied by deficiencies and need to be supplemented. In this paper, two basic aspects: discharge and sediment supply, which are the two most basic conditions in river morphology, have been studied.

Sediment supply plays a vital role because the imbalance of sediment supply from the upper river reaches sediment transport capacity, causing bed aggradation or degradation in the downstream reach and controlling sediment transport features and overall river morphologies. Some studies clearly show an inseparable relationship

Figure 1.1. Alternate bars in Japan

between sediment supply and river morphodynamics [19,20]. However, despite the common knowledge regarding the importance of sediment supply to river morphodynamics, there are still deficiencies in understanding the scale and intensity of the impact from the imbalance of sediment supply to the capacity transport rate. Some studies show that the imbalance of sediment supply affecting river morphology is a very long process for decades and will not appear in a short time; also, the effect varies with distance: the farther the distance is, the less obvious the effect will be, which seems to be a common sense but the length of the distance is difficult to calculate [21-24]. These opinions indicate that even though the sediment supply plays an important role in downstream river morphodynamics, we must consider the effective temporal and spatial scales of the sediment supply to the downstream environment.

Discharges are basic conditions that cannot be ignored. But it seems that most of the studies about alternate bars have been done under a steady flow condition, for it always takes weeks to form stable alternate bars and giving such a long unsteady flow condition is not realistic. In fact, discharge unsteadiness, which has been a long-ignored concept, plays a critical role in sand bar formation and dynamics. Tubino performed a linear stability analysis of free river bars under unsteady discharge conditions, indicated the importance of flow unsteadiness to bar dynamics and further motivated the understanding of alternate bar dynamics under unsteady discharge conditions [25]. Several following studies have also shown the importance of discharge unsteadiness to river morphodynamics [26-28]. However, such studies focus on short-term morphodynamics as only a single or a few repeated hydrographs are considered. How the river bars were formed and continue to develop in the long term, under the complex sequence of hydrographs remains unclear. This is mainly owing to a lack of field observations pertaining to long-term hydrological and spatiotemporal river bars interactions, as well as the difficulty in performing long-term flume experiments, even under simplified conditions. Researchers may have a deep understanding of the morphodynamics of alternate bars under steady flow conditions. Still, we are hoping to find some regular morphodynamics properties of alternate bars under unsteady flow conditions. Therefore, long-term unsteady flow conditions simulation has been performed in this research.

This study is based on a flood disaster that happened in 2011 at the Otofuke River, Japan, in which bank collapse and road damage were reported (Figure 1.2). Disasters have occurred on the river from time to time in recent decades, and studies have been made based on the situation of this river [18,29,30], giving us an appropriate research object. Here, 2-D numerical simulations are performed via Nays2DH, a functional numerical model in iRIC software [31-37].

1.2 Study objectives

The main objectives of this dissertation are

1) To test the applicability of the concept of Hydrograph Boundary Layer in the 2-D simulation proposed by Wong and Parker under 1-D conditions.

2) To test the effective temporal and spatial scales of the sediment supply imbalance.

3) To find the regular morphodynamics properties of alternate bars under unsteady flow conditions.

4) To analyze the change of morphodynamics of the alternate bar with the unsteady flow.

Figure 1.2. Bank erosion disaster happened in Otofuke river, 2011 (Otofuke River, Japan, Nagata, 2014)

1.3 Layout of the dissertation

In Chapter 2, we focus on the role of sediment supply in the downstream morphology. In this regard, Wong and Parker [18] proposed an important concept called the hydrograph boundary layer (HBL), which indicates that bed elevation responds to the sediment supply variation can travel only a short distance. This short river reach, which is affected by the upstream sediment imbalance, is termed as the hydrograph boundary layer (HBL), and in the downstream of HBL, the mobile-bed equilibrium, which indicates no bed elevation change, is achieved. Most study related to the HBL concept has been done under 1-D simulation, make us wonder if it can also behave in 2-D simulation. In Chapter 2, we investigated the effect of sediment supply on the morphodynamics of free alternate bars in gravel-bed rivers in terms of the HBL concept. Two-dimensional morphodynamic calculations regarding sand bar development were performed under cycled, single triangle-shaped hydrographs with different sediment supply conditions, more specifically, constant and equilibrium feed conditions.

In Chapter 3, we started with a special case we found in Chapter 2, in which the alternate bars can reach a morphodynamics equilibrium state, that is, the wavelength and migration period of alternate bars remained constant, and the migration period was the same as the hydrograph cycle. After further study, we found that the morphodynamics of alternate bars under a specific combination of discharge variation and hydrograph cycle reached an equilibrium state. This might be a unique morphodynamic feature of alternate bars under unsteady conditions because the steady discharge counterparts demonstrated a dynamic equilibrium state with slightly time-dependent features of the wavelength and migration period but did not exhibit non-time-dependent features. In this chapter, we focused on the effect of the hydrograph cycle on river morphology and performed dozens of numerical simulations under different discharge and hydrograph cycle conditions. Meanwhile, we tried to give the discharge process an abrupt change to observe the morphodynamics of alternate bars to find the intriguing consistency of the hydrograph cycle and migration period under morphodynamics equilibrium.

In Chapter 4, we summarize the conclusions of the previous chapters and give some recommendations based on the previous study and the existing results.

Chapter 2

Effect of Sediment Supply on Morphodynamics of Free Alternate Bars: Insights from Hydrograph Boundary Layer

2.1 Introduction

Catastrophic flood events result in intense sediment transport and subsequent changes in river morphology, causing water and sediment-related disasters. For instance, riverbank erosion, levee collapse, and the movement of sandbars lead to urban flooding [38,39], road damage [40,41], and bridge failure [42,43]. Therefore, a better understanding of the river morphodynamics and the factors controlling the system is essential for managing rivers and their floodplain environment and mitigating flood risks.

The river morphologies and their dynamics are influenced by numerous physical and environmental factors such as water discharge [44], bed slope [45], grain size [46], anthropogenic stresses [47], and sediment supply [48]. Among these factors, sediment supply plays a vital role because the imbalance of sediment supply from the upper river reaches sediment transport capacity, causing bed aggradation or degradation in the downstream reach and controlling sediment transport features and overall river morphologies. For instance, Constantine et al. investigated the relationship between the sediment supply rate and meander migration rate in the Amazon River basin [19], and a strong positive correlation between these factors was observed. Stähly et al. studied the reservoir sediment ejection process in the Sarine floodplain [20]. Before the ejection, the downstream alternate bar disappeared because the block of the dam considerably reduced the sediment supply. Sediment ejection events extensively restored the formation of the downstream alternate bar. These studies clearly show that an inseparable relationship exists between sediment supply and river morphodynamics.

However, despite the common knowledge regarding the importance of sediment supply to river morphodynamics, there are still deficiencies in understanding the scale and intensity of the impact from the imbalance of sediment supply to the capacity transport rate. For example, the Mississippi Delta has been suffering significant drowning, and the decline of the sediment transport rate from the upper Mississippi River due to dam construction is thought to be one of the causes [21]. Nittrouer and Viparelli [22], however, investigated the sediment transport rate in the Mississippi River and highlighted that the downstream sediment transport rate did not decline significantly despite dam construction, which is far upstream from the river mouth. This is because upstream degradation of the riverbed causes the sand to be supplied to the downstream instead of the sediment supply from the upper reach. Gaeuman et al. studied the response of the Duchesne River flow and sediment reduction caused by water development in the 1920s [23]. The results show that it took approximately 30 years for a 14 km channel to restore stability. The results show that the elevation change due to sediment supply conditions is closely related to the distance from the source. Such processes can be described as translation (or advection): i.e., dispersion of the sediment wave [24], and the importance of these two factors determines the effectiveness of the sediment source. These studies indicate that even though the sediment supply plays an important role in downstream river morphodynamics, we must consider the effective temporal and spatial scales of the sediment supply to the downstream environment.

In this study, we focus on the role of sediment supply in the downstream morphological changes in gravel-bed rivers during flood events. In this regard, Wong and Parker [49] proposed an important concept called the hydrograph boundary layer (HBL). They performed simple movable bed experiments and numerical simulations under cycled hydrographs and a constant sediment feed rate. Under these conditions, the upstream riverbed is forced to undergo repeated aggradation/degradation due to the imbalance of the constant sediment feed rate to the transport capacity, which is determined by the hydrograph. However, the bed elevation responds to the hydrograph only in a specific reach near the sediment feed point, indicating that upstream bed fluctuation can travel a short distance. This short river reach, which is affected by the upstream sediment imbalance, is termed as the hydrograph boundary layer (HBL), and in the downstream of HBL, the mobile-bed equilibrium, which indicates no bed elevation change, is achieved. This sediment feed condition is unlikely to occur in natural streams; however, this concept is helpful for a clear understanding of how the riverbed change caused by the imbalance of sediment feed to the capacity rate can propagate to the downstream river reach in a single flood event. So far, studies have been conducted based on the concept of HBL. Parker et al. tested several variables, such as hydrograph duration, grain size distribution, and bed slope, to determine their influence on the HBL. An et al. [50] applied the HBL theory to a massive sediment supply into a river caused by an earthquake to determine how the riverbed will react under such sediment supply conditions.

These studies shed some critical light on understanding the relationship between sediment feed conditions and river responses; however, further studies and discussions are required for a more complex situation. For example, An et al. [51] pointed out a breakdown of the HBL concept in poorly sorted sediment cases, showing that low-amplitude bedload sheets can travel beyond the HBL. The other limitation of this concept is that most previous studies were performed under one-dimensional flow and sediment transport fields. In other words, even though mobile-bed equilibrium can be achieved downstream of the HBL, it remains unclear whether the upstream effect has no role in complex morphological elements such as sand bars or channel meandering. The 2D river morphologies can also be affected by sediment supply conditions [52,53], but an interpretation of the effect of sediment supply on river morphodynamics is not always straightforward because of the difficulty of sediment transport measurement in the field. Therefore, the concept that HBL is also valid for 2D cases must be focused on to better understand the effect of sediment supply on downstream morphodynamics. In this study, a series of two-dimensional morphodynamic calculations regarding the alternate bar development with the HBL effect were conducted. According to the concept of HBL, the sediment transport rate outside the HBL region will reach equilibrium because there is almost no change in the bed elevation. It can be inferred from the properties of the HBL that if two cases have the same cycled hydrograph but different sediment supply conditions, more specifically, constant and equilibrium feed rate, the river morphology outside the HBL may not change as well as the bed elevation. However, this study aimed to determine how HBL acts in two-dimensional cases and how river morphology responds to the imbalance of sediment supply during a flood event.

2.2 Methods

2.2.1 Numerical Model

We used the Nays2DH model [31], a two-dimensional morphodynamic model enclosed in the iRIC software [32]. This model has been applied to various morphodynamic phenomena in rivers [54], and the model can simulate the alternate bar morphodynamics focused on in this study [55,56].

The flow model is an unsteady two-dimensional shallow water flow model. The governing equations of this model are written for a generalized coordinate system; however, for simplicity, here, we describe the governing equations in the Cartesian coordinate system:

$$\frac{\partial h}{\partial t}+\frac{\partial uh}{\partial x}+\frac{\partial vh}{\partial y}=0 \tag{2.1}$$

$$\frac{\partial u}{\partial t}+u\frac{\partial u}{\partial x}+v\frac{\partial u}{\partial y}=-g\left(\frac{\partial h}{\partial x}+\frac{\partial z}{\partial x}\right)-\frac{gn^2u\sqrt{u^2+v^2}}{h^{\frac{4}{3}}} \tag{2.2}$$

$$\frac{\partial v}{\partial t}+u\frac{\partial v}{\partial x}+v\frac{\partial v}{\partial y}=-g\left(\frac{\partial h}{\partial y}+\frac{\partial z}{\partial y}\right)-\frac{gn^2v\sqrt{u^2+v^2}}{h^{\frac{4}{3}}} \tag{2.3}$$

where x and y are the downstream and transverse coordinates, h is the water depth, z is the riverbed elevation, t is time, u and v are depth-averaged velocity components in the x and y directions, respectively, g is the gravitational acceleration, and n is the Manning coefficient.

Because we focus on the morphodynamics of the gravel-bed river, we only consider bedload transport as a mode of sediment transport. The Meyer-Peter and

Müller formula was used here, and the sediment was considered to have a uniform grain size. The sediment transport model used was as follows:

$$q_{bs} = 8(\tau_* - \tau_{*c})^{\frac{3}{2}}\sqrt{sgd^3} \tag{2.4}$$

$$q_{bn} = q_{bs}\left(\frac{u_{bn}}{V} - \sqrt{\frac{\tau_{*c}}{\mu_s \mu_k \tau_*}}\frac{\partial z}{\partial n}\right) \tag{2.5}$$

where τ_* is the Shields number, τ_{*c} is the critical Shields number, s is the submerged specific gravity of the sediment, d is the grain size of the bed material, q_{bs} and q_{bn} are the bedload transport rates in the x and y directions, respectively, u_{bn} is the flow velocity near the riverbed in the n direction, V is the composite velocity near the riverbed, and μ_s and μ_k are the static friction coefficient and dynamic friction coefficient, respectively. The following Exner equation updates the bed elevation:

$$(1-\lambda)\frac{\partial z}{\partial t} + \frac{\partial q_{bx}}{\partial x} + \frac{\partial q_{by}}{\partial y} = 0 \tag{2.6}$$

where λ is the void ratio of the bed.

2.2.2 Computational Conditions

As a case study, we simplified the condition of the Otofuke River, which is a typical gravel-bed river [18]. This river was affected by a large flood in 2011, which caused significant development of sand bars and subsequent channel meandering; therefore, this is a relevant example for the 2D river morphodynamics in gravel-bed rivers. The channel for the calculation is straight with a width of 70 m and length of 21 km, and the slope of the initial riverbed was set to 0.005. A Manning roughness coefficient of 0.028 s/m$^{1/3}$ and a uniform particle size of 40 mm were used. This is the simplified channel configuration of the main channel of the Otofuke River.

The observed hydrograph is modeled as a simple triangle-shaped hydrograph; that is, the water discharge linearly increases from 100 to 600 m^3/s within 20 h and decreases from 600 to 100 m^3/s linearly within the next 20 h, which makes the whole cycle of 40 h, as shown in Figure 2.1.

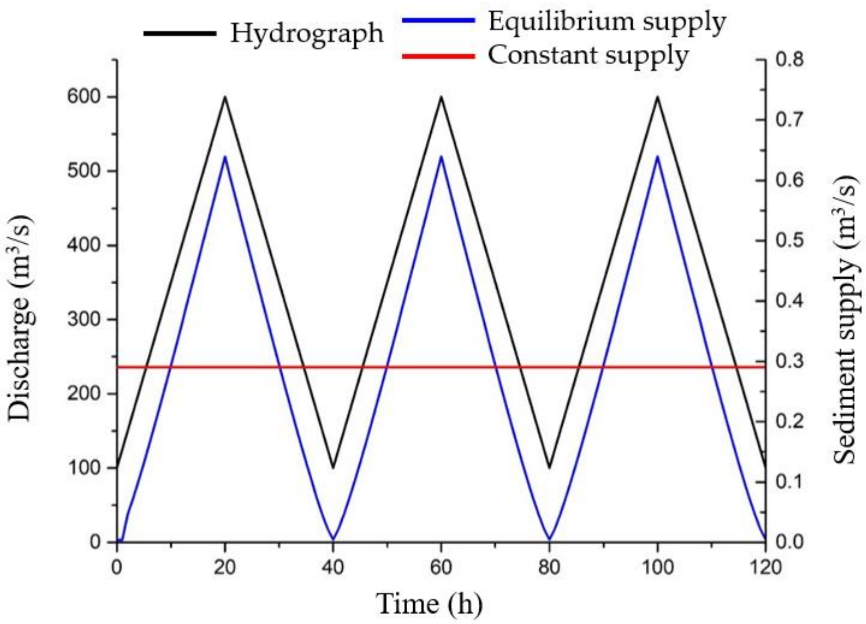

Figure 2.1. Hydrograph and sediment supply conditions used for the base calculation (Case 1). The three hydrographs are shown here as an example, but in the calculation, 50 hydrographs were obtained.

We set two sediment supply conditions, namely equilibrium and constant sediment feed conditions. The equilibrium condition provides the equilibrium sediment transport rate calculated using the flow parameters from the upstream end. This feed rate is the sediment transport capacity of this modeled river, and the supply rate depends on the hydrograph, as shown in Figure 2.1. Because the feed rate is equivalent to the transport capacity, the bed elevation at the upstream end does not change over time under this condition.

The constant-feed condition is intended to obtain the hydrograph boundary layer at the upstream end [49]. The constant-feed rate obtained from the upstream end is a type of averaged sediment transport rate over the hydrograph, so that the bed elevation at the upstream end varies over the hydrograph, but the average bed elevation over the hydrograph does not change. This feed condition makes the bed slope remain constant throughout the calculation, and the total sediment supply rate under this condition becomes the same as the equilibrium condition. Note that we slightly modified the original model of the Nays2DH code to provide a constant sediment feed rate from the upstream end.

The difference between the two conditions is only the persistent bed fluctuation over the hydrograph; the former case provides no bed variation, whereas the latter condition provides the fluctuation of bed elevation caused by the imbalance between the sediment transport capacity and the sediment feed rate. According to Wong and Parker [49], the bed fluctuation of the latter run propagates downstream but has an influential role within the limited river reach from the upstream end, that is, HBL; thus, there should be no difference in the morphodynamic features downstream of the HBL in both conditions. This is valid for 1D cases; however, in this study, we investigated whether this concept is still valid for the 2D morphodynamic phenomena developed beyond HBL, such as the formation and development of alternate bars that take place far downstream from a sediment source into the river.

In addition to this hydrograph condition, as a parameter study, we performed two additional computations by changing the features of the hydrograph but retaining the triangular shape. The computational conditions above are defined as Case 1, and in Case 2, a longer hydrograph duration (i.e., 80 h) with the same peak discharge as Case 1 was used. In Case 3, a higher peak discharge (i.e., 1200 m^3/s) with the same hydrograph duration as Case 1 was adopted, as summarized in Table 2.1. The large ensemble climate and runoff calculations have been used to predict this kind of hydrograph variation in past and future climates [57-59], so the condition of this numerical experiment is realistic.

We obtained 50 hydrographs for all calculations. This numerical experiment was intended to understand how the hydrograph duration and peak discharge influence the HBL characteristics and the downstream sand bar characteristics beyond the HBL.

Table 2.1. Hydrograph duration and variation in the numerical experiment.

	Hydrograph Duration	**Discharge Variation**
Case 1	40 h	100–600 m^3/s
Case 2	80 h	100–600 m^3/s
Case 3	40 h	100–1200 m^3/s

2.3 Results

2.3.1 Two-Dimensional Study of the Hydrograph Boundary Layer: Alternate Bar Formation

Figure 2.2 shows the bed elevation change along the right bank after 25 hydrographs are provided in Case 1 with a constant sediment feed condition. Figure 2.2 (a) and (b) illustrate the 1D morphodynamic features in the entire calculation at reach at the lowest and peak discharges (i.e., 100 and 600 m^3/s, respectively). The structured bed variation observed in the downstream reach (5–21 km) corresponds to alternate bars. At the upstream end, the lowest discharge causes the highest elevation change (i.e., aggradation), whereas the peak discharge provides the lowest elevation change (i.e., degradation). This elevation change is caused by the imbalance of the sediment feed rate to the sediment transport capacity; when the water discharge is low (high), the sediment feed rate is larger (smaller) than the sediment transport capacity, resulting in aggradation (degradation). This elevation difference at the upstream end within a single hydrograph is not small, approximately 2 m, which is almost the same as the bar height developed at the downstream reach. However, this bed elevation change enables the propagation to only short distances such as 1.5 km from the source, that is, the upstream end, as shown in Figure 2.2. This feature is precisely what Wong and Parker obtained in their 1D morphodynamic calculation (i.e., HBL); thus, this result clearly shows that the HBL also formed in our 2D simulation. This figure also demonstrates that an alternate bar was developed outside this HBL zone. There is a reach between these two zones where no elevation fluctuation exists or bars are formed. Hereafter, we refer to these three zones as the HBL zone (0–1.3 km), buffer zone (1.3–5 km), and bar zone (5 km, downstream end).

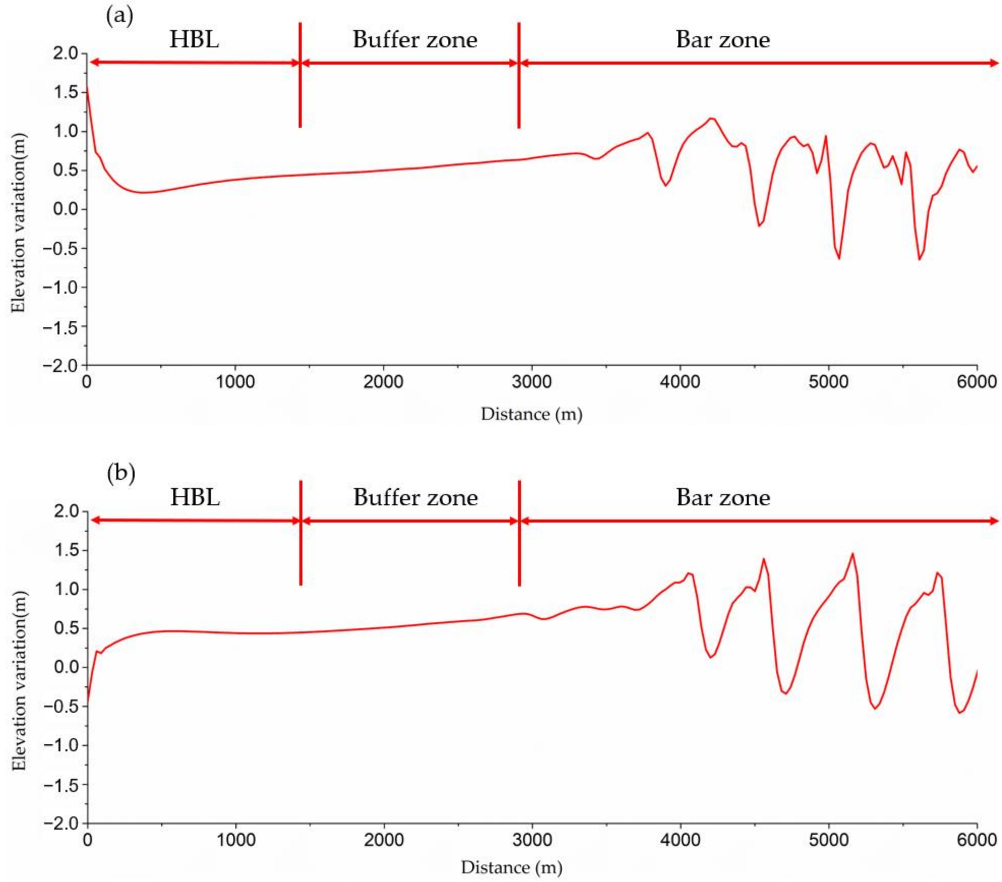

Figure 2.2. Bed elevation change along the right bank 6000 m upstream after 25 hydrographs in the case of constant sediment feed condition. (**a**) At lowest discharge. (**b**) At peak discharge.

Figures 2.3 and 2.4 compare the 1D bed profiles of Case 1 between the equilibrium and constant sediment feed conditions. Because the sediment feed rate is equivalent to the capacity rate, there is no bed elevation change at the upstream end in the equilibrium feed condition. Except for this difference, the other morphodynamic features, namely downstream bar characteristics and emerging points of the bars, are quite similar in both runs, regardless of the sediment feed condition. The only difference is the phase difference of the trains of alternate bars between the two runs. To highlight the similarity of the alternate bar characteristics more clearly, Figure 2.5 shows the elevation variation comparison at the right bank in both runs by removing the phase difference. Regardless of the discharge (i.e., the low or high discharge states), the bar height and wavelength in both runs were almost the same.

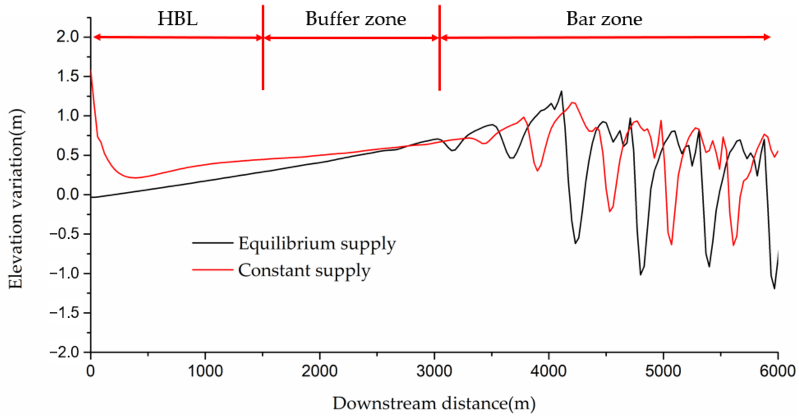

Figure 2.3. 1D bed profiles of Case 1 along the right bank 6000 m upstream after 25 hydrographs.

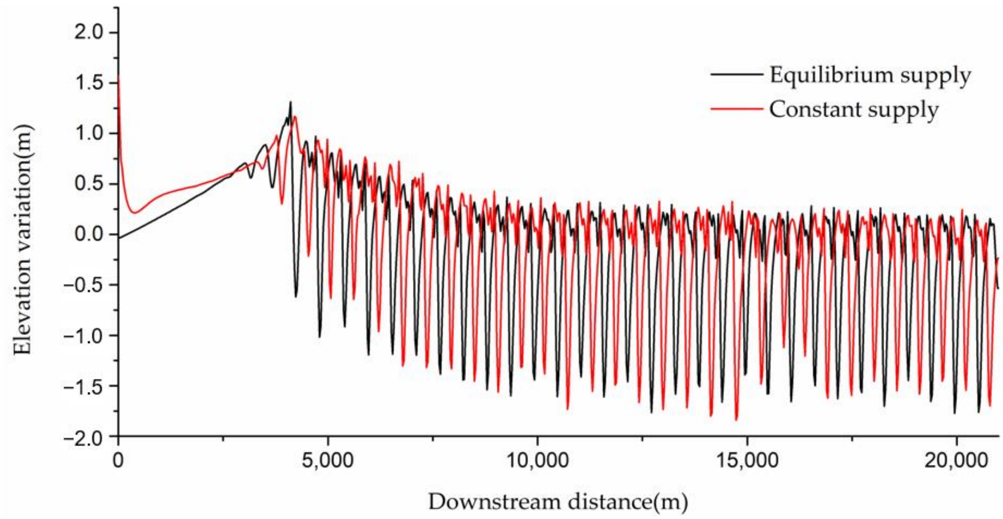

Figure 2.4. Elevation variation comparison at the right bank in both runs after 25 hydrographs.

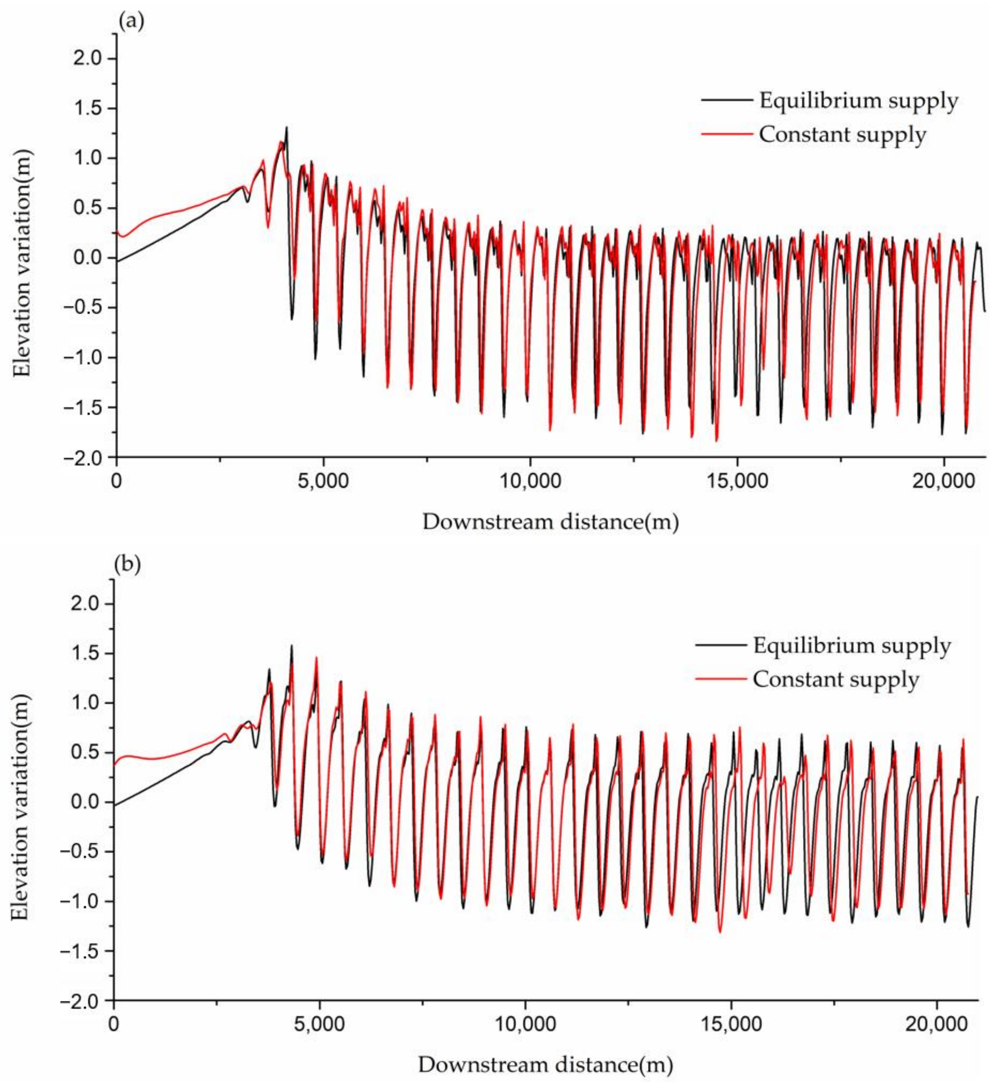

Figure 2.5. Elevation variation comparison at the right bank in both runs after removing the phase difference: (**a**) At lowest discharge. (**b**) At peak discharge.

Figure 2.6 shows the 2D top view of the bar area for a better illustration of the similarity and difference in spatial features of the alternate bar shape. Because the width–length ratio of this computational reach is too small, the downstream distance from approximately 10 km to 12 km was taken as a sample. As also observed in this figure, the alternate bar characteristics (not only the wave height and wavelength but also the 2D shape) are almost identical at the same time points. Meanwhile, the migrating processes were also similar in both cases; the bar moved almost the same distance downstream within 20 h.

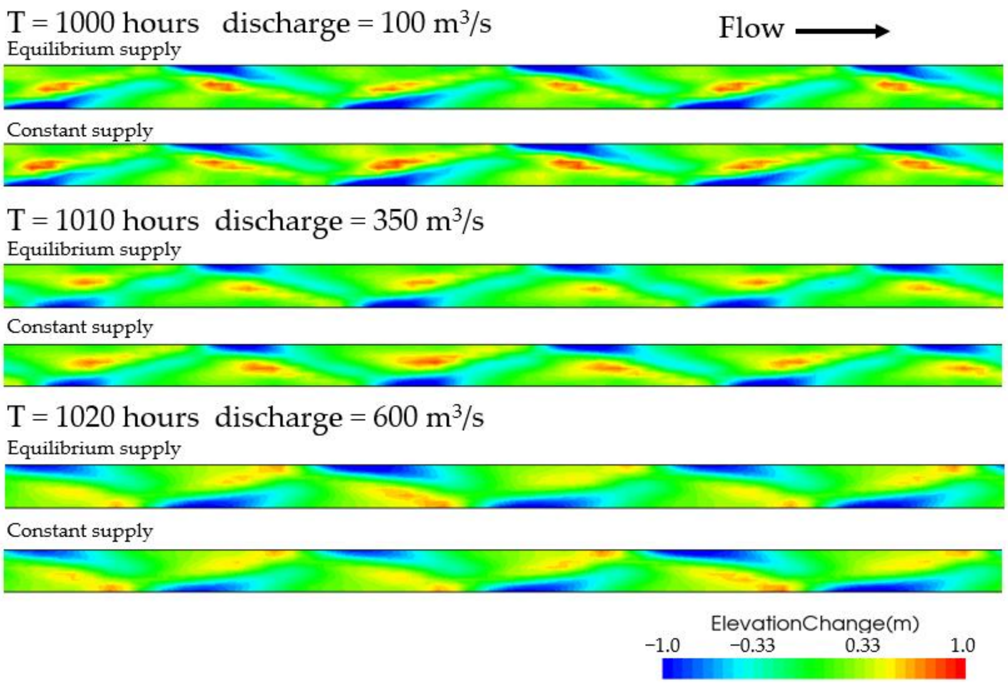

Figure 2.6. 2D top view of alternate bars simulated in Case 1.

The discussion above is based on specific time points and the distance of the channel. For a more qualitative evaluation of the results, the bar characteristics over the entire calculation time must be overviewed. We apply the fast Fourier transform analysis to the time series of 1D bed elevation changes (e.g., Figure 2.2). Figure 2.7 shows the FFT analysis result, indicating that the 2D contour map of the spectrum power in the time-wavelength domain in Case 1. As expected from the quantitative comparison above, this diagram seems very similar in both runs, suggesting that the bar characteristics (e.g., dominant wavelength) and their temporal changes are quantitatively similar. However, after approximately 1500 h, the dominant bar wavelength obtained in the constant sediment feed condition extends to approximately 600 m. Figure 2.8 shows the elevation change along the right bank after 1800 h. This comparison shows that the bar characteristics are almost similar in the upper bar area (i.e., the downstream distance is 3–13 km). This is also seen in the spectrum diagram (Figure 2.7), which shows a second peak in the spectrum at a wavelength of 550 m under constant-feed conditions. However, at the further downstream reach, the elevation variation and wavelength increase, thus increasing the amplitude and period in the FFT analysis, which makes the dominant wavelength 600 m in the constant-feed case. In contrast, the bar characteristics in the equilibrium feed case seem somewhat spatially consistent, leading to only a single, strong peak in the spectrum diagram.

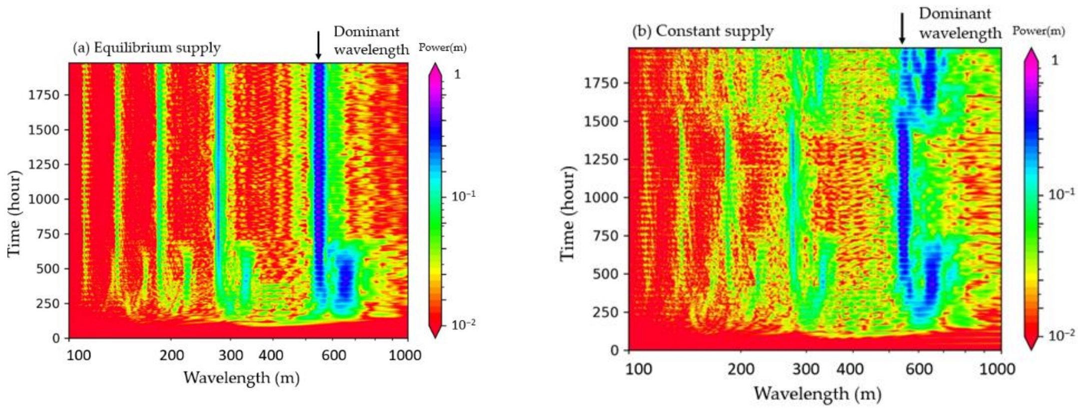

Figure 2.7. FFT analysis of dominant wavelength in case 1: (**a**) Equilibrium sediment supply. (**b**) Constant sediment supply.

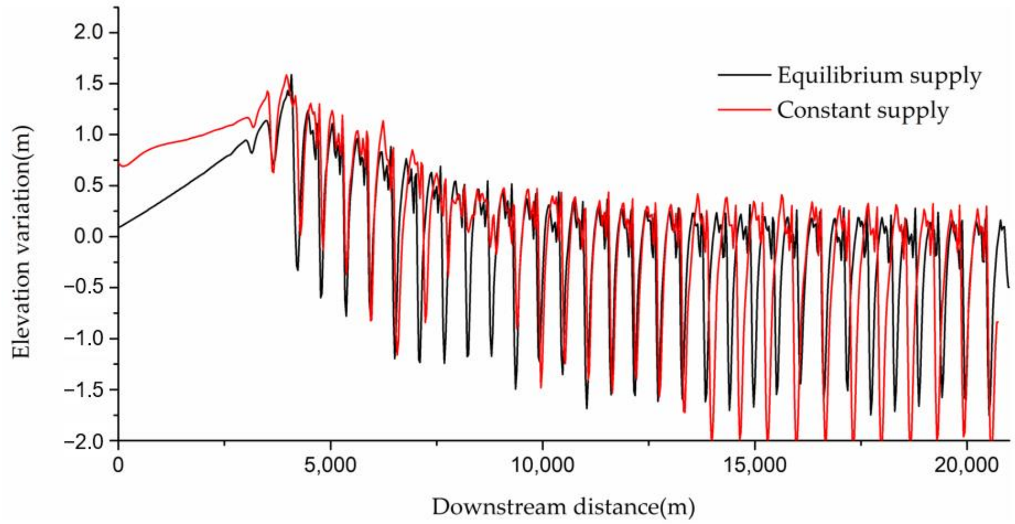

Figure 2.8. Elevation variation comparison at the right bank in both runs after 1800 h removed phase difference.

The cause of this difference at a later time might be an increase in elevation in the buffer zone. To investigate this, three specific points in three zones (i.e., 900 m, 2400 m, and 9000 m downstream) were selected based on the results after removing the phase difference. In Figure 2.9, comparisons are made according to the elevation variation in these points. Both runs show this elevation increase in the buffer zone; however, this feature is more significant in the constant-feed case. This makes the slope steeper, and this difference may affect the bar characteristics. This bed elevation increase is observed

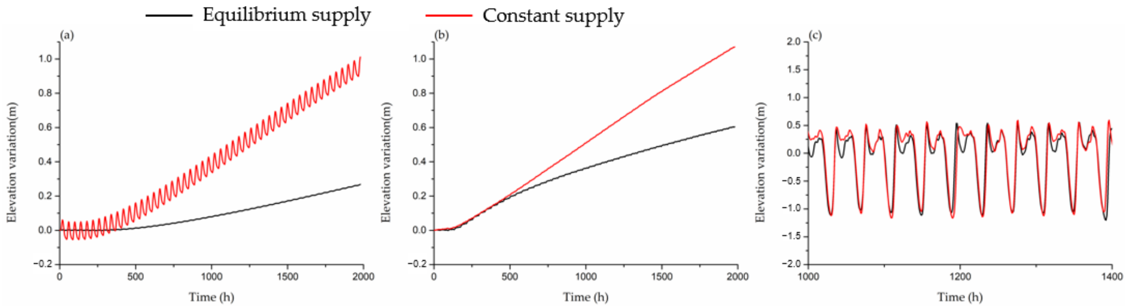

Figure 2.9. Elevation variation comparison of three specific points in three zones. (**a**) The point 900 m downstream in the HBL zone. (**b**) The point 2400 m downstream in the buffer zone. (**c**) The point at 9000 m downstream in the bar zone (i.e., to make the comparison clear, the time range from 1000 to 1400 h is selected).

after bar development, so that the alternate bar formed in the downstream reach has some roles in the upstream bed elevation change. Generally, alternate bars have a negligible effect on the flow resistance, but they play a role in the sediment transport rate [60]. These effects may affect the width-averaged bedload transport rate, causing some deposition (or erosion) upstream of the alternate bars. This point must be investigated; however, this effect is essentially not related to sediment feed conditions. The bar characteristics are very similar in the early stage before the elevation increase in the buffer zone is not significant (i.e., 500 h). In addition, even at a later stage, there is still a very similar bar area upstream.

In summary, regardless of the sediment supply condition, the alternate bar feature formed downstream of the HBL is quantitatively very similar. This suggests that the findings regarding HBL [49] are almost valid for dynamics of alternate bars developed beyond HBL, that is, sediment disturbance at the upstream end has a negligible effect on the mobile-bed dynamic equilibrium downstream of the HBL.

2.3.2. Sensitivity Analysis

We present two additional results, that is, Cases 2 and 3, to highlight the effect of hydrograph shape, more specifically, the hydrograph duration and peak discharge, on the HBL features and dynamics of alternate bars. Figure 2.10 shows the elevation variation at the upper reach of the channel under a constant sediment supply in each case to highlight the properties of the HBL. The two lines used in each case were chosen

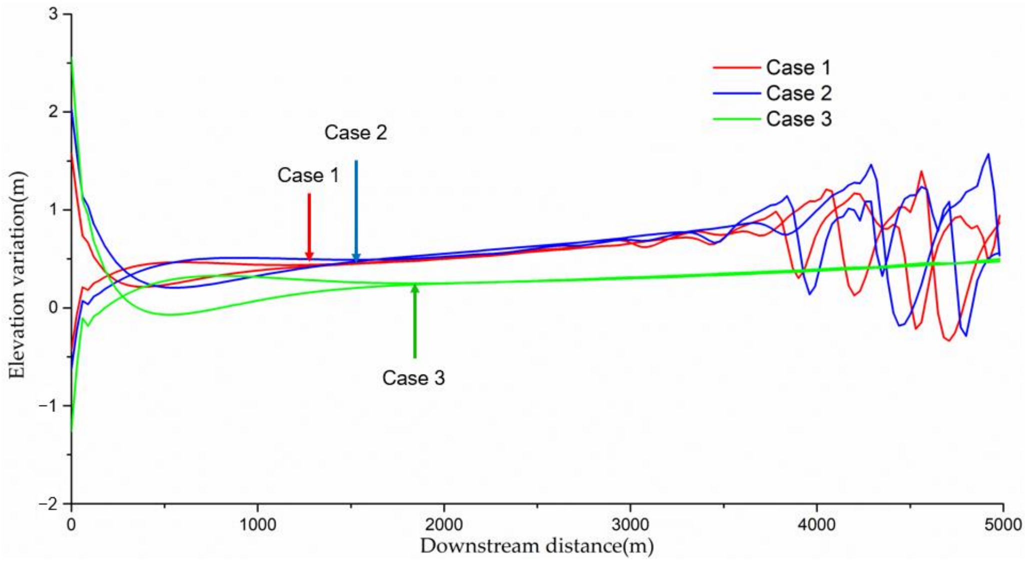

Figure 2.10. Elevation variation at the upper reach of the channel of Cases 1, 2, and 3 when discharge is maximum/minimum.

to show the highest and lowest bed profiles within the hydrograph. This figure clearly demonstrates that the longer and larger hydrograph extends the length of the HBL; this length is approximately 1.3, 1.5, and 1.8 km in Cases 1, 2, and 3, respectively.

As shown in Figure 2.10, alternate bars are formed outside the HBL in Cases 2 and 3, so we again investigated the difference in the bar properties downstream of the HBL. figures 2.11 and 2.12 demonstrate the temporal change in the spectrum power provided by the FFT analysis applied to the 1D bed profile in Cases 2 and 3. The bar properties, such as the dominant wavelength and time-dependent features, are different for each case. For instance, in Case 2, the dominant bar wavelength is approximately 720 m in both sediment feed conditions; however, there are several secondary peaks in the spectrum around the dominant one. In addition, the time-dependent features of such secondary peaks are relatively significant, indicating that the bar properties become less stable than those in Case 1. The FFT results for Case 3 indicate two clear peaks in the spectrum diagram. The corresponding dominant wavelengths were approximately 450 and 550 m, respectively. Although the dominant wavelengths are similar between the two sediment feed conditions compared with Cases 1 and 2, the differences in the bar characteristics indicated by the FFT analysis in Case 3 are slightly more evident than those in Cases 1 and 2.

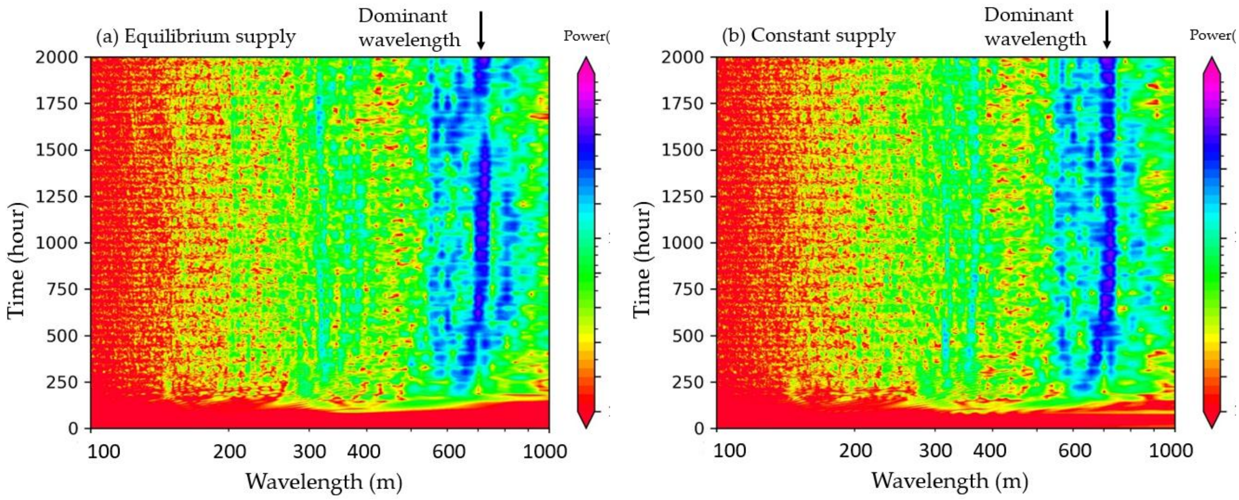

Figure 2.11. FFT analysis of the dominant wavelength in Case 2. (**a**) Equilibrium sediment supply. (**b**) Constant sediment supply.

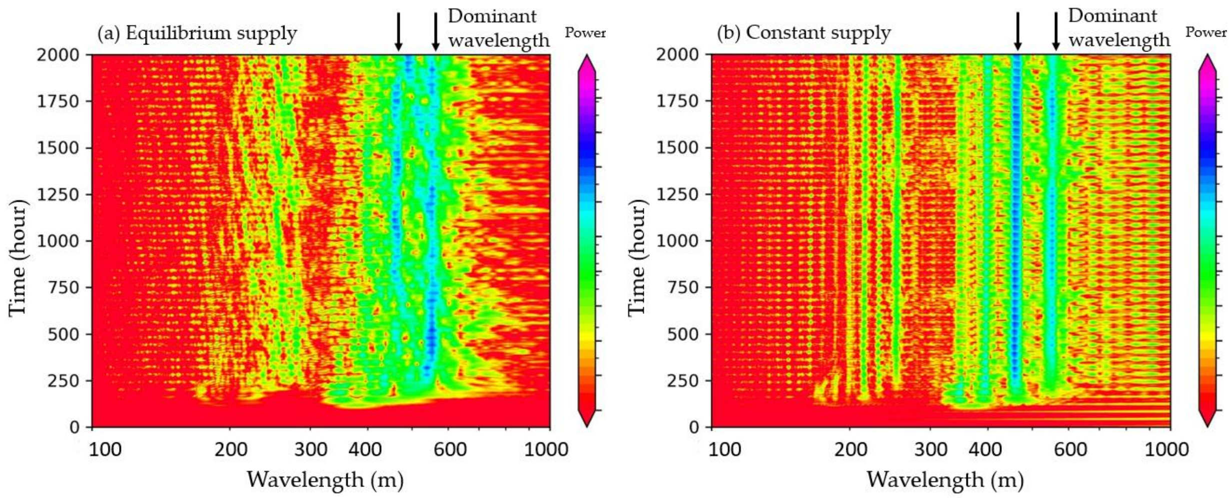

Figure 2.12. FFT analysis of dominant wavelength in Case 2. (**a**) Equilibrium sediment supply. (**b**) Constant sediment supply.

There are some differences in the characteristics of alternate bars formed outside the HBL, particularly time-dependent features, between equilibrium and constant sediment feed conditions. In Cases 2 and 3, HBL is more significant than Case 1, so this effect might be seen as a slight difference in the time-dependent features of the alternate bars. However, the spectrum diagram generally seems very similar regardless of the sediment feed conditions. The results may indicate that as long as the alternate bars develop far outside the HBL, the bed elevation change caused by the feed condition does not propagate beyond the HBL; the difference in bar properties between the two sediment feed conditions eventually becomes negligible.

2.4. Discussion

2.4.1. Implications

The present results indicate that the length of the HBL is an effective spatial scale of the additional sediment input into the river during a single flood event, so that the sediment supply condition in the upstream boundary has little effect on the river morphologies far downstream from the source. Numerous studies have suggested that massive sediment supply into rivers caused by, for instance, dam removal or landslides, causes reorganization of the river morphologies, grain size distribution, and environments [61,62]. This is inevitably valid for a specific river reach from the sediment source; however, at a more downstream reach, such as beyond the HBL, the effect of sediment disturbance will be very small or no longer measurable. In particular, in gravel-bed rivers, where sediment dispersion is dominant rather than in translation, the sediment pulse has a limited effect on downstream channel morphologies such as bar-pool structures [63,64]. This is what the concept of the HBL suggested, and in addition to the 1D mobile-bed equilibrium outside the HBL, the upstream sediment feed condition has a limited role in the 2D morphodynamics such as alternate bar dynamics focused herein at such a river reach. Because the effective length is limited, predicting the HBL length scale might be helpful for effective sediment replenishment works [65].

However, we must mention that the effective length scale of the sediment disturbance scaled by the HBL is short term, similar to the hydrograph scale, and is not applicable for long-term effects, such as a continuous decline in the sediment supply rate due to dam construction [66]. In this case, the upstream sediment condition eventually propagates far downstream by long-term flow-sediment transport processes. In addition, the transport feature of the sediment disturbance highly depends on its properties, such as the mass, size, and grain size of the sediment augmentation [67] and hydraulic conditions [68], so some of the sediment disturbance likely propagates beyond the HBL and affects the river morphology.

The increase in the hydrograph duration and peak discharge we tested in the sensitivity analysis (i.e., by a factor of 2 from the observed significant flood event in this river), is an extreme change in the hydrological perspective, but the difference in the HBL length caused by this extreme hydrograph difference is not significant. This might suggest that, practically speaking, the HBL length can be assumed as a constant in a single river (or some specific reach focused). Because this length is a type of adaptation length scale of the river subject to the imbalance of the sediment feed to the capacity within a single flood event, it will be useful to predict the length of the HBL through a simpler way. Wong and Parker [49] theoretically predicted this length using the linearized governing equation, as follows:

$$\delta \sim \left[\frac{T_h q_{bf}}{(1-\lambda)S_0}\right]^{1/2} \tag{2.7}$$

where q_{bf} is the constant bedload transport rate, which achieves the mobile-bed equilibrium state over the hydrograph, S_0 is the bed slope of such an equilibrium state, and T_h is the hydrograph duration. The conditions of our calculation obtained the right-hand side of Equation (2.7) as 454, 642, and 700 m for Cases 1, 2, and 3, respectively. Multiplying the factor 2.5 to these numbers is a good predictor for the δ we obtained (Figure 2.10). By verifying this equation this way, we might be able to use this predictor for non-linear systems as well. Again, the features of the HBL should be related to the intensity of the hydrograph and sediment condition [51] as well as the hydraulic conditions [68]. Therefore, this point needs to be investigated for different types of river reaches such as sandbed or lowland rivers.

2.4.2. Limitations

One of the limitations of our study was the assumption of a single grain size of the sediment. In gravel-bed rivers, the effect of graded sediment on sediment transport and morphodynamics is significant [51,69,70], which might have altered our findings. For example, An et al. [51] showed that low-amplitude bedload sheets can propagate long distances beyond the HBL in the case of poorly sorted graded sediment. The bar dynamics in the graded sediment case are more unstable than those in the case of uniform sediment [71]; therefore, it is likely that the low-amplitude bedload sheets or some small fluctuations caused by sediment feed conditions can drastically change the dynamics of the graded sediment sand bars.

This limitation is also critical in cases where suspended sediment transport should be considered [72]. The length scale of the suspended sediment transport is much longer than that of the bedload, so that the effect of sediment supply into the river can reach more downstream. Landslides or debris flow events bring finer sediment than those in the riverbed [73]; therefore, this type of sediment supply has a different role in the bedload-dominated condition. Our focus is on gravel-bed rivers, so this is beyond the scope of this study, but the inclusion of suspended sediment transport is an essential piece of sediment transport worth investigating in future research.

The other limitation that should be noted here is the simple channel configuration or fixed bank assumption. In this study, we used a straight channel with a non-erodible bank. In general, the channel width and curvature can vary in space and time and play an important role in river morphodynamics [74]. Nelson et al. investigated the response of riffle-pool morphology in a width-varying channel to the sediment supply condition, showing that the sediment supply has little effect on the riffle-pool features and that the width variation has a primary role in controlling the overall morphologies. The combination of planimetric channel geometry and sediment supply conditions is also necessary for future research.

Morgan performed flume experiments on gravel bar dynamics under unsteady water discharge and constant sediment feed conditions. This condition satisfies the alternate bar dynamics in the presence of HBL. Because the duration of the hydrograph is much shorter than the morphodynamic time scale, the HBL is not evident in their experiment, but such an attempt will be a good dataset in the future. Furthermore, it is necessary to test this 2D calculation for other types of river morphology, such as bedforms [53,75] and meandering rivers [19], which have been extensively investigated in the context of the effect of sediment supply conditions.

2.5. Conclusions

We investigated the effect of sediment supply on the morphodynamics of free alternate bars in gravel-bed rivers in terms of the HBL concept proposed by Wong and Parker, using a 2D morphodynamic numerical model, iRIC-Nays2DH. Two-dimensional morphodynamic calculations regarding sand bar development were performed under cycled, single triangle-shaped hydrographs with different sediment supply conditions, more specifically, constant and equilibrium feed conditions. The 1D morphodynamic perspective suggests that both feed conditions provide the same mobile-bed equilibrium downstream of the HBL. In contrast, it remains unclear whether the morphodynamic features at such a reach are identical even if the condition is extended to 2D cases, including complex bedforms such as alternate bars.

In the present condition, the simulated alternate bars develop outside the HBL, and characteristics of the alternate bars such as wavelength, bar height and migration speed are almost identical in both sediment feed conditions. This result suggests that the HBL concept is still valid for 2D cases, where the upstream sediment disturbance is difficult to propagate beyond the HBL, and eventually, has a negligible effect on the downstream morphological characteristics. We also changed the hydrograph characteristics, that is, the hydrograph duration and peak discharge were increased by a factor of 2, to understand the sensitivity of this result to the extreme change in the hydrograph from a practical perspective. The larger and longer hydrographs extend the length of the HBL, but the upstream sediment boundary condition does not affect the general characteristics of the downstream alternate bars. In summary, the findings regarding HBL [49] are almost valid for the dynamics of alternate bars developed beyond the HBL, that is, sediment disturbance at the upstream end has a negligible effect on the mobile-bed dynamic processes, including alternate bar formation and development downstream of the HBL.

The HBL is likely an effective temporal or spatial scale of the sediment disturbance (e.g., sediment pulse, sediment wave, gravel augmentation, etc.) in a single flood event, so this cannot be applied to larger-scale issues driven by long-term sediment increase/decline effects (e.g., dam construction). Moreover, this characteristic is highly dependent on the magnitude of the disturbance (size, shape, and texture) and hydraulic conditions. With more complex channel or bed configurations, some experimental or field observational validation will be necessary in future work.

Chapter 3

Morphodynamic equilibrium of alternate bar dynamics under repeated hydrographs

3.1 Introduction

Understanding river morphology and its dynamics is an important topic in many research fields, and the alternate bar morphology is a specific field of interest. Owing to their spontaneous alternating transformation and migration, alternate bars could be the main contributing factor for channel engineering or watershed topography problems such as river bank protection, navigation, agriculture, or river construction [76, 77, 78, 79]. In the last few decades, extensive studies have investigated the fundamental physical mechanisms of the alternate bars [1, 5, 80]. To understand river morphodynamics, the concept of formative (or dominant, effective) steady discharge, which determines the overall characteristics of river morphology, is adopted. River bars and related morphodynamics (e.g., meandering) have been thoroughly investigated using steady discharge conditions based on formative or effective discharge concepts. Generally, this simplification does not affect the fundamental physics of the formation and development of river bars and provides some important insights such as alternate bar wavelength and height, growth rate, and migration [6, 11, 82]. Crosato et al. performed experiments and numerical simulations of alternate bar morphodynamics under long-term steady discharge conditions, demonstrating cyclic behavior of the alternate bar morphodynamics and the possibility of non-migrating alternate bars [83]. However, these studies consider alternate bars to be in a relatively stable discharge condition, focusing on their long-term behavior and development.

The discharge unsteadiness, which has been a long-ignored concept, plays a critical role in the sand bar formation and dynamics. Tubino performed a linear stability analysis of free river bars under unsteady discharge conditions, showing generally good agreement with the experimental results, which demonstrates the temporal changes in the wavelength and wave height of bars under unsteady discharge conditions [25]. This first theoretical attempt indicated the importance of flow unsteadiness to bar dynamics and further motivated the understanding of alternate bar dynamics under unsteady discharge conditions [26,27,28]. Visconti et al. conducted movable bed and bank experiments under unsteady discharge conditions, showing that a specific combination of hydrograph features and migration characteristics of bars enhance or suppress the development of pseudo-meandering channels [44]. Iwasaki et al. performed a numerical simulation of the bar and bank erosion in the vegetated floodplain during a large flood in a natural river (Otofuke River, Japan), suggesting similar importance of the discharge unsteadiness to the amplification of meandering channels [18].

The aforementioned studies emphasize the significance of discharge unsteadiness on the morphodynamics of river bars. Such studies focus on short-term morphodynamics as only a single or a few repeated hydrographs are considered. A lack of understanding of the long-term morphodynamic behavior subjected to multiple unsteady hydrographs exists. In other words, exactly how the river bars were formed and continue to develop in the long term, under the complex sequence of hydrographs remains unclear. This is mainly owing to a lack of field observations pertaining to long-term hydrological and spatio-temporal river bars interactions, as well as the difficulty in performing long-term flume experiments, even under simplified conditions. Notably, in this regard, Carlin et al. proposed a novel framework for obtaining the long-term equilibrium characteristics of river bars (i.e., wavelength and wave height) using a linear, and nonlinear stability analysis with the flow duration curve, which is a bulk treatment complex sequence of discharge variation in long-term [13]. Their analyses were in agreement with field observations of the river bar geometry. This is a robust framework to understand the equilibrium state of bars under discharge variation; however, bar dynamics must be discussed in detail as discharge variations are simplified into a flow duration curve. Nelson and Morgan conducted flume experiments of gravel bedform development under repeated simple triangle hydrographs and a constant sediment feed rate [52]. This is, to our knowledge, only the flume experiment to pursue long-term equilibrium of bedforms under unsteady discharge conditions. Their results showed that flow unsteadiness has a negligible effect on channel-scale morphologies. However, the bedform resembling the alternate bars in their experiment might be a combination of dunes and alternate bars (i.e., three-dimensional bedforms [84]), as the observed geometry does not satisfy the river bar categories derived from linear stability analysis that adopts the shallow flow approximation [5, 85]. In this case, the bedform can adjust its shape to the discharge variations, although there is a hysteresis effect [86]. However, the large-scale bars have a longer morphodynamic timescale, so the effect of the hydrograph might be more complex. In summary, the discharge variation (or discharge unsteadiness) has been considered only recently in morphodynamic modeling, but it remains unclear how large-scale bedform alternate bars reach a state of equilibrium, especially in the long term.

This study focuses on the long-term behaviors of alternate bars under the influence of repeated hydrographs. The questions we pursue in this study are 1) Do alternate bars attain the equilibrium state under unsteady flow discharge conditions? 2) What are the equilibrium characteristics of alternate bars under this condition? 3) What controls the long-term behaviors of alternate bars? To understand these points, we perform several numerical simulations of alternate bar formations under repeated hydrographs and corresponding steady discharge conditions using a two-dimensional morphodynamic model, iRIC-Nays2DH. The simulated alternate bar morphodynamics, i.e., the wavelength, bar height, and migration period are investigated to understand the effect of hydrographs on long-term alternate bar characteristics, and the relation between hydrograph and morphodynamic timescales.

3.2 Method

3.2.1 Numerical model

We used the Nays2DH model [31], a two-dimensional morphodynamic model embedded in the iRIC software [32]. This model was applied to various sediment transport-related simulation studies [33,34,35], and is suitable for simulation applications of alternate bar morphodynamics focused on in this study [36, 37]. In addition to such previous results, in the Appendix A, we show that the model reasonably captures the formation and migration of alternate bars under repeated simple hydrographs observed in a laboratory experiment. Also, the characteristics of alternate bars simulated in the present study are generally consistent with the observed one in the Otofuke River, which is a modeled river in this study (see below and Appendix A). These validations of the model suggest that the Nays2DH model may be an acceptable tool to pursue the long-term morphodynamics of alternate bars under repeated hydrographs focused on in this study. Meanwhile, the flow model used is an unsteady two-dimensional shallow water flow model. As we focus on morphodynamics of alternate bars in gravel-bed rivers, we only consider bedload transport as a mode of sediment transport. The Meyer-Peter and Müller formula was used here, and the sediment was assumed to have a uniform grain size.

3.2.2 Computational conditions

To understand the morphodynamics of alternate bars under repeated hydrographs, we used the condition of the Otofuke River as an example. This river is a typical gravel-bed river and the alternate bars are one of the dominant river morphologies [18, 29]. The modeled channel has a 21 km length and 70 m constant channel width with a uniform slope of 0.005, which is a simplified configuration of the upper Otofuke River [29]. A Manning roughness coefficient of 0.028 $s/m^{1/3}$ and a uniform particle size of 40 mm were used.

We derived the hydrograph shape based on the large flood event observed in 2011, such that the migrating alternate bars could form and develop [30]. Figure 3.1 shows repeated hydrographs used in the calculation. The observed hydrograph was modeled as a simple triangle-shaped hydrograph; that is, the water discharge linearly increased from 100 to 600 m^3/s within 20 h and subsequently decreased from 600 to 100 m^3/s linearly in 20 h, forming a 40 h cycle.

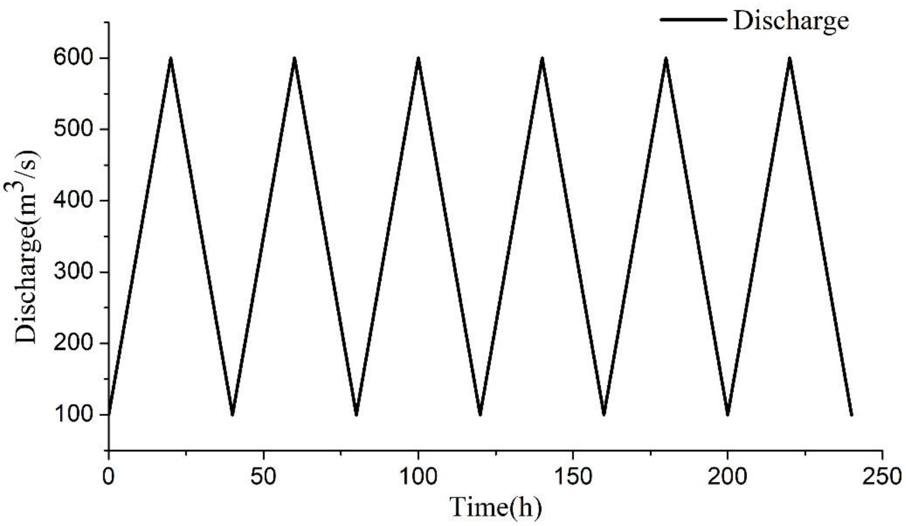

Figure 3.1 Hydrograph condition used for the calculation.

The six hydrographs are shown here as an example. In the calculation, 50 hydrographs were obtained. The aforementioned computational condition is the same as our previous studies that focus on the effect of sediment supply on the alternate bar formation [36]. However, the sediment transport rate used in this study was calculated from the upstream end flow parameters. This feed rate is the sediment transport capacity of this modeled river, and the supply rate depends on the hydrograph, as shown in Figure 3.1. As the feed rate is equivalent to the transport capacity, the bed elevation at the upstream end does not change over time under this condition.

3.2.3 Wavelet analysis of migration periods of alternate bars

Wavelet analysis was introduced by Grossman and Morlet for the treatment of geophysical seismic signals [87]. This analysis is considered as a milestone in Fourier analysis development because it can achieve higher accuracy in unstable signal analysis by localizing the process.

Currently, wavelet analysis is an efficient mathematical solution in many fields and makes up for a few drawbacks of the Fourier analysis. However, few applications have been made with respect to river morphology. Yovanni used wavelet analysis on the migrating ripple sand dunes observed in an experiment on a meandering channel. In this study, bed elevation and distance were considered as amplitude and process respectively, and the processed data helped identify the location and geometric dimensions of erosional and depositional regions in meandering channels [88]. Mahdade introduced new wavelet analysis tools in the field of geomorphic analysis to identify the pseudo-periodicity of alternating morphological units from a general point of view for six small French rivers [89].

Our study data deals with the elevation variation at one position with respect to time. As the time for each alternate bar to pass through varies, the Fast Fourier Transform (FFT) method cannot determine the instability over time. Wavelet analysis is a better solution to process the elevation variation with respect to time. In this study, Morlet wavelet with a central frequency of two was used as the parent wavelet.

3.3 Results

Figure 3.2 shows the elevation change at the right bank of the computational river with respect to time. In this figure, the migration of alternate bars can be inferred from the pattern of elevation variation, that is, erosional and depositional patterns of this figure move from bottom-left to top-right. This pattern shows that the morphology (i.e., alternate bars) keeps migrating downstream, and the slope of this pattern shows the migration velocity of bars, as this figure represents the bed elevation contour of the time-space domain. It can be shown that although the migration velocity varies owing to the unsteady water discharge, the average migration velocity of the alternate bars, which is akin to long-term behavior, appears constant. Additionally, the spacing between each depositional or erosional point, which corresponds to the wavelength of alternate bars, is consistent with respect to space and time. Figure 3.3 shows the temporal change of alternate bars during the last hydrograph of this computation. Here five typical time points in one hydrograph cycle are selected to present the characteristics of the alternate bars during a hydrograph, The points are 0 (beginning of the hydrograph cycle), 1/4T (one-quarter of the hydrograph cycle), 1/2T, 3/4T, and T (end of the hydrograph cycle), where T denotes the hydrograph cycle. As shown by the red arrow line, the migration velocity changes with respect to discharge, while the wavelength remains constant at 580 m with respect to time. Moreover, when t = 0 and t = T, the positions and shapes of alternate bars are identical; thus, the elevation of the river bed returns to its original value after one hydrograph cycle because alternate bars migrate exactly one wavelength downstream within one hydrograph.

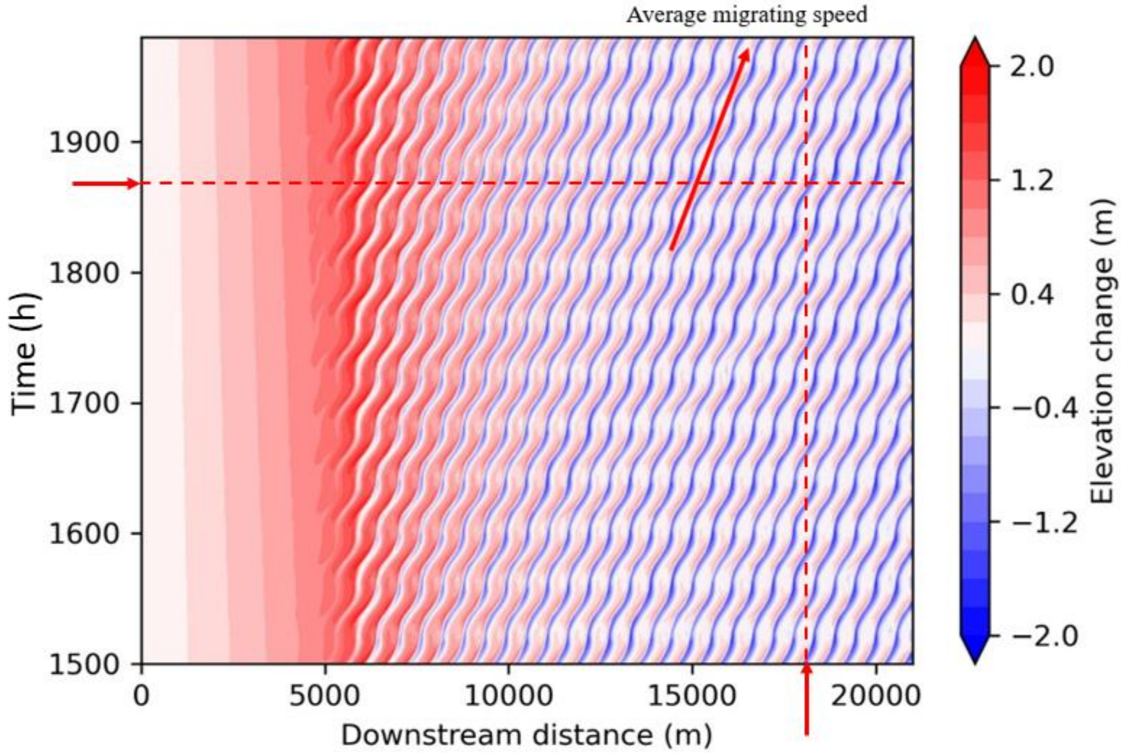

Figure 3.2. Elevation variation at the right bank along time and downstream distance.

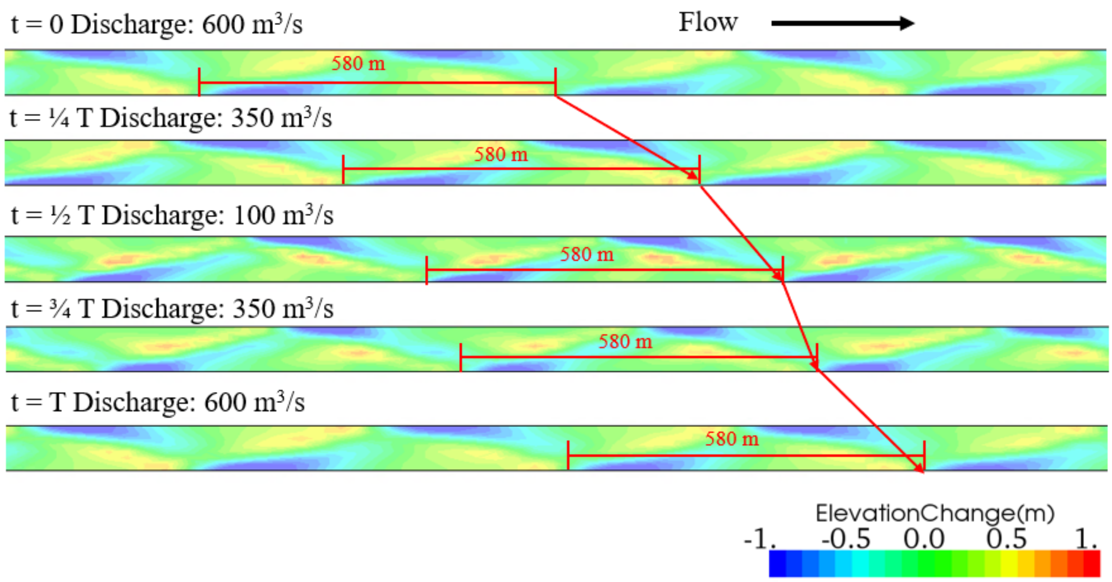

Figure 3.3. Alternate bars migration within one hydrograph cycle of last hydrograph in the computation, where T is the hydrograph cycle (40 h).

To investigate the migration characteristics in a greater detail, as shown n in Figure 3.2, we selected a point at the distance axis and demonstrated that the elevation variation with the time as shown in Figure 3.4(a). The space between two adjacent minimum values represents the time taken by an alternate bar needs to pass through this point. To simplify this description, we define this time as the "migration period." Similarly, if we select a point on the time axis, we can obtain elevation variation at the right bank for this time point in Figure 3.4 (b). The space between two adjacent minimum values represents the wavelength of an alternate bar.

Figure 3.4 shows a simple introduction of the elevation variation with respect to time and space. Figure 3.4 (a) shows the migration period of alternate bars, which is equal to the hydrograph cycle of 40 h; Figure 3.4 (b) reflects the wavelength of alternate bars, which is a constant (580 m).

However, elevation variation at a single position or a single point in time, as shown in Figure 3.4, is not sufficient in obtaining the overall characteristics of simulated alternate bar dynamics. For this, we performed Fast Fourier Transform (FFT) on the bed elevation data along the right bank to obtain the temporal change of the dominant wavelength. In addition, we applied wavelet analysis for the temporal change of the bed elevation at a certain fixed point to detect the migration period of the alternate bars, which is the time required for the bar to migrate by exactly one wavelength. Figure 3.5 shows the result of FFT and wavelet analysis. The results show that during the entire calculation time, the wavelength and migration period of alternate bars remain at 580 m and 40 h, respectively, suggesting that the migration and shape characteristics of

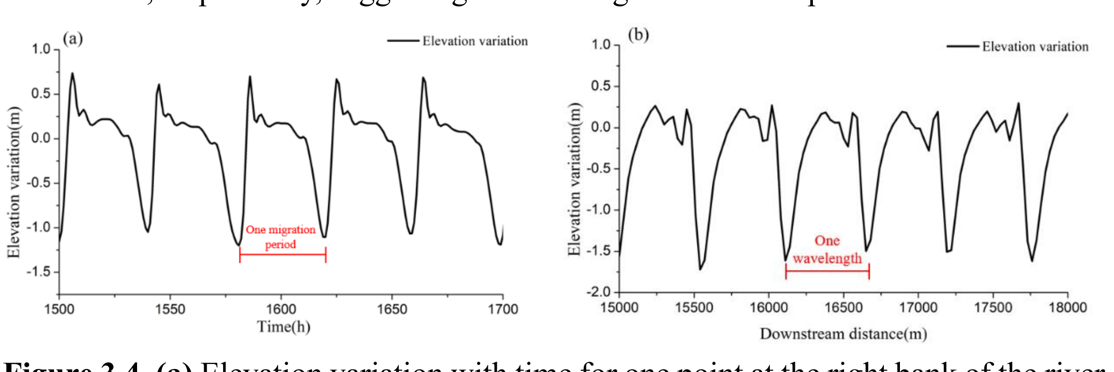

Figure 3.4. (a) Elevation variation with time for one point at the right bank of the river. **(b)** Elevation variation along the river in a downstream direction and at a single point in time.

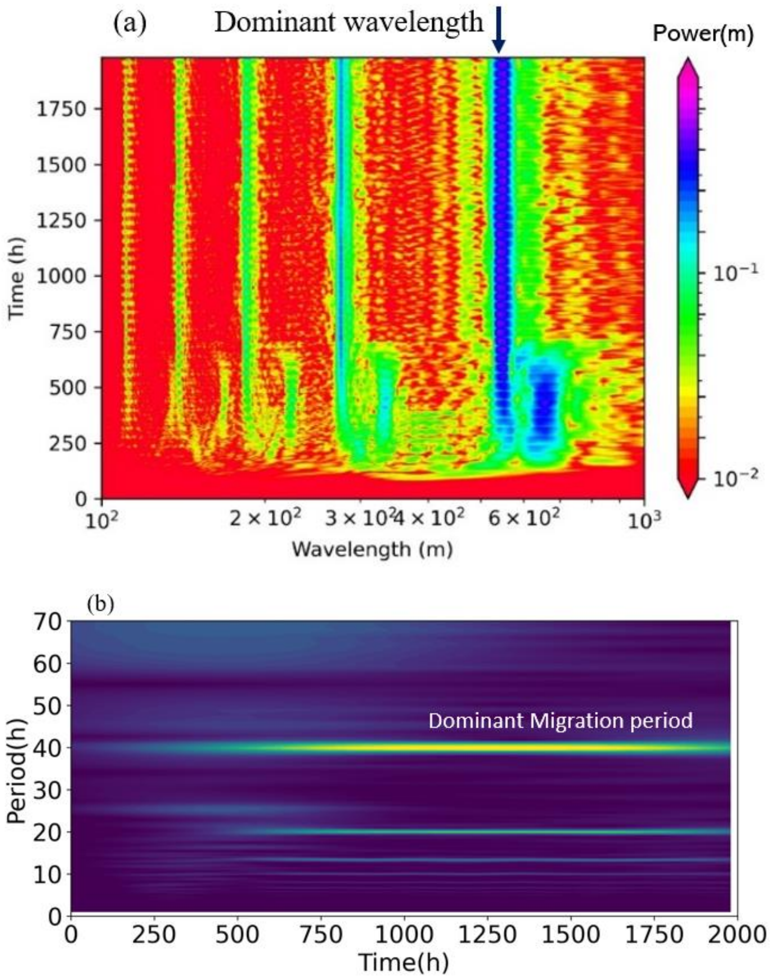

Figure 3.5. (a) FFT analysis of the dominant wavelength. (b) Wavelet analysis of the migration period.

alternate bars are consistent with respect to time and space. In addition, the migration period was equal to the hydrograph cycle. This result shows that even under an unsteady water discharge condition, the bar shape and migration pattern reach an equilibrium state in the context of long-term morphological change.

We imposed a repeated, identical, simple triangle-shape hydrograph for this alternate bar calculation, such that properties of the hydrograph, i.e., cycle and discharge range, might control this morphodynamic equilibrium state. Alternate bars showed unconventional characteristics such as constant wavelength and migration periods after reaching morphodynamic equilibrium.

To confirm whether this phenomenon widely occurs in various unsteady flow conditions or is unique under this condition, we performed simulations considering other unsteady flow conditions by changing the minimum and maximum discharges as well as the hydrograph cycle as shown in Table 3.1. For discharge variation, the lowest discharge of 400 m^3/s resulted in a fully transported condition of alternate bars, while the bars remained submerged and actively moved downstream. The highest discharge of 1000 m^3/s can be determined by the upper transition limit between alternate bar formation and a no-bar condition based on the linear stability analysis [90]. This condition is intended to make the migration of alternate bars active throughout the computation. This also implies that our attention is limited to the actively migrating alternate bars.

As an example of this sensitivity analysis, Figures 3.6 and 3.7 show the FFT and wavelet analyses of the discharge varying between 400 and 1000 m^3/s, with varying hydrograph cycles. These figures show that hydrograph cycles of 10 and 20 h resulted in a constant wavelength and migration period with respect to time, suggesting that in both the cases, alternate bars reached morphodynamic equilibrium. The constant wavelengths for the 10 and 20 h cases were 480 m and 680 m, respectively. Meanwhile, the alternate bars with hydrograph cycles of between 40 and 80 h did not reach morphodynamics equilibrium, implying that the dominant wavelength and migration period vary with time. Also, a sensitivity analysis has been presented in Appendix B, we use smaller mesh size to ensure that the current mesh size has no decisive impact on the calculation results (i.e., morphodynamic equilibrium explained above).

The occurrence of this kind of morphodynamic equilibrium in the sensitivity analysis is summarized in Table 3.1, where the existence of the morphodynamics equilibrium is marked with a circle. In each case wherein the equilibrium state is achieved, the alternate bars have a unique constant wavelength, and their migration periods are equal to the hydrograph cycle. However, most of the unsteady flow cases with a hydrograph cycle of 20 h can reach morphodynamic equilibrium. Furthermore, certain hydrograph cycles can also facilitate the alternate bars in reaching an equilibrium state. The results of FFT and wavelet analysis of the morphodynamics equilibrium states that is not included in the main text can be seen in the Appendix C.

Table 3.1. Hydrograph features for sensitivity analysis and existence of morphodynamic equilibrium.

Discharge (m^3/s)		Hydrograph cycles (hours)			
Min.	Max.	10	20	40	80
100	600			○	○
100	700		○		
200			○		
300			○		
400			○		
400	600		○		
	800		○		
	900		○		
	1000	○	○		

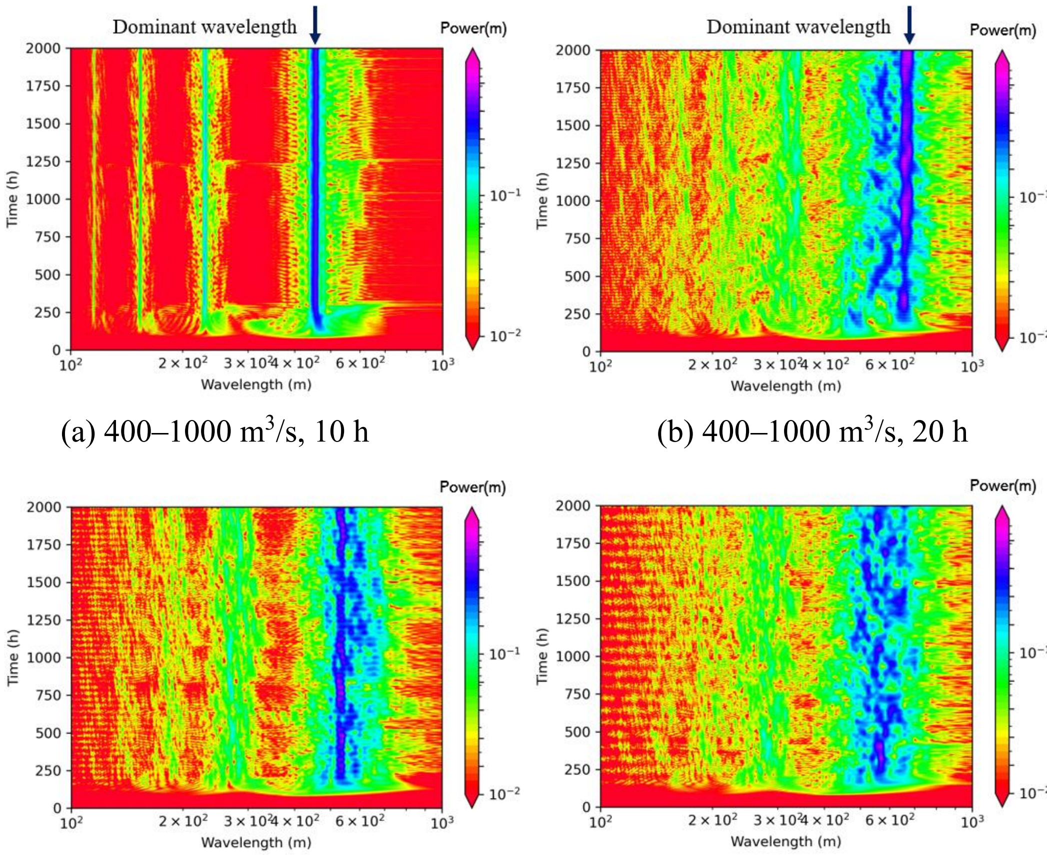

(a) 400–1000 m^3/s, 10 h (b) 400–1000 m^3/s, 20 h

(c) 400–1000 m^3/s, 40 h (d) 400–1000 m^3/s, 80 h

Figure 3.6. (a)–(d) FFT analysis of dominant wavelength in cases 400–1000 m^3/s, cycles of 10, 20, 40 and 80 h.

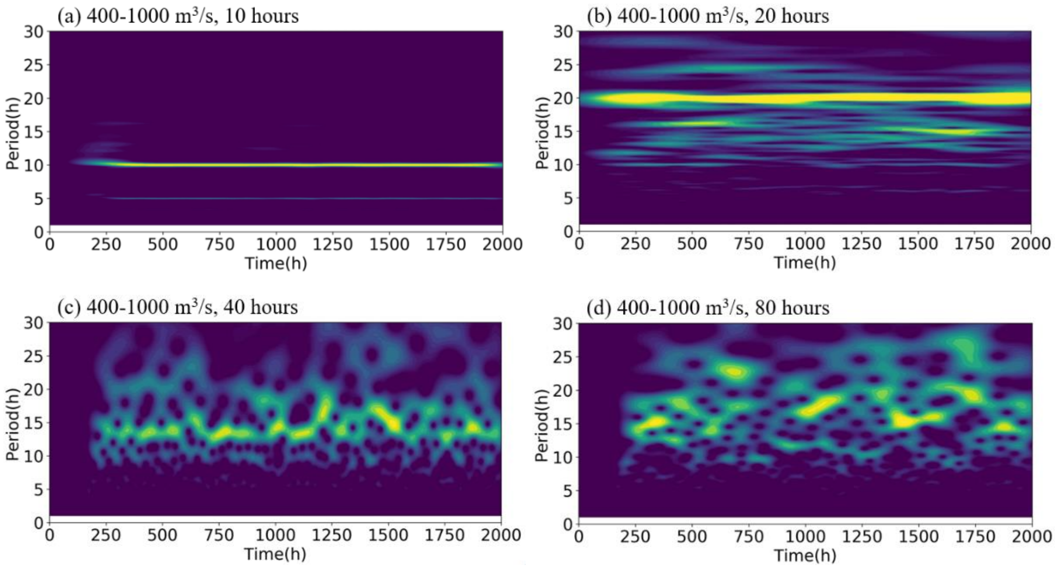

Figure 3.7 Wavelet analysis of the migration periods of the unsteady flow cases of 400-1000 m^3/s with hydrograph cycles of (a)–(d)10, 20, 40, and 80 h.

The results of the sensitivity analysis led to the following observations: First, the cases of 10 and 20 h indicate that under fixed discharge variation, morphodynamics equilibrium is reached in a value range of the hydrograph cycle; second, different constant wavelengths in the two cases indicate that hydrograph cycles determine the characteristics of alternate bars of this state, and it appears that wavelengths will increase as the hydrograph cycle increase.

We compared the results of unsteady versus steady discharge conditions as the latter is generally used to understand the equilibrium state of alternate bars. In this regard, steady water discharges at 400, 500, 600, 700, 800, 900, and 1000 m^3/s were considered, which were in the range of unsteady cases. The results of wavelength and migration periods of steady flow cases derived from FFT and wavelet analysis are shown in Table 3.2. The steady discharge case of 700 m^3/s was selected as a typical example to demonstrate FFT and wavelet analyses, as shown in Figure 3.8. This figure suggests that the dominant wavelength and migration period vary slightly with time, and thus exhibit a dynamic equilibrium behavior, but they do not achieve a single equilibrium value. All the runs demonstrated comparable results, that is, similar alternate bars developed and migrated downstream in the entire calculation reach, but their morphodynamics showed slight time-dependent features. This result is consistent

Table 3.2. Wavelength and migration periods for steady flow cases

Discharge (m^3/s)	400	500	600	700	800	900	1000
Migration period (h)	25–40	18–30	15–25	12–20	10–15	8–13	5–10
Wavelength (m)	500–700	500–700	500–700	550–650	500–650	500–600	450–500

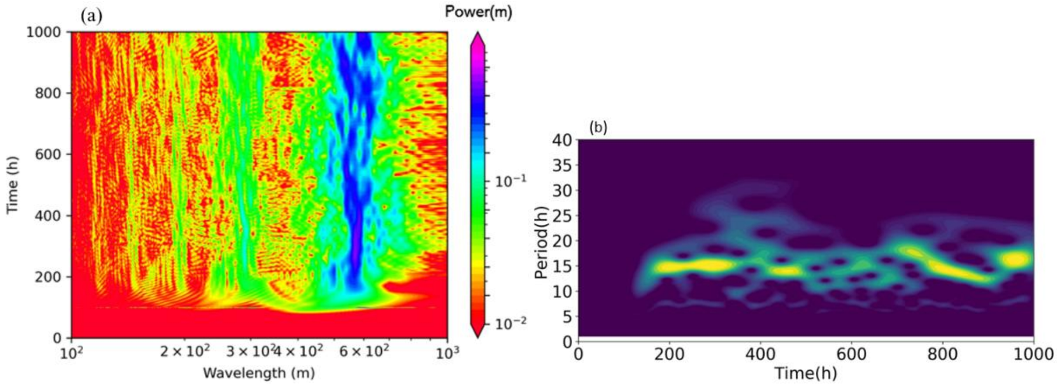

Figure 3.8. (a) FFT analysis of alternate bar wavelengths. **(b)** Wavelet analysis of the migration period for steady flow conditions at 700 m^3/s.

with previous numerical and experimental studies: the migrating alternate bars can elongate in their development state even under steady water and sediment supply conditions [1, 91], and the alternate bars show cyclic development in the context of long-term morphodynamic behavior [83]. The present results for a unique morphodynamic equilibrium show that the specific combination of hydrographs and other physical conditions can cause a different equilibrium state in terms of temporal change of wavelength and migration periods as compared to cases of steady discharge conditions.

The morphodynamic equilibrium state explained above, (that is, the unchanged wavelength and migration periods under repeated hydrographs) appears as a unique feature of the migrating alternate bars under unsteady discharge conditions. This is because the steady discharge counterpart cannot achieve such an equilibrium state. To understand this equilibrium state in more detail we investigated 1) the role of the hydrograph cycle in determining alternate bar characteristics, and 2) the possible range and criteria of the hydrograph cycle to produce morphodynamic equilibrium in certain discharge variations.

As the hydrograph cycles of 10 and 20 h provide the equilibrium state for a discharge variation of 400–1000 m^3/s, a cycle period around 10 and 20 h was selected, that is, 6, 8, 12, 14, 16, 18, 25, and 30 h hydrograph cycles were used.

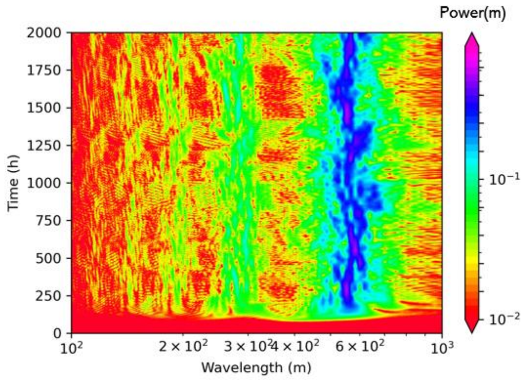

(a). 400–1000 m^3/s, 6 h

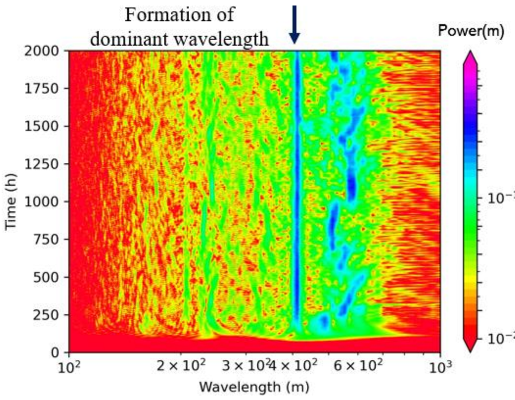

(b). 400–1000 m^3/s, 8 h

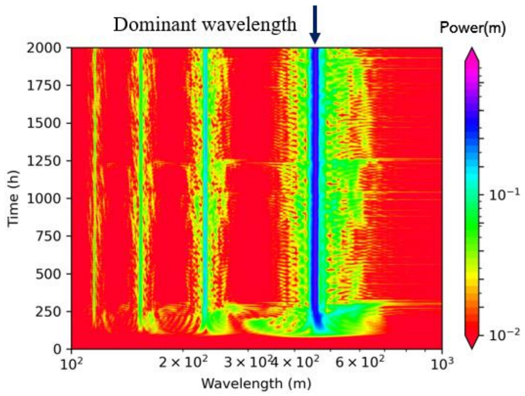

(c). 400–1000 m^3/s, 10 h

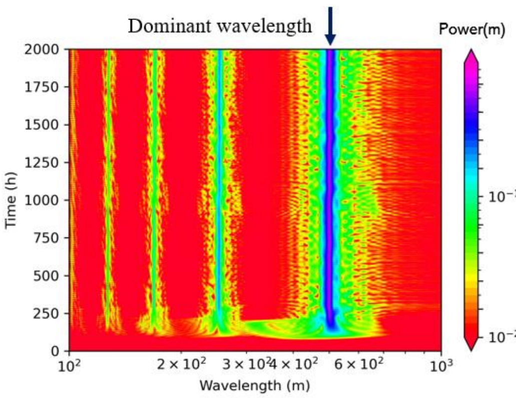

(d). 400–1000 m^3/s, 12 h

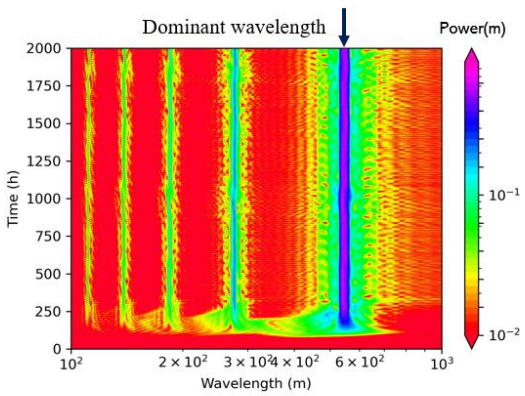

(e). 400–1000 m^3/s, 14 h

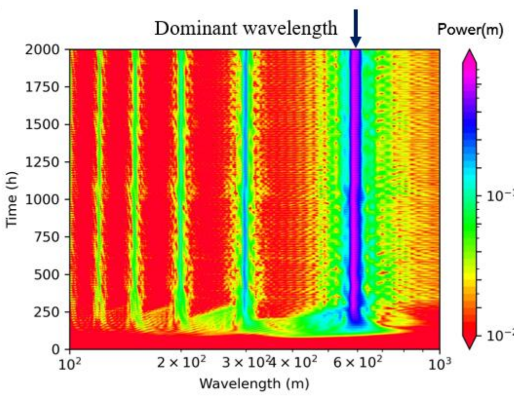

(f). 400–1000 m^3/s, 16 h

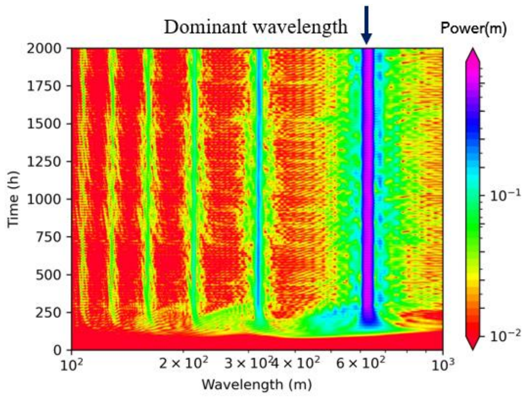

(g). 400–1000 m^3/s, 18 h

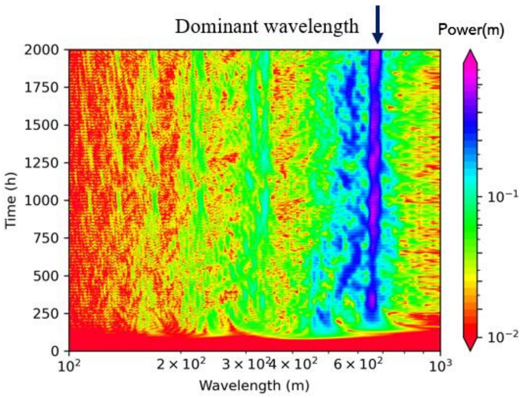

(h). 400–1000 m^3/s, 20 h

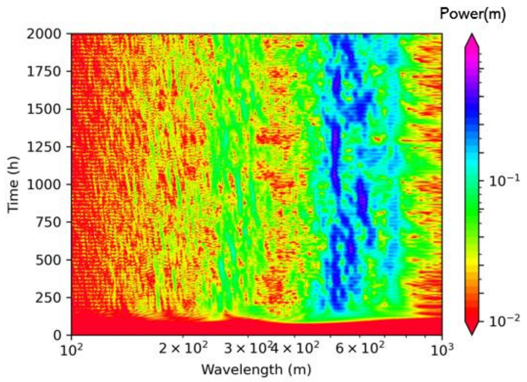

(i). 400–1000 m^3/s, 25 h

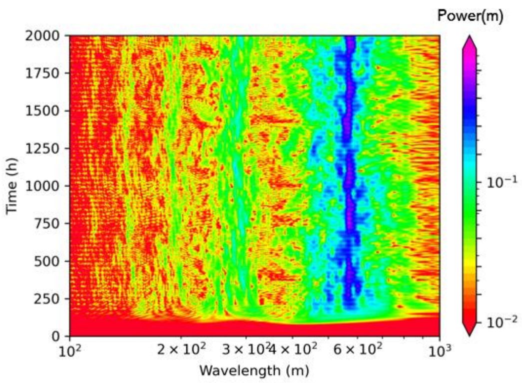

(j). 400–1000 m^3/s, 30 h

Figure 3.9. (a)–(j) FFT analysis of wavelengths in cases 400–1000 m^3/s, cycles of 6, 8, 10, 12, 14, 16, 18, 20, 25, and 30 h.

Figure 3.9 shows the results of FFT analysis of these cases, showing that when the hydrograph cycle is in the range between 10 and 20 h, it results in an equilibrium state. Under this equilibrium state, the dominant wavelength caused by the 10, 12, 14, 16, 18, and 20 h hydrograph cycles are 457, 500, 539, 584, 637, and 678 m respectively, and the migration periods of these cases are identical to their hydrograph cycles, suggesting that the hydrograph cycle is a dominant factor in determining the morphology of migrating alternate bars, that is, increasing the hydrograph cycle causes a longer wavelength and migration period. Conversely, the other cases show time-dependent morphodynamic features, i.e., dominant wavelength and migration period are highly variable with time.

Figure 3.10 shows the temporal change of dominant wavelengths of the steady flow cases of 400 and 1000 m^3/s, and unsteady flow cases of 400–1000 m^3/s with hydrograph cycles of 10, 12, 14, 16, and 18 h obtained from the FFT analysis. Notably,

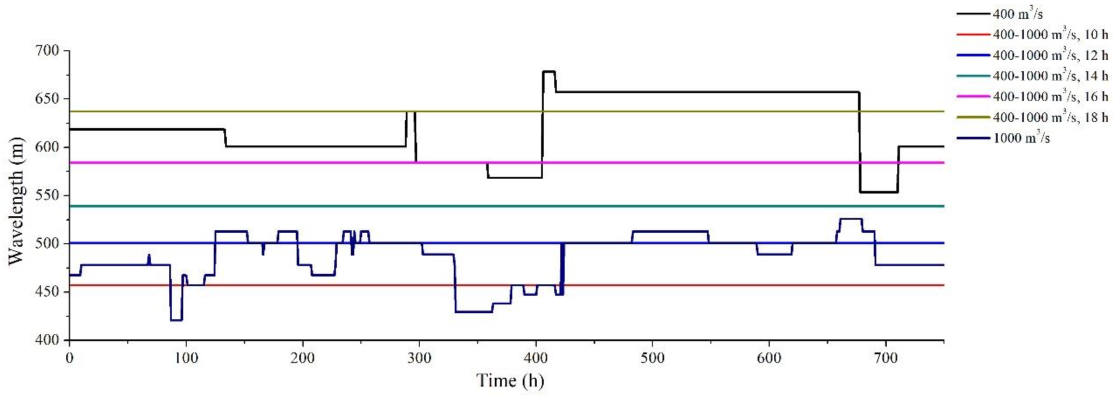

Figure 3.10. Temporal change of dominant wavelengths for steady and unsteady discharge cases.

the dominant wavelength of the hydrograph cycle of 10 h, which is the shortest cycle that could provide an equilibrium state, is close to the dominant wavelength of the steady discharge condition of 1000 m^3/s (450–500 m). Similarly, by increasing the hydrograph cycle from 10 to 18 h, and as long as the equilibrium state is satisfied, the dominant wavelength approaches that of the steady state discharge condition of 400 m^3/s (that is, 550–700 m). These wavelengths of alternate bars caused by the highest and lowest discharge under steady flow conditions, appear to be the lower and upper limits of the dominant wavelength of the alternate bars in equilibrium under unsteady conditions respectively. Furthermore, the equilibrium state under the repeated hydrographs is bound by the alternate bar morphodynamics under the steady discharges of the lowest and highest discharge of hydrographs.

The same is true for the migration period, that is, the migration period of 1000 m^3/s steady case might be an upper limit for unsteady cases, with a period of 400 m^3/s as the lower limit. The hydrograph we used here is a constant flow state, with linear variation between the maximum and minimum of two discharge rates. For example, in the case of the 400–1000 m^3/s flows, we define the migration period of steady flows of 400 m^3/s and 1000 m^3/s as P_{400} and P_{1000} respectively and the migration period of unsteady flow 400–1000 m^3/s case as P_U. Figure 3.11 shows the dominant migration periods of steady flow cases of 400 and 1000 m^3/s, as well as unsteady flow cases between 400 and 1000 m^3/s with hydrograph cycles of 10, 20, 40, and 80 h.

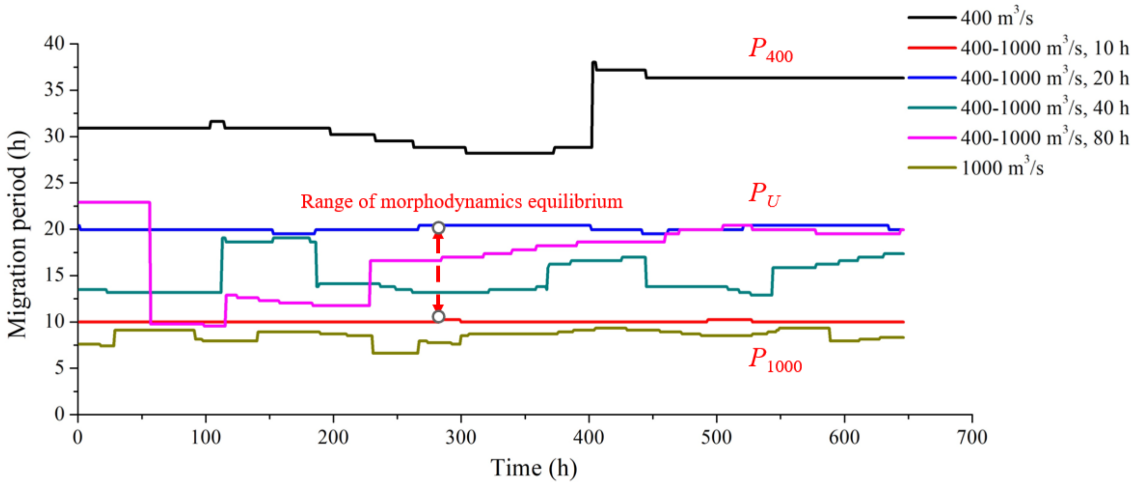

Figure 3.11. Temporal change of dominant migration periods for steady discharge cases of 400, 1000 m^3/s, and unsteady discharge cases of 400–1000 m^3/s with hydrograph cycles of 10, 20, 40, and 80 h.

The numerical results for the migration period caused by the different hydrograph cycles suggest that the migration period of unsteady flow P_U is bounded by P_{1000} and P_{400}, that is, $P_{1000} < P_U < P_{400}$. The value range of P_{400} and P_{1000} are 25–40 and 7–9 h respectively, and the ranges of unsteady flow cases are approximately 10–25 h, which roughly satisfies the condition $P_{1000} < P_U < P_{400}$. However, the temporal change of the dominant migration period is highly dependent on the hydrograph cycle, namely, the 10 and 20 h hydrograph results in a steady value, which is an equilibrium state. Conversely, the migration periods of the hydrograph cycle for 40 and 80 h varies within the range between P_{400} and P_{1000}. As P_U in the case of a hydrograph cycle of 10 and 20 h appears close to P_{1000} and P_{400}, this condition might be a boundary that causes the equilibrium state of the alternate bars under unsteady flow conditions.

Because the migration period of alternate bars, P_U, is identical to the hydrograph cycle, T, in this equilibrium state, the condition $P_{1000} < T < P_{400}$ might be necessary to achieve this equilibrium state of alternate bars under repeated hydrographs. Generally, when the discharge change is from A to B and the migration period of steady discharge A and B are defined as P_A and P_B, this condition might be $P_B < T < P_A$. This is a likely criterion of the hydrograph cycle that could lead to the morphodynamic state; however, the physical meaning should be further explored. However, P_A and P_B are related to a representative morphodynamic timescale of sand bar migration; therefor, this criterion may suggest a relationship between hydrodynamic (i.e., hydrograph cycle) and morphodynamic (migrating bars) timescales. Particularly, the speed of forming and migrating alternate bars under varying discharge conditions might be key to studying the relationship between morphological change and the hydrograph cycle.

To explore this further we performed a numerical simulation of alternate bars with an abrupt discharge change condition of 400–1000 m^3/s as shown in Figure 3.12. The purpose of this case is to study the response time of alternate bars when the discharge rate changes. Low (or high) steady discharge first develops migrating alternate bars in a dynamic equilibrium state, and the abrupt change of discharge reshapes the bars to form another dynamic equilibrium state according to the high (or low) steady discharge. The adjustment timescale of bar shape due to the discharge change might be an important factor in understanding the relation between hydrodynamic and morphodynamic timescales.

Figure 3.13 shows the time-space change of bed elevation at the right bank as we showed in Figure 3.1, and Figure 3.13 demonstrate the temporal change of the bed elevation at the right bank within a certain time, when the discharge is abruptly decreased from 1000 m^3/s to 400 m^3/s and increased from 400 m^3/s to 1000 m^3/s,

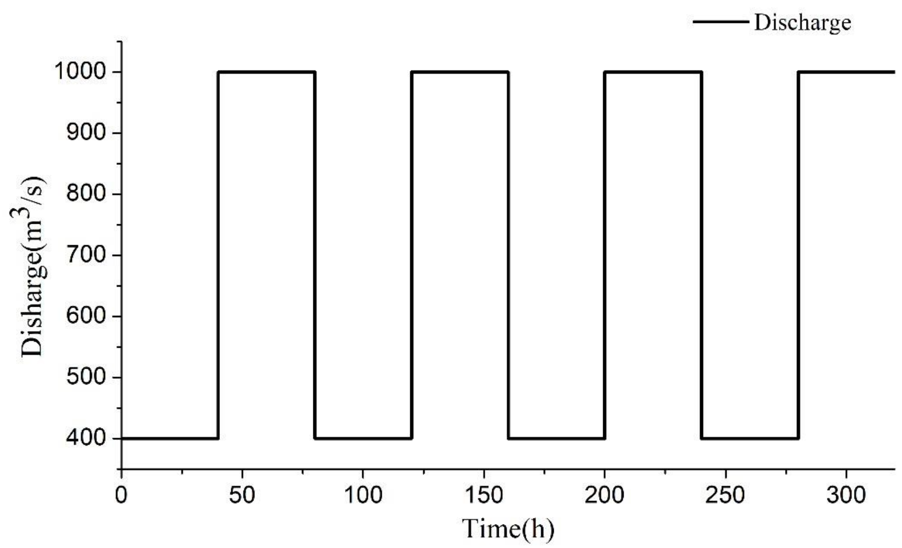

Figure 3.12. Hydrograph of the abrupt discharge change of 400–1000 m^3/s.

respectively. In the decreasing discharge process, elevation variation between 797–820 h is shown in Figure 3.14 (a), and the discharge decreases after 800 h. In the increasing discharge process, elevation variation from 837–860 h is shown in Figure 3.14 (b), and the discharge increases after 840 h.

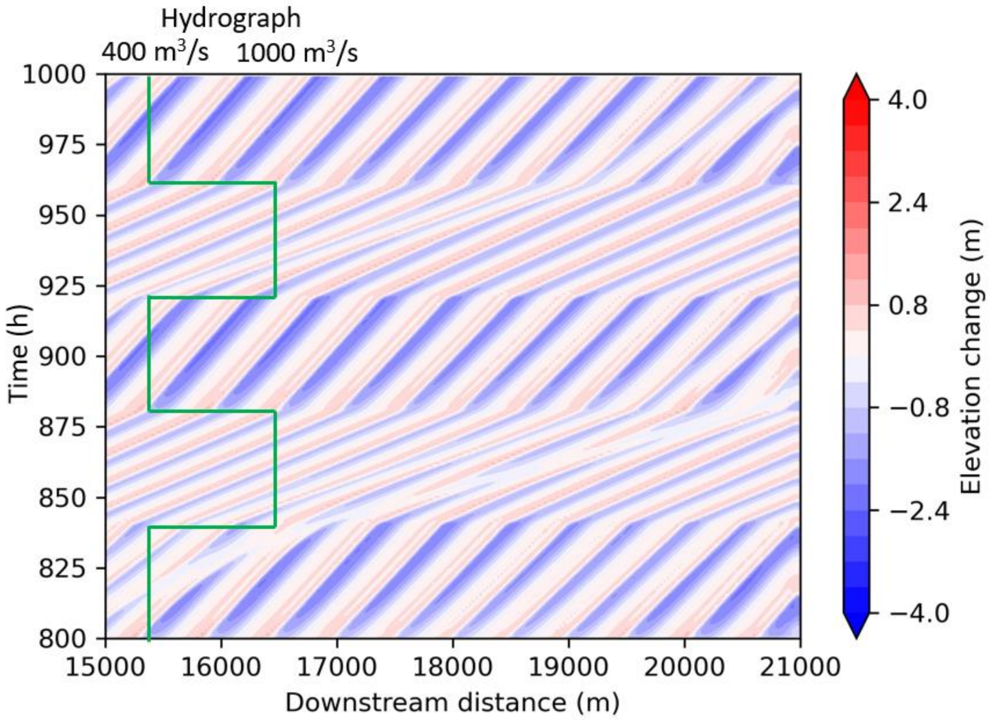

Figure 3.13. Elevation variation at the right bank along time and downstream distance with the hydrograph.

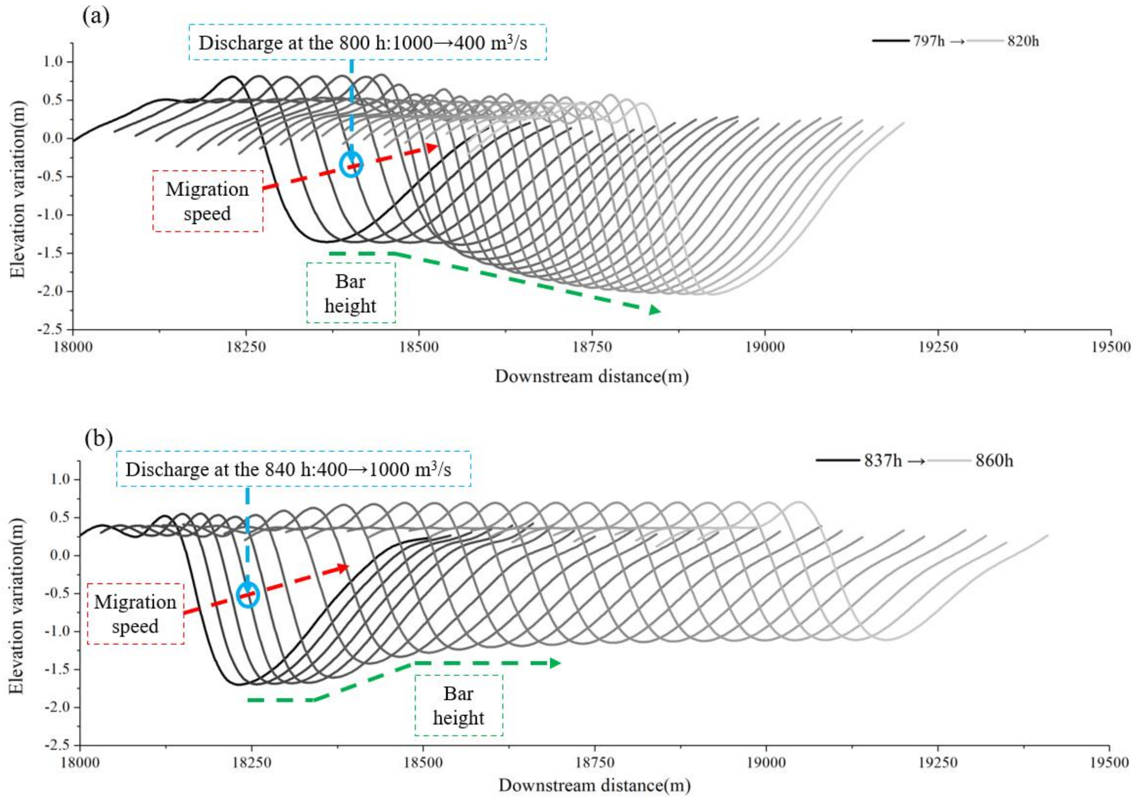

Figure 3.14. Elevation variation of the right bank when discharge (a) decreases from 1000 m^3/s to 400 m^3/s; (b) increases from 400 m^3/s to 1000 m^3/s.

Figure 3.13 shows that the migration speed of alternate bars changes rapidly as the discharge abruptly changes. The same phenomenon can be observed in Figure 3.14, which has been marked with a red dotted arrow, that is, the migration speed of the alternate bar high points changed rapidly within 3–4 h after the discharge changed. Figure 3.14 (a) shows a discharge reduction from 1000 m^3/s to 400 m^3/s, and a subsequent decrease in the bottom of the alternate bars indicated by the green dotted arrow, increasing bar height. However, unlike the rapid change in the migration speed, the change in bar height is a longer process. In Figure 3.14 (a), the decrease in the elevation of the bottom point lasts for 20 h, and still maintains a decreasing trend. In Figure 3.14 (b) shows a discharge increase from 400 m^3/s to 1000 m^3/s, and a subsequent increase in the bottom of the alternate bars indicated by the green dotted arrow, decreasing bar height. Similarly, the migration speed changes rapidly, and the change in bar height is a long-term process. However, in Figure 3.14 (b), the bar height appears to reach an equilibrium state after 6–8 h. The elevation variation due to discharge increase is much faster than that when the discharge decreases from 1000 m^3/s to 400 m^3/s .

The short response time of migration speed shows that this speed and the discharge rate changes simultaneously. In our study, the hydrograph is linear and smooth. The migration speed changes without any lag, contributing to the migration pattern shown in Figure 3.2. The migration speed of all alternate bars changes with discharge and eventually maintains an approximate constant of the average velocity. Contrastingly, the longer response times of the bar height show that, for different discharge changes, different time periods are required for the alternate bars to reach the corresponding bar height and wavelength. For lower discharge rates, a much longer time is required for alternate bars to reach elevation stability because of low sediment transport capacity. The alternate bars reach elevation stability quicker for higher discharge rates because the sediment transport capacity is high.

(a)

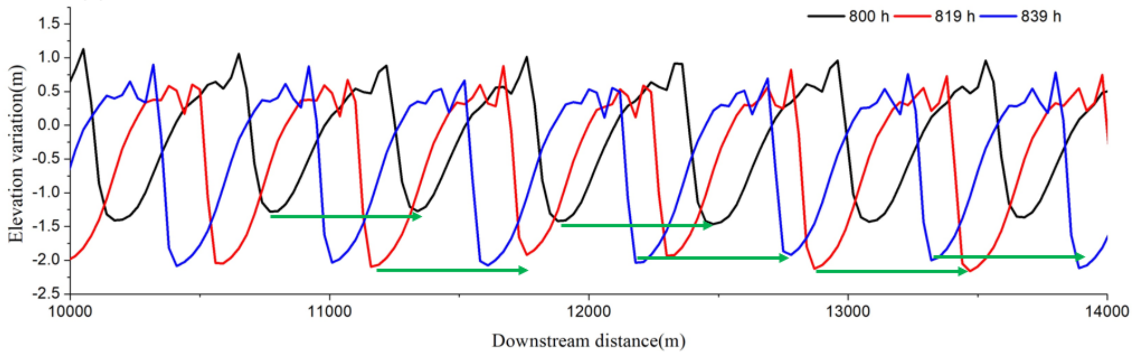

(b)

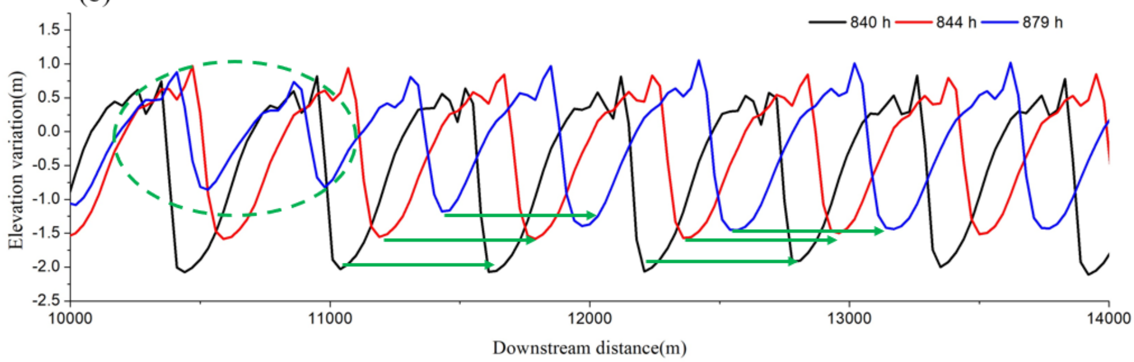

Figure 3.15. (a) Elevation variation of the right bank at 800, 819, and 839 h when discharge drops from 1000 m^3/s to 400 m^3/s. **(b)** Elevation variation of the right bank at the 800, 819, and 839 h when discharge increase from 400 m^3/s to 1000 m^3/s.

Figure 3.15 shows the response conditions of elevation and wavelength to a discharge change from 1000–400 m^3/s and 400–1000 m^3/s. The green arrow line represents a 570 m length and is used to measure the wavelength of the alternate bars. Figure 3.15 (a) shows that the wavelength of bars does not change during the discharge dropping process. On the contrary, in the discharge increasing process shown in Figure 3.15 (b), different wavelengths appear at 879 h, while the wavelengths at 840 h and 844 h remain 570 m. Furthermore, the shape of alternate bars may also change, as depicted inside the green dotted circle. The results show that the wavelength of alternate remain stable in the discharge dropping process as opposed to the increasing process. During the response time of elevation variation, the wavelength remains the same in both processes, but after the elevation change is complete during the discharge increasing process, the wavelength changes, as shown at 844 h and 879 h. This is because after the alternate bars reaches a steady discharge pattern, it is much easier for the bar to change its wavelength. However, for the discharge dropping process, the response time is much longer, and the alternate bars cannot reach a steady discharge pattern, and the wavelength remain constant for a longer period. This difference in response time is caused by the sediment transport rate in lower and higher discharges, implying that the higher sediment transport rate makes the adjustment time for the discharge change faster.

According to the result, there are three response stages of the alternate bars to discharge change. First is the quick response of the migration speed, while elevation variation occurs until the dynamics of alternate bars reach the corresponding discharge level, which maintains the alternate bars in a state of steady flow. The required time for the alternate bars to reach a steady flow state is dependent on the discharge, ranging from 5 h (during 400–1000 m^3/s) to more than 20 h (during 1000–400 m^3/s). After the alternate bars reach the steady flow state, their wavelengths might change according to the alternate bar properties.

The hydrograph cycle that provides the morphodynamics equilibrium state might lie between the two response times above. The hydrograph cycle should be long enough for the alternate bars to respond to discharge variation, but not too long to allow the alternate bars to reach the equilibrium bar height and begin to deform their wavelength as they do in steady flow conditions. If the hydrograph cycle is too short, the alternate bars can be unstable as the 400–1000 m^3/s, 6 h case shows. If the migration speed is not constant and stable, alternate bars cannot be formed upstream. If the hydrograph cycle is too long, the alternate bars have enough time to deform, and the wavelength will be similar to the 400–1000 m^3/s, 80 h case, in which the alternate bars have a chance to develop and become unstable or show cyclic behaviors [83].

3.4 Discussion

In this study, we performed numerical simulations of alternate bar morphodynamics under unsteady discharge conditions, focusing on the influence of hydrograph cycles. Some hydrograph cycles bring the alternate bars to an equilibrium state, with a constant long-term wavelength and migration period, and the migration period is equal to the hydrograph cycle. The results suggest that the hydrograph cycle could also be a key factor in river morphodynamics. Studies on alternate bar morphodynamics under unsteady discharge condition shows that hydrographs with the same discharge variation but differing cycles give rise to different morphodynamic features. Tubino performed flume experiments on sand bar dynamics under unsteady discharge conditions, that is, the same discharge with differing hydrograph cycle conditions were evaluated. In addition, Tubino proposed a theoretical framework to predict the bar height and migration speed under different hydrograph cycles. The results show that short hydrograph cycles yield bar heights that are lower than the expected value from the steady discharge perspective, and long hydrograph cycles yield bar heights that are in equilibrium state [25]. Watanabe et al. also investigated unsteady flow and alternate bar formations with a flume experiment and linear stability analysis, and the results also showed that the hydrograph cycle influences the alternate bar morphodynamics such as wavelength and bar height [92].

The findings of the aforementioned two studies might correspond to the timescales of bar dynamics we introduced: a short hydrograph cycle might not provide sufficient time for the alternate bars to develop, thus resulting in lower bar heights or shorter wavelengths; a long hydrograph cycle might, contrastingly, provide the alternate bars too much time to deform, and alternate bars will elongate significantly [1, 91], deepen and end up with a higher bar height. For example, the experiments of Watanabe et al. adopted a long hydrograph compared to the time scale of bar formation, such that the morphodynamics of alternate bars is strongly changed within a single hydrograph. Our result, however, suggests a constant wavelength or migration periods under unsteady flow conditions (i.e., repeated hydrographs). This morphodynamic equilibrium might be achieved under the specific condition that the timescale of hydrodynamics (i.e., hydrograph cycle) is similar to the morphodynamic timescale. To understand this point, we calculate the following unsteadiness parameter, $\widehat{U}$ proposed by Tubino [25].

$$\widehat{U} = \frac{\sigma}{\epsilon \alpha_{1R}}, \quad \sigma = \frac{\sigma^* B^*}{\overline{U_0^*}}, \quad \epsilon = \frac{\bar{\beta} - \beta_c}{\beta_c}, \quad \bar{\beta} = \frac{B^*}{\overline{D_0^*}} \tag{3.1}$$

where, B^*: half of channel width, $\overline{U_0^*}$, $\overline{D_0^*}$: uniform flow velocity and depth of reference base state, $\bar{\beta}$, β_c: width-depth ratio of reference base state and critical condition, $\sigma^* = 1/T$ and T: hydrograph cycle and α_{1R}: linear growth rate of perturbation. This unsteadiness parameter is the ratio of the timescale between basic unsteadiness of flow and bar growth. $\widehat{U} \gg 1$ corresponds to much slower bar development than the discharge change, so that the alternate bars cannot change their shape corresponding to the discharge change. $\widehat{U} << 1$ provides a much faster growth of bars than the hydrograph cycle, resulting in the equilibrium state of bars given by the steady discharge condition. According to the method of Tubino, some hydrograph cycles were evaluated for 400–1000 m^3/s case, namely, 6, 10, 20, and 40 h provides $\widehat{U}$ =0.47, 0.28, 0.14, and 0.07, respectively. The longer hydrograph cycle (i.e., 40 h) yields small unsteadiness parameters, and in this case, the bar behavior is like a steady discharge case (Figures 3.6, 3.7 and 3.8). The hydrograph cycles which lead non-time dependent wavelength and migration periods of alternate bars, leads to $\widehat{U} \sim O(0.1)$, suggesting that the timescale of morphodynamics is of a smaller order than the hydrodynamic scales, but it is not too small. This result supports our results on the response time of alternate bars. This consideration might suggest that a moderately long hydrograph compared to the bar growth scale will be a key factor in achieving this morphodynamic equilibrium under repeated hydrographs.

The equilibrium state of migrating alternate bars between steady and unsteady discharge conditions may seem similar in terms of bar dynamics, i.e., constant wavelength and the continuously migrating feature. However, it might play different roles in the development of other morphodynamic features, such as bank erosion and channel meandering. To show this, we selected the unsteady case of 100–600 m^3/s with a hydrograph cycle of 40 h, and the steady flow case of 400 m^3/s. Two points A and B on the right bank with a downstream distance is 10,200 m and 10,500 m shown in Figure 3.2, respectively, were selected to evaluate their elevation variation from 700–900 h in both cases. The chosen period was sufficiently long to allow for equilibrium bar development, and the distance between two points was determined by the half wavelength of alternate bars observed in the unsteady case.

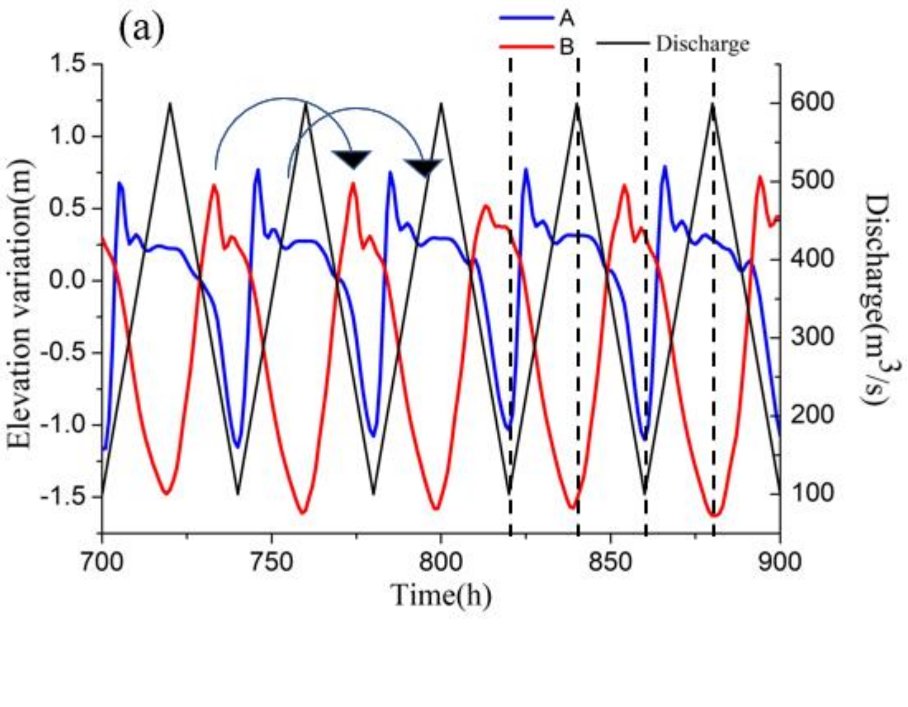

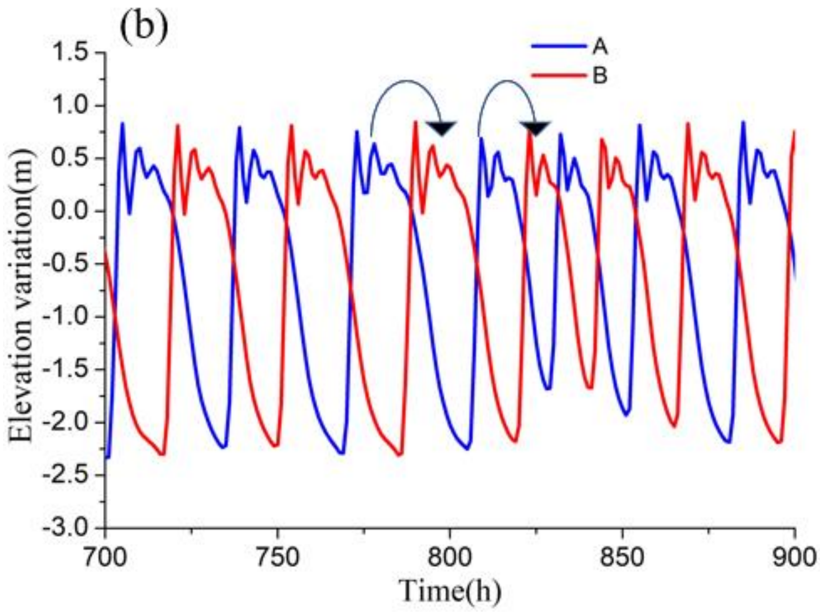

Figure 3.16. Elevation variation at two fixed points (downstream distance = 10,200, and 10,500 m, see Figure 2) under **(a)** unsteady flow condition (The discharge variation is from 100 to 600 m^3/s) and **(b)** steady flow condition (The discharge is 400 m^3/s). The black solid line in a) represents the hydrograph.

Figures 3.16 (a) and (b) show the elevation variation in unsteady and steady flow cases, respectively. The elevation variation at the selected two points at the maximum and minimum discharges are marked with dotted lines. We found that when discharge reaches the maximum value of 600 m^3/s, the elevation variation of point A is always positive whereas that of point B is always negative, even reaching the minimum value. This is because the bars migrate downstream exactly one wavelength within one hydrograph under the equilibrium state. In this case, the morphodynamic changes of fixed points are completely different and are highly dependent on the discharge variations.

Conversely, in the steady discharge case, observing the elevation variation at A and B can be used to determine their relation in Figure 3.16 (b), and that similarity exists in every variation of A and B. The variation appearing in the upstream point (A) appears in the downstream point (B), in a similar form as denoted by curvilinear arrows, demonstrating that the alternate bars which reached equilibrium shape are migrating downstream.

The results of the elevation variation shown above indicate completely different migration patterns and riverbed deformations between the steady flow condition and the unsteady flow condition, which has reached morphodynamics equilibrium. This might cause different morphodynamic features in the context of bank erosion and meandering, as follows:

1. Steady discharge leads to continuous downstream migration of the same alternate bars throughout the channel, implying that the riverbed and riverbank experience the same erosion and deposition processes caused by alternate bar migration.
2. Under an unsteady flow condition that has reached morphodynamics equilibrium, the erosion and deposition at each bank point differ. They exhibit their own varying pattern associated with the hydrograph, implying that some points might suffer more erosion than others. For example, the variation of point B in Figure 3.16 (a) always reaches the minimum value when discharge is at a maximum, implying that A will always be in an eroded state during the flood period. On the contrary, the elevation change of point A during the high flow period remains at a safe position, represented by a positive number, and the elevation change reaches a negative number during the low flow period, implying that point A is a safe position relative to point B.

The hydrograph cycle is a key factor controlling this morphodynamic equilibrium, making it a vital role in the bank erosion and meandering development. Visconti et al. experimentally showed comparable results above: a specific combination of hydrograph shape and migration celerity of bars causes bank erosion at the same point, contributing to the maintenance of the pseudo-meandering channel [44]. However, if the specific combination is not met, bank erosion occurs evenly in both riverbanks, similar to the steady discharge case above, resulting in the formation of a braiding channel. Additionally, in the real-scale Otofuke River, which was selected to determine our numerical conditions, Nagata et al. and Iwasaki et al. pointed out the importance of hydrograph shape in amplifying meandering channels caused by significant bank erosion [18,30]. Although our numerical setup is quite simple, i.e., identical, triangle shape hydrographs are repeated in a straight channel, the results have important implications for the morphodynamics of bar and meandering channel development in alluvial rivers.

Our computational condition and associated results are limited to the continuously migrating alternate bars in a straight channel, neglecting the interaction between flat-bed (no bar) and multi-bar or braided morphodynamics. The present results will be applicable for gravel-bed rivers with high bed slope in upper river reaches, where the bar dynamics is highly active (e.g., [93]). On the contrary, we need to investigate this phenomenon in detail for sand bed rivers, as in such cases other factors (e.g., suspended sediment load) affect the dynamics of alternate bars, and the unsteadiness parameter is generally large, implying that the bar growth is a much slower process than the hydrodynamics [94, 95]. In addition, the reasoning behind this kind of equilibrium state of migrating alternate bars remains unclear under repeated hydrograph conditions. These issues need to be investigated for further understanding of the morphodynamics of alternate bars under unsteady discharge conditions.

5. Conclusions

In this study, we numerically investigated the morphodynamics of alternate bars under unsteady flow conditions. Particularly, the morphodynamics of migrating alternate bars subjected to repeated simple triangle hydrographs was simulated using a two-dimensional morphodynamic model, iRIC-Nays2DH, to understand long-term behaviors of alternate bars under unsteady discharge conditions. We found that the morphodynamics of alternate bars under a specific combination of discharge variation and hydrograph cycle reached an equilibrium state, that is, the wavelength and migration period of alternate bars remained constant, and the migration period was the same as the hydrograph cycle. This might be a unique morphodynamic feature of alternate bars under unsteady conditions because the steady discharge counterparts demonstrated a dynamic equilibrium state with slightly time-dependent features of the wavelength and migration period but did not exhibit non-time-dependent features. When morphodynamic equilibrium was reached, the hydrograph cycle was the dominant factor for alternate bar characteristics. If this morphodynamic state was achieved, the wavelength of alternate bars increased with the hydrograph cycle, and the migration period was always identical to the hydrograph cycle. The hydrograph cycle that corresponds to this equilibrium state can be determined from the relation between hydrodynamic and bar growth timescales. Under a short hydrograph, the bar growth occurred much slower than the discharge changes, implying the bars cannot respond to the discharge variation. Meanwhile, the long hydrograph provided sufficient time for the deformation and development of alternate bars, causing a significant change in bar characteristics (e.g., wavelength) within one hydrograph, which is a similar process obtained under the steady discharge condition. The hydrograph cycle that achieves this equilibrium state must be moderately long so that the timescale of the hydrograph is similar but slightly smaller than the bar growth timescale, but not too small to allow equilibrium bar behaviors caused by steady discharge conditions.

As the morphodynamic equilibrium of alternate bars, subject to the repeated simple hydrographs discussed herein differs from a dynamic equilibrium state provided by the steady discharge analysis, the findings of this study will shed some light on the alternate bar dynamics and related channel-scale morphodynamics such as a river meandering under long-term unsteady discharge. However, the discussion in this paper is still limited because, for example, physical mechanisms of this equilibrium state and applicability of other river and hydraulic conditions remain unsolved. Further research is of immense importance in contributing to a comprehensive understanding of the long-term processes involved in migrating alternate bars under unsteady discharge conditions.

Appendix A: Model validation for alternate bar behavior under unsteady discharge

The iRIC-Nays2DH model we use in this study is a two-dimensional morphodynamic model, which has been applied to many types of morphodynamic phenomena [54]. More specifically, for current study, the model performance for simulating sand bars has been valid, for example, alternate and multiple row bar formation with erodible bank under steady condition has been reproduced by Jang and Shimizu. Also, Kobayashi et al. [96] applied this type of model to flume experiments regarding sand bar behavior under unsteady discharge condition performed by Watanabe and Kuwamura [97]. The numerical result shows general agreement with the experimental result, i.e., the temporal change of bar wavelength and bar height due to discharge change. In addition to these efforts, we herein apply the iRIC-Nays2DH to the laboratory experiments of alternate bar formation under repeated hydrograph, which is similar to our present numerical experiments.

The experiment is performed in 42 m long and 0.9 m wide straight channel at Civil Engineering Research Institute for Cold Regions, Hokkaido, Japan. A well-sorted sand, of which the mean diameter is 0.76 mm, is used for material of bed and supplied sediment. The sand supply rate from the upstream end is equilibrium transport rate, which does not cause bed aggradation and degradation at the upstream end. The longitudinal slope of initial bed is 0.005, and the bed surface is set to be flat. The simple triangle shape hydrograph such as we used in this paper is adopted; highest and lowest discharges are 8 and 4 l/s, and hydrograph cycle is set to 2 hours. The duration of rising and falling stages of discharge is identical (i.e., 1 hour for each stage) and the discharge is linearly changed in time between highest and lowest discharges. This simple hydrograph is obtained 6 times in total, but, firstly, 3 hydrographs are given to the initial bed for formation of sand bars. After a time interval for a few days to measure the bed surface in dry condition using a 3D laser scanner, later 3 hydrographs are obtained to bar-developed bed. In entire experiment, the sand bar behavior at the reach between 17 to 35 m from the upstream end is recorded by three digital cameras from the top of the channel with the time interval of 2 min. Using the photographs taken from the top of channel, we identify the location of migrating alternate bars to capture the migration pattern of the bars. Also, the bathymetric data taken after 3 and 6 hydrographs is available to understand spatial orientation of the alternate bar geometry.

The computational conditions are set based on the experimental condition. The Manning's roughness coefficient is set to 0.0145, which is equivalent to the grain size roughness, to reproduce the uniform water depth at the initial state. The sediment is treated as a uniform sediment of the diameter of 0.76 mm. The grid sizes for streamwise and transverse directions are 0.1 and 0.045 m, respectively. Main difference between the experimental and computational conditions is channel length and number of hydrographs we obtain. In general, time necessary for bar development in the numerical simulation is longer than the experiments, maybe because of the difference in degree of the perturbation. In same way, it takes longer distance to ensure the formation and development of sand bars. More specifically, in the experiment, the bars start developing within first hydrograph at a few meters downstream from the upstream end, on the other hand, in the numerical simulation, the bars start emerges almost at the end of 2^{nd} hydrographs at the 20 m downstream from the upstream end. By considering these "spin-up" time and distance for the system [91], we use 80 m length channel and give 8 hydrographs for the computation. It also means that the computational result during first 2 hydrographs and in 21 m upstream reach in the computation are not used for the comparison.

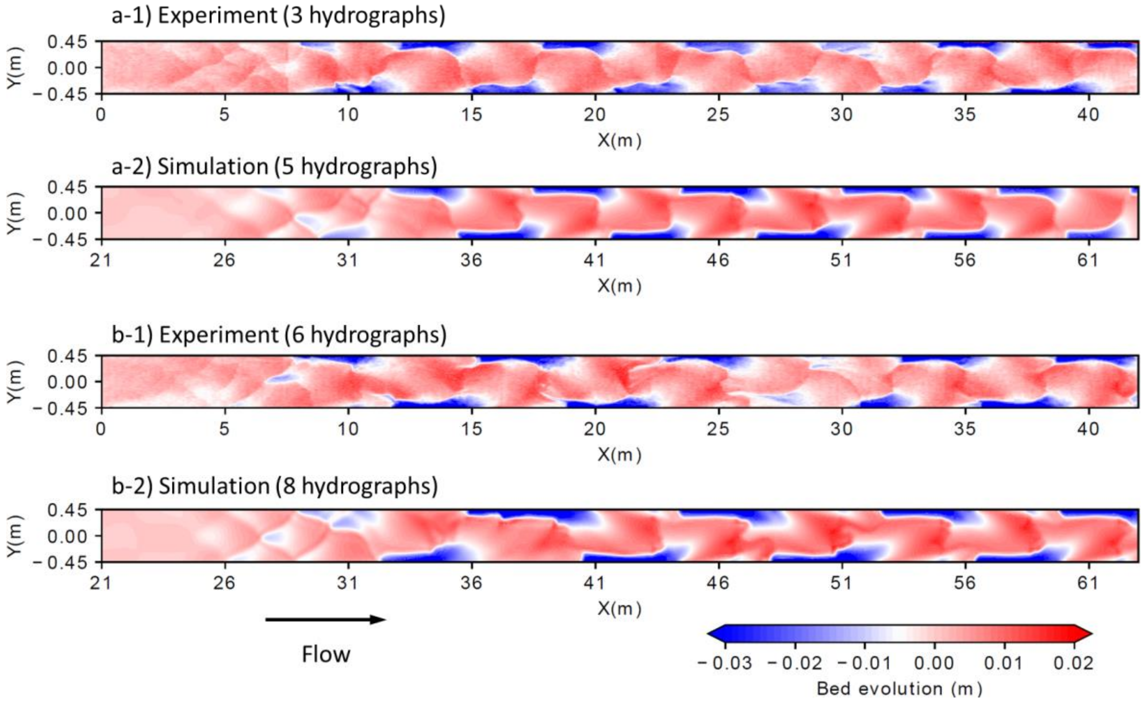

Figure A1. Comparison of the bar geometry between experiment and numerical simulation after a) 3 hydrographs and b) 6 hydrographs. Note that because of the spin-up time and distance in the numerical simulation, the numerical result during first 2 hydrographs and 21 m upstream reach are not used for this comparison.

Figure A1 shows the geometry of sand bars in the experiment and numerical simulation after three and six hydrographs. As the experimental result shows, the multiple row bars form at the upstream reach and its change their characteristics to alternate bars downstream reach. Because of the multiple hydrographs we obtained, the wavelength of alternate bars slightly increases in time. This figure clearly demonstrates that the numerical model is able to capture such morphodynamic trend observed in the experiments.

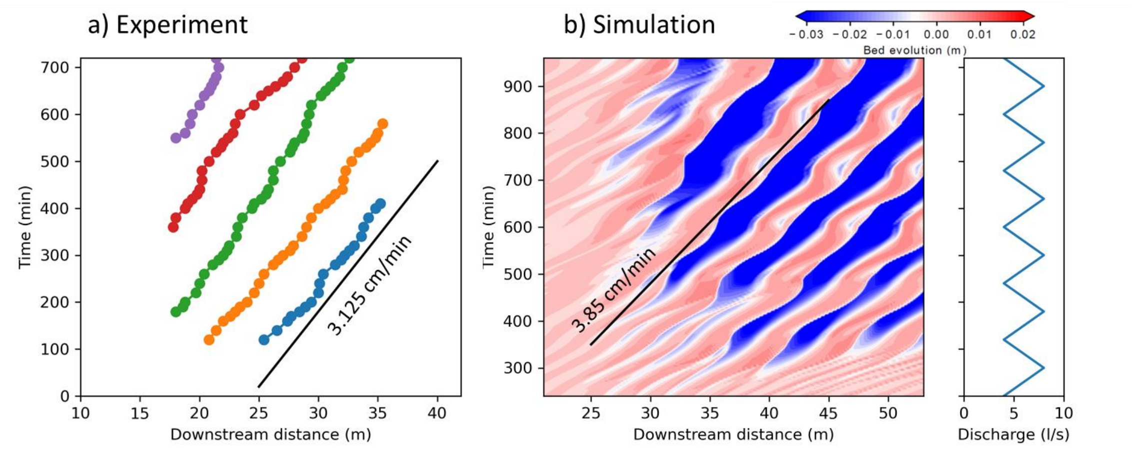

Figure A2. Migration pattern of observed and simulated alternate bars.

Figure A2 compares the migration pattern of the alternate bars in the experiment and numerical simulations. In the experiment, we identify the location of bar front near the right wall of the channel from the photographs taken, on the other hand, numerical results show the pattern of erosion and deposition of bed at the right bank as we show in the main part of the paper as well. This result suggests that the model slightly underpredicts the observed migration velocity of alternate bars, but, generally this result shows good agreement with the experimental data.

Field-scale validation of the model performance for this study is difficult issue since there might not be sufficient field dataset available for alternate bar morphodynamics under repeated hydrographs in a straight channel. Instead, the iRIC-Nays2DH generally captures the sand bar development and associated meandering development caused by large flood event in a field-scale river, the Otofuke River, Japan, which is also used as a modelled river in this study [18,29]. In addition to such previous works, the general features of alternate bars simulated in this study is agreed with the bed and channel characteristics in the field. Figure A3 demonstrates the morphodynamic changes of the upper Otofuke River, Japan, showing that the dominant river morphology is alternate bars and associated meandering development. Two large floods took place at 7th, Sep. 2011 and the end of Aug., 2016, causing great changes of sand bars and channel pattern at Fig. A3 b-c and A3 c-d, respectively. The resultant characteristics, i.e., wavelength of the alternate bars and meandering in this figure can be in the range from 500 to 800 m, which is consistent with the characteristics of alternate bars formed under even simplified discharge condition in this study. It should be noted that since the bars are highly vegetated in this river reach, causing slowdown of migration speed of bars or even non-migrating bars (e.g., Serlet et al [98]), the migration pattern cannot be directly compared with non-vegetated bars in our study. In addition, the significant bank erosion widens channel greatly, on the other hand, in this study, we assume that the channel is a constant width with non-erosible side banks. In spite of these limitations, the numerical model generally captures the morphodynamics of alternate bars of the target river reach.

The results above might suggest that the iRIC-Nays2DH model is a potential tool to pursue the alternate bar dynamics under unsteady discharge condition as we perform in this study. It is worth noting that although the present experiment will be relevant for the validation data of this study, the model needs to be carefully validated further, especially, from long-term perspectives. It means that experimental studies focusing on the morphodynamic behaviors of alternate bars under many repeated hydrographs will be of great interest. In addition to this, the field scale observation of alternate bar behaviors in detail will be surely necessary to understand the effect of unsteady discharge on the alternate bar dynamics for long-term and further validation of the morphodynamic model.

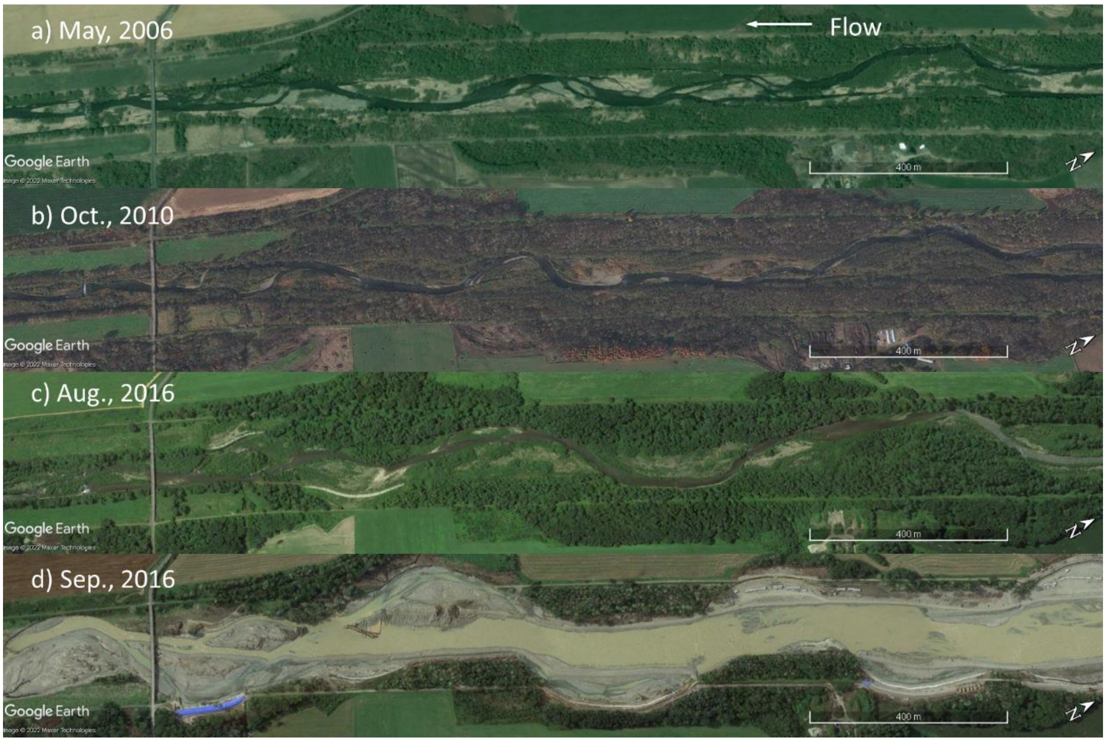

Figure A3. Morphological changes of alternate bars and associated channel meandering observed in the upper Otofuke River, Japan. Two large floods took place at 7th, Sep. 2011 and the end of Aug., 2016, causing large changes of sand bars and channel pattern between b-c and c-d.

Appendix B: Sensitivity test to numerical mesh size

The mesh size is an important parameter for hydraulics numerical simulations. A hydrograph condition may lead to different results according to the mesh size, Horrit et al [99] performed a same flow simulation under different size of mesh, showing different errors, especially modelling a large magnitude event. In this study, an unsteady flow condition is given, though the morphodynamic equilibrium state is observed, there is still possibility that mesh size will influence the results. The mesh size used in this study is 70×10 m^2, and we decrease the length and width to only half of them to 35×5 m^2 to test the sensitivity. Meanwhile, unsteady flow cases of 400-1000 m^3/s with the hydrograph cycles of 10, 20 and 40 hours were tested here, to confirm whether the grid resolution could change the morphodynamic features of the alternate bars we simulated.

Because more grids will consume a lot of extra computing time, for the 10-hour case, we reduce the process to 1000 hours. Figure B1 shows the FFT analysis of the results:

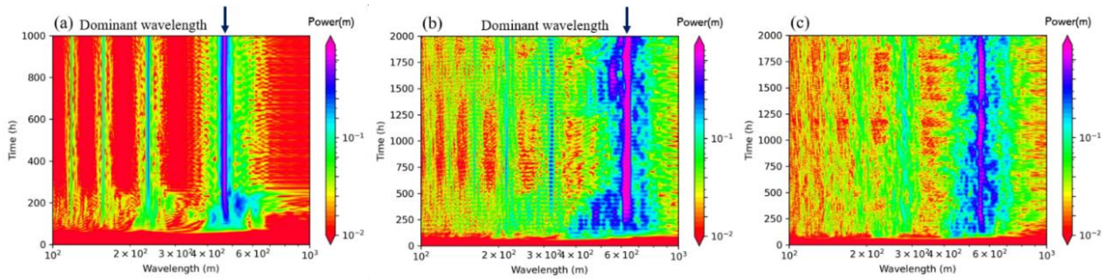

Figure B1. FFT analysis of unsteady flow cases of 400-1000 m^3/s under 35×5 m^2 mesh size with the hydrograph cycles of (a)10, (b)20 and (c)40 hours.

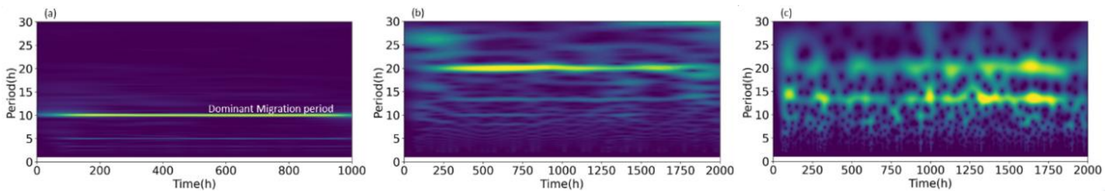

Figure B2. Wavelet analysis of unsteady flow cases of 400-1000 m^3/s under 35×5 m^2 mesh size with the hydrograph cycles of (a)10, (b)20 and (c)40 hours.

Compared Figure B1 to Figure 6, and Figure B2 to Figure 7, it is clearly shown that in every flow condition under 35×5 m^2 mesh size, alternate bars will still show the same morphodynamics properties: morphodynamic equilibrium (10 hours), morphodynamic equilibrium under critical state (20 hours) and alternate bars under general state (40 hours). Figure B1(a)(b) and Figure B2(a)(b) show the dominant wavelengths and constant migration periods. Though Figure B1(c) show a similar dominant wavelength, it is worth to noticed that migration period in Figure B1(c) is not 40 hours, and that doesn't satisfy our definition for morphodynamics equilibrium state. However, it is noticed that the dominant wavelengths in Figure B1 decrease about 20 m in each case, which is 3-5 % of the wavelength, indicating that mesh size will slightly influence the alternate bars' properties. But still, it can be confirmed that the mesh size doesn't influence the morphodynamics equilibrium states which is the main finding of this study.

Appendix C: FFT and wavelet analysis of the equilibrium cases in Table 3.1

Technically speaking, FFT analysis is used to solve periodic signal [100]. To dealing with aperiodic signal like elevation variation, adding window function to transform the signal can reduce error [101].

Figure C1 shows the original and windowed data. We have banished the upstream no-bar area and selected the valid distance from 6000 m to 19000 m in the bar zone.

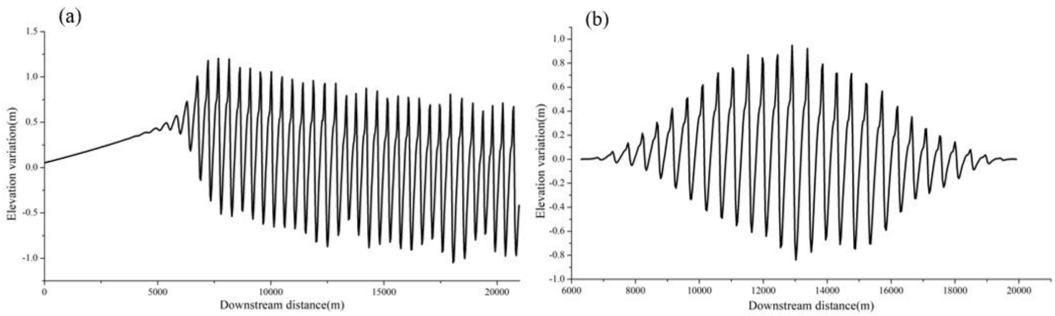

Figure C1. (a)Original and (b)windowed data of elevation variation along the distance.

Figure C2 and C3 show the FFT analysis of the unsteady flow cases 400-1000 m^3/s with the hydrograph cycles of 10 and 40 hours.

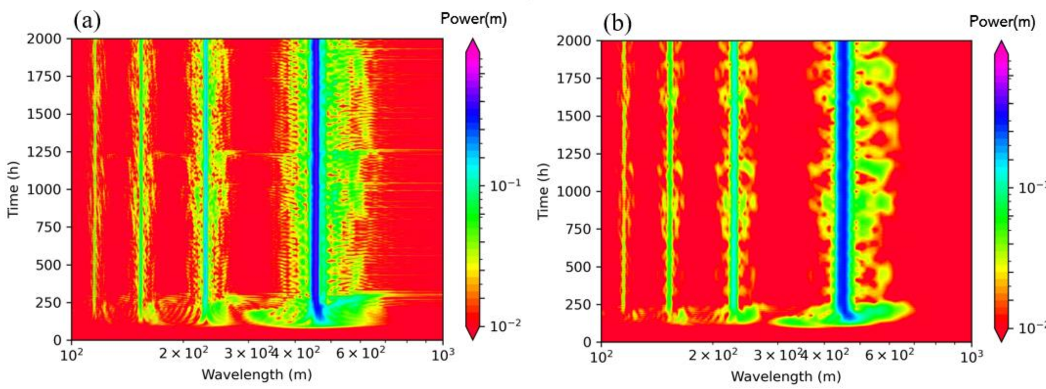

Figure C2. Comparison of FFT analysis of dominant wavelength in cases 400-1000 m^3/s,10 hours with the (a)original and (b)windowed data.

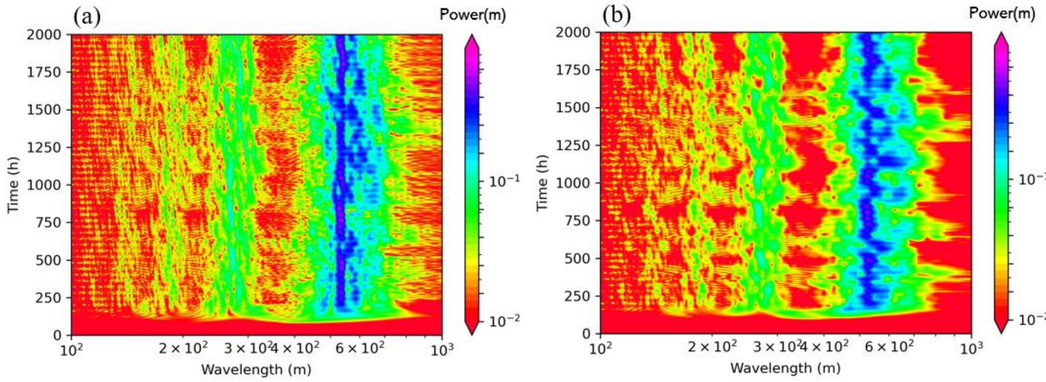

Figure C3. Comparison of FFT analysis of dominant wavelength in cases 400-1000 m^3/s,40 hours with the (a)original and (b)windowed data.

Figure C2 and C3 show that the windowed data give almost the same results as the original data. For equilibrium case of 400-1000 m^3/s,10 hours, constant wavelength is shown clearly; for non- equilibrium case of 400-1000 m^3/s,40 hours, the results are also similar. However, as windowing reduces the effective data, the graphics resolution is reduced. Also, as the original data will not affect the correctness of the results, so we decided to use the original data for FFT analysis.

Figure C4 to C11 show the results of FFT analysis of the dominant wavelengths of the cases in Table 3.1; Figure C12 to C19 show the results of wavelet analysis of the dominant migration periods of the cases in Table 3.1

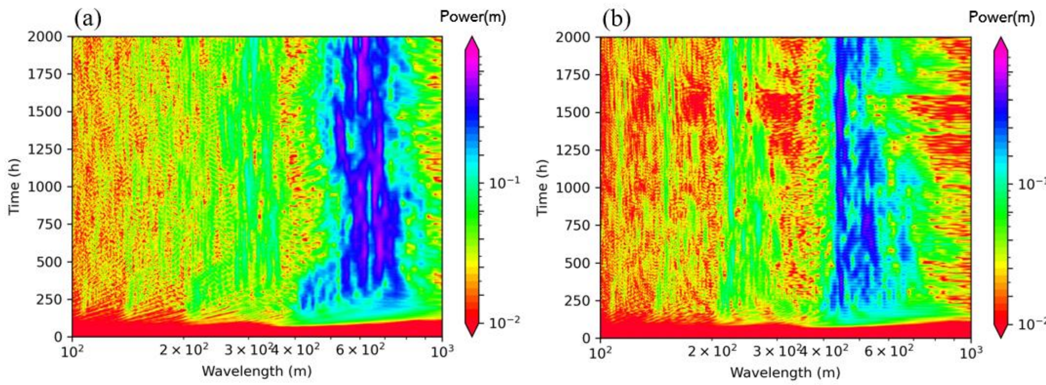

(a). 100-600 m^3/s, 10 hours (b). 100-600 m^3/s, 20 hours

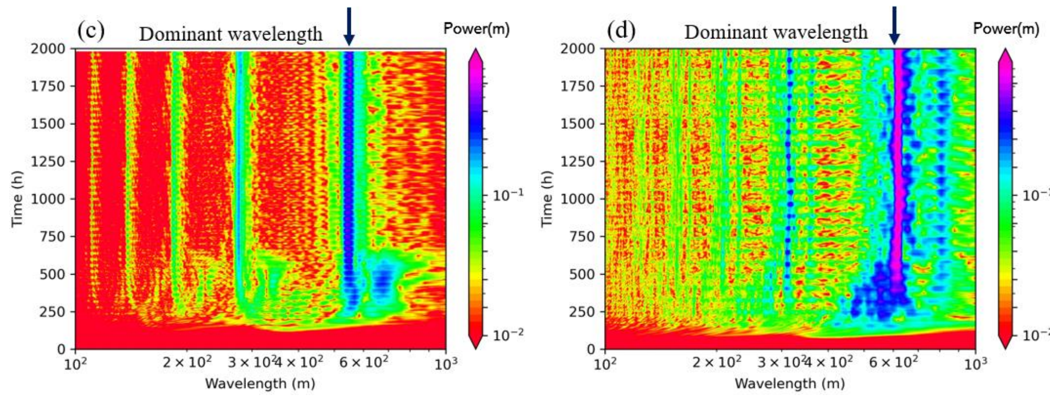

(c). 100-600 m^3/s, 40 hours (d). 100-600 m^3/s, 80 hours

Figure C4. (a)-(d) FFT analysis of dominant wavelength in cases 100-600 m^3/s, cycles of 10, 20, 40 and 80 hours.

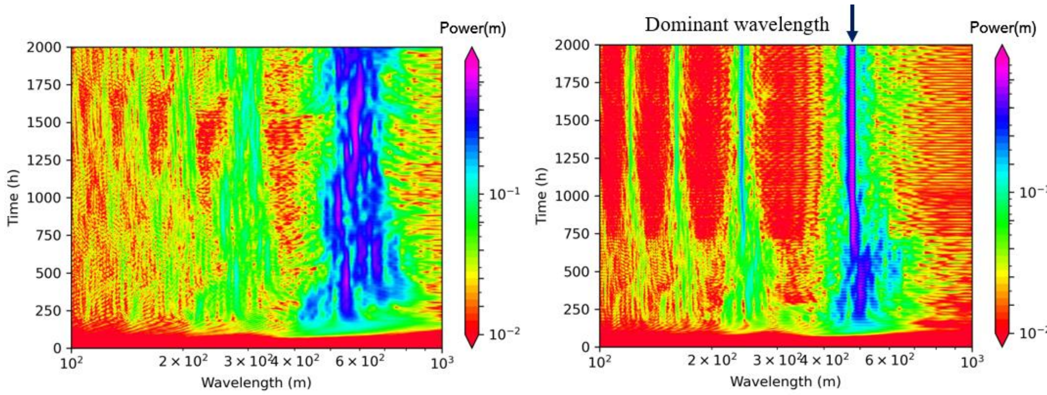

(a). 100-700 m^3/s, 10 hours (b). 100-700 m^3/s, 20 hours

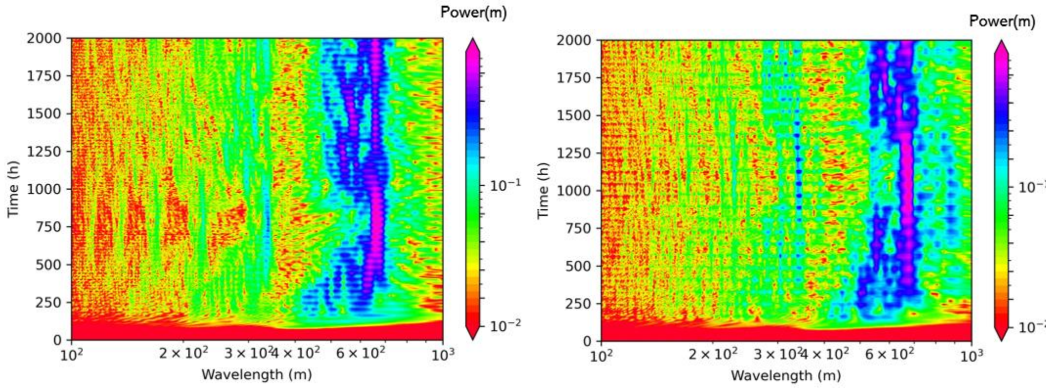

(c). 100-700 m^3/s, 40 hours (d). 100-700 m^3/s, 80 hours

Figure C5. (a)-(d) FFT analysis of dominant wavelength in cases 100-700 m^3/s, cycles of 10, 20, 40 and 80 hours.

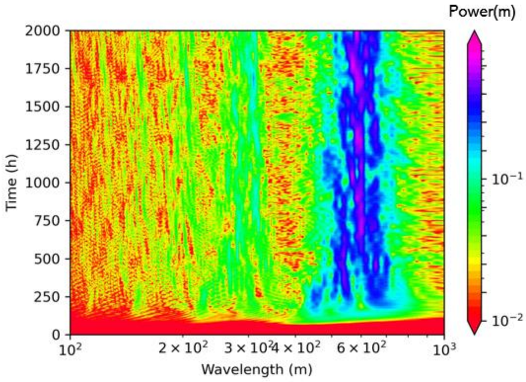

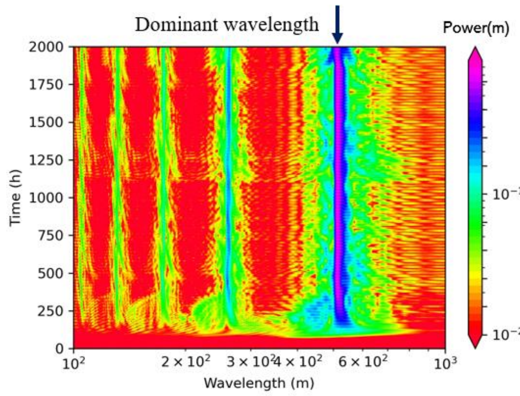

(a). 200-700 m^3/s, 10 hours (b). 200-700 m^3/s, 20 hours

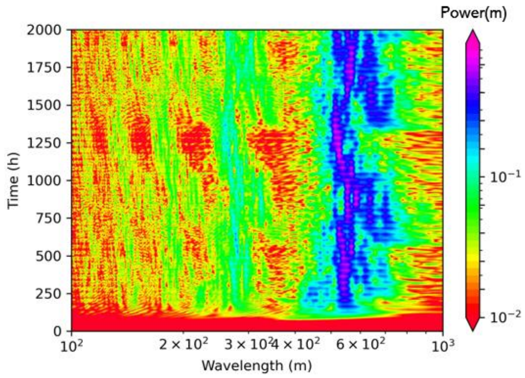

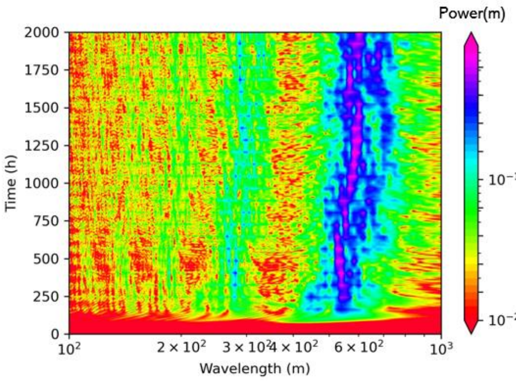

(c). 200-700 m^3/s, 40 hours (d). 200-700 m^3/s, 80 hours

Figure C6. (a)-(d) FFT analysis of dominant wavelength in cases 200-700 m^3/s, cycles of 10, 20, 40 and 80 hours.

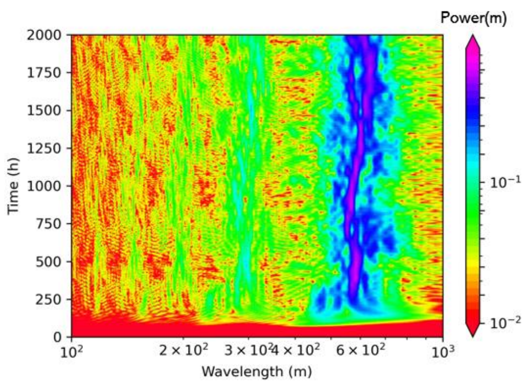

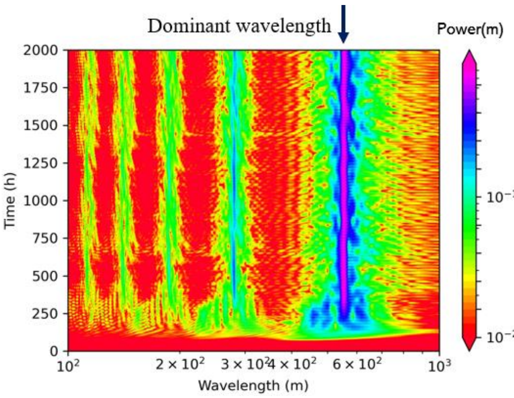

(a). 300-700 m^3/s, 10 hours (b). 300-700 m^3/s, 20 hours

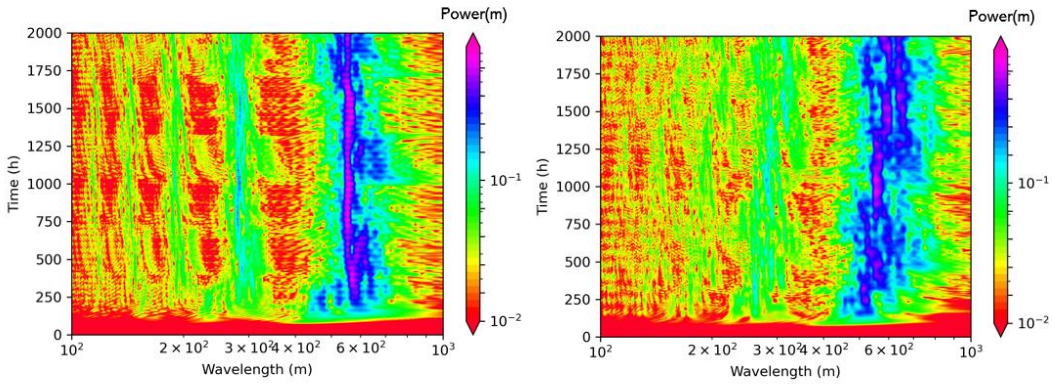

(c). 300-700 m^3/s, 40 hours (d). 300-700 m^3/s, 80 hours

Figure C7. (a)-(d) FFT analysis of dominant wavelength in cases 300-700 m^3/s, cycles of 10, 20, 40 and 80 hours.

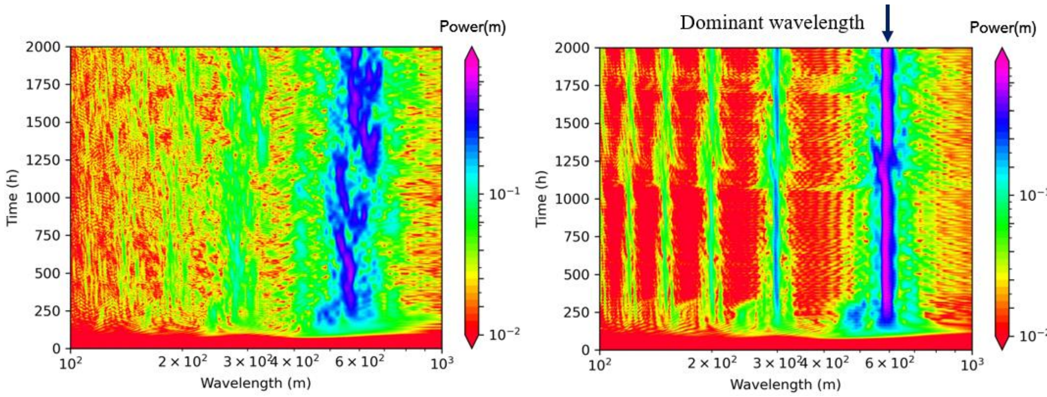

(a). 400-700 m^3/s, 10 hours (b). 400-700 m^3/s, 20 hours

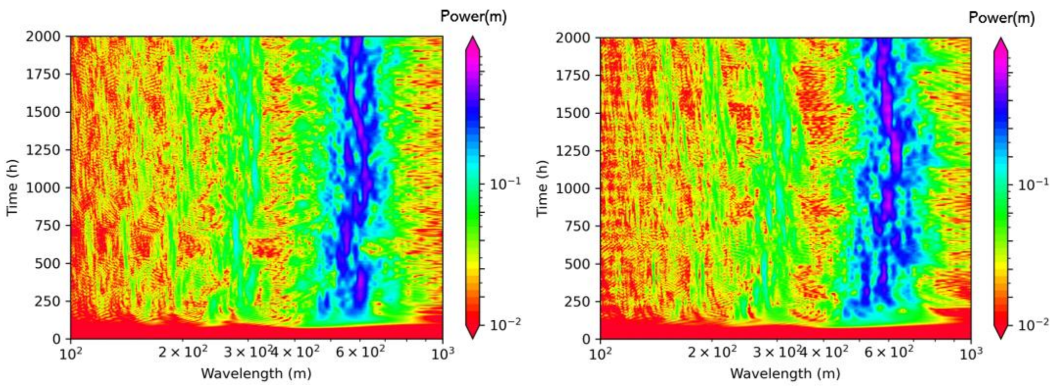

(c). 400-700 m^3/s, 40 hours (d). 400-700 m^3/s, 80 hours

Figure C8. (a)-(d) FFT analysis of dominant wavelength in cases 400-700 m^3/s, cycles of 10, 20, 40 and 80 hours.

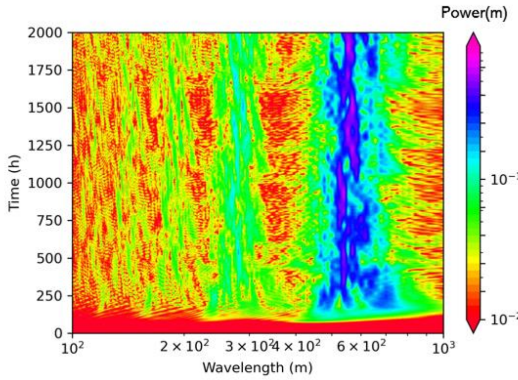

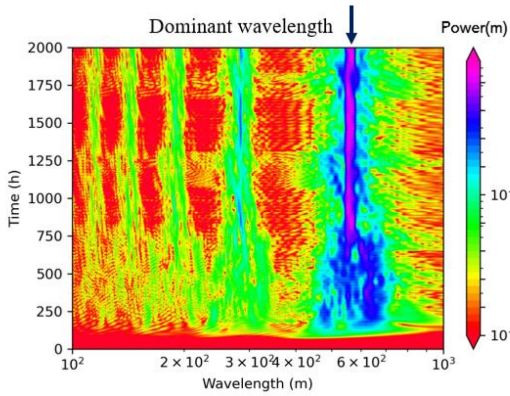

(a). 400-600 m^3/s, 10 hours

(b). 400-600 m^3/s, 20 hours

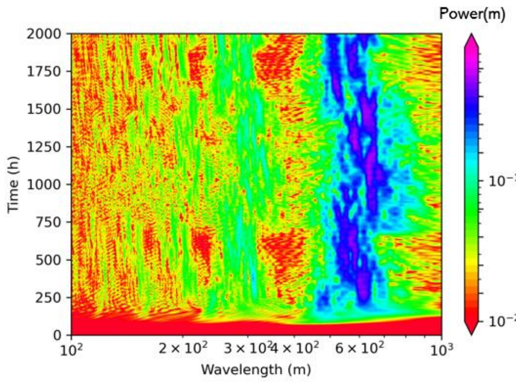

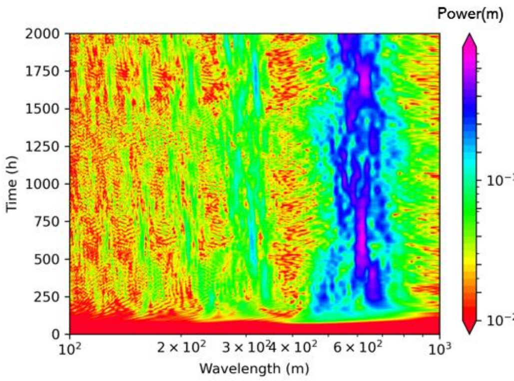

(c). 400-600 m^3/s, 40 hours

(d). 400-600 m^3/s, 80 hours

Figure C9. (a)-(d) FFT analysis of dominant wavelength in cases 400-600 m^3/s, cycles of 10, 20, 40 and 80 hours.

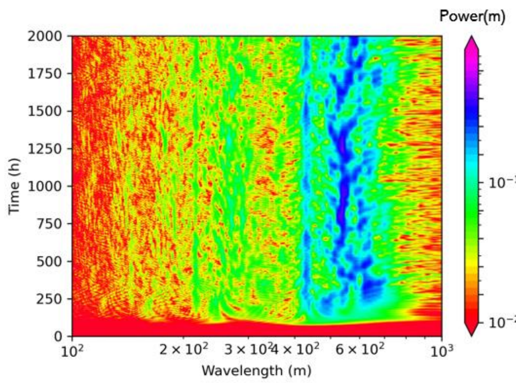

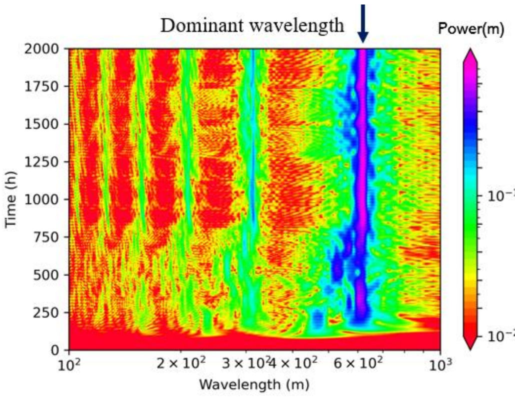

(a). 400-800 m^3/s, 10 hours

(b). 400-800 m^3/s, 20 hours

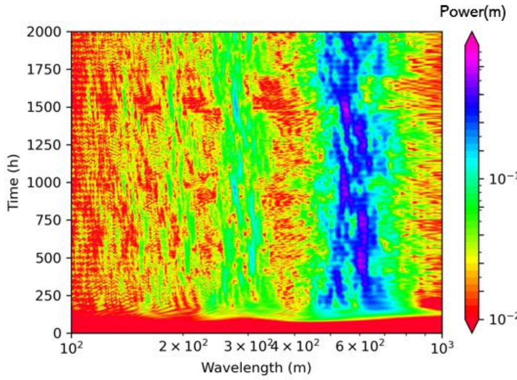

(c). 400-800 m^3/s, 40 hours

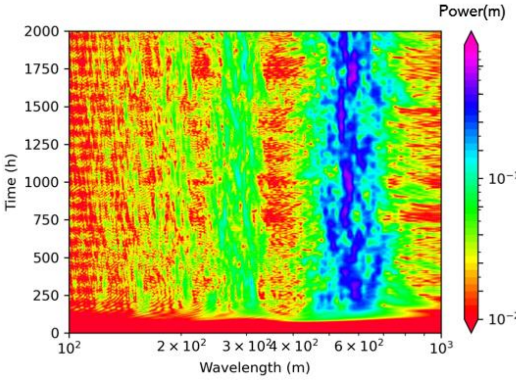

(d). 400-800 m^3/s, 80 hours

Figure C10. (a)-(d) FFT analysis of dominant wavelength in cases 400-800 m^3/s, cycles of 10, 20, 40 and 80 hours.

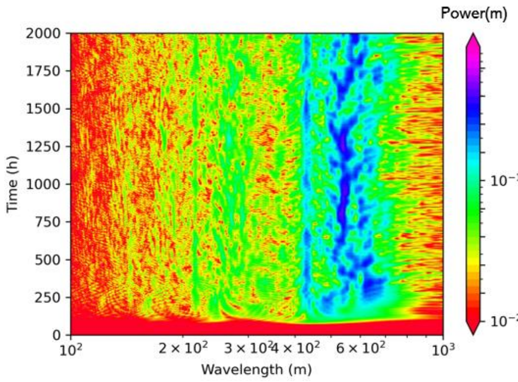

(a). 400-900 m^3/s, 10 hours

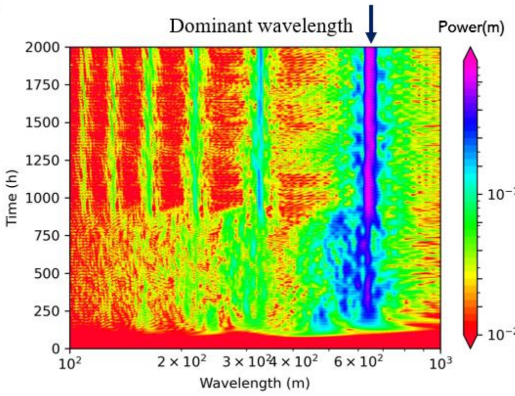

(b). 400-900 m^3/s, 20 hours

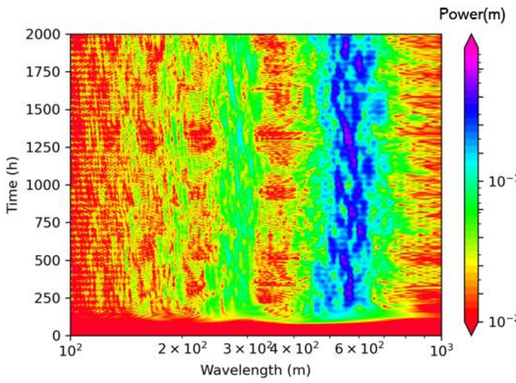

(c). 400-900 m^3/s, 40 hours

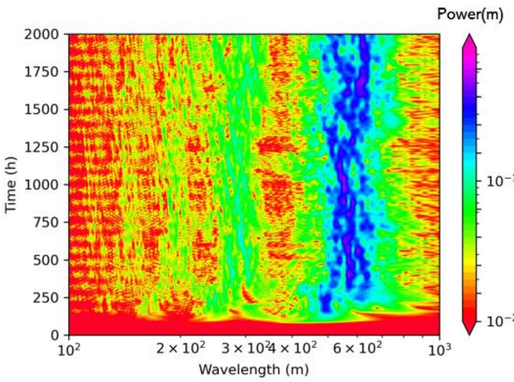

(d). 400-900 m^3/s, 80 hours

Figure C11. (a)-(d) FFT analysis of dominant wavelength in cases 400-900 m^3/s, cycles of 10, 20, 40 and 80 hours.

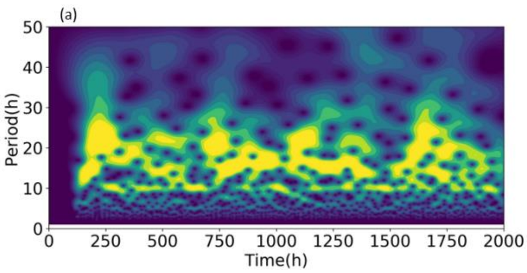

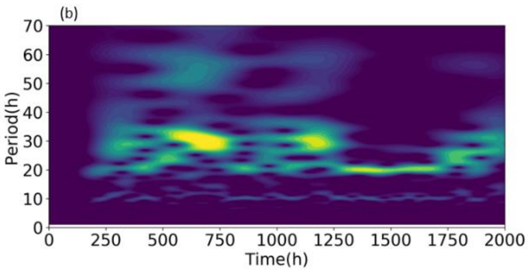

(a). 100-600 m^3/s, 10 hours

(b). 100-600 m^3/s, 20 hours

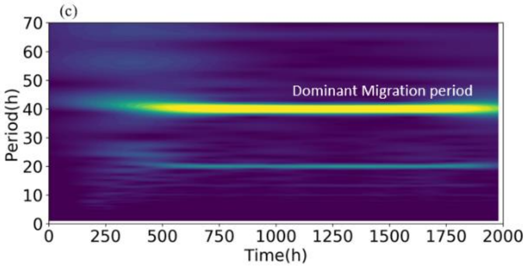

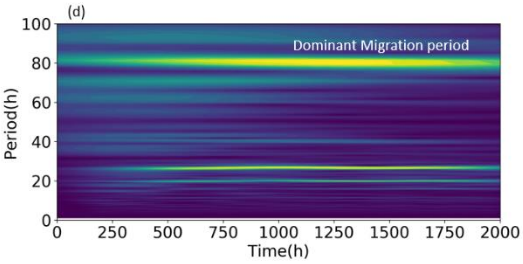

(c). 100-600 m^3/s, 40 hours

(d). 100-600 m^3/s, 80 hours

Figure C12. (a)-(d) Wavelet analysis of dominant migration periods in cases 100-600 m^3/s, cycles of 10, 20, 40 and 80 hours.

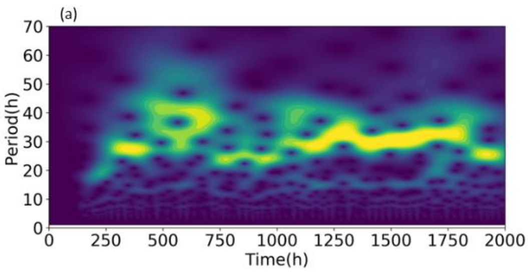

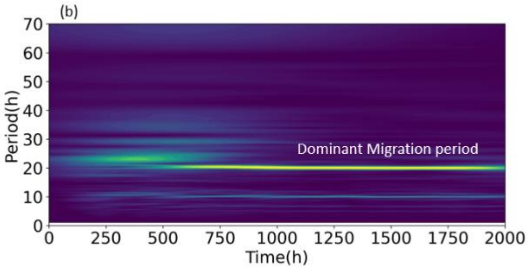

(a). 100-700 m^3/s, 10 hours

(b). 100-700 m^3/s, 20 hours

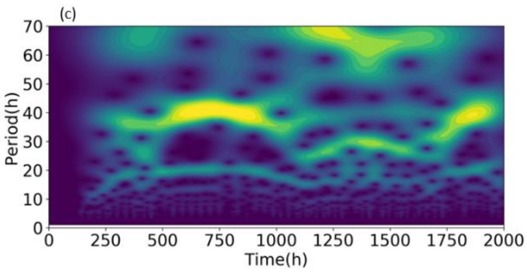

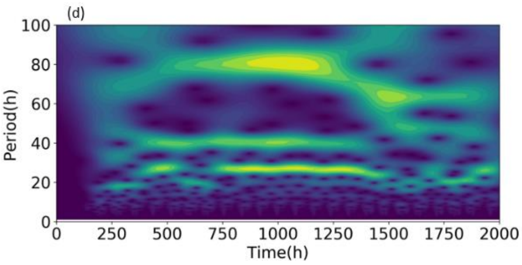

(c). 100-700 m^3/s, 40 hours

(d). 100-700 m^3/s, 80 hours

Figure C13. (a)-(d) Wavelet analysis of dominant migration periods in cases 100-700 m^3/s, cycles of 10, 20, 40 and 80 hours.

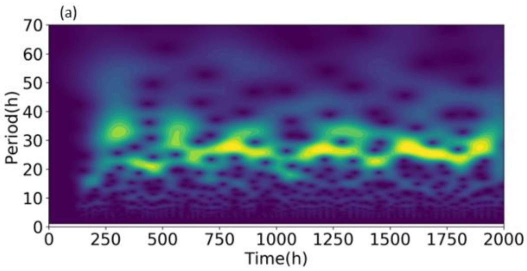

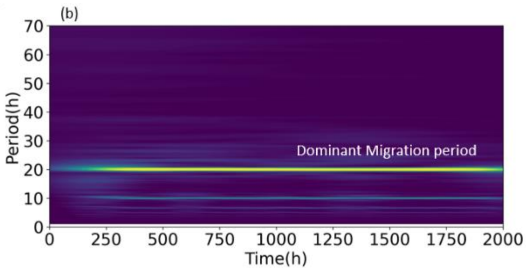

(a). 200-700 m^3/s, 10 hours

(b). 200-700 m^3/s, 20 hours

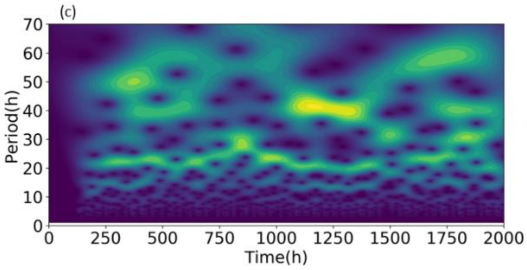

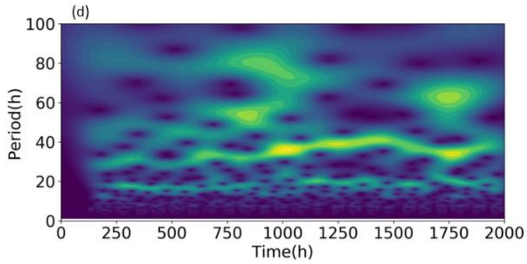

(c). 200-700 m^3/s, 40 hours

(d). 200-700 m^3/s, 80 hours

Figure C14. (a)-(d) Wavelet analysis of dominant migration periods in cases 200-700 m^3/s, cycles of 10, 20, 40 and 80 hours.

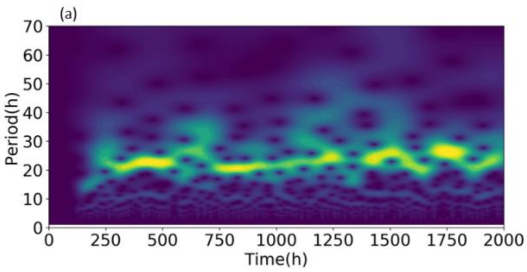

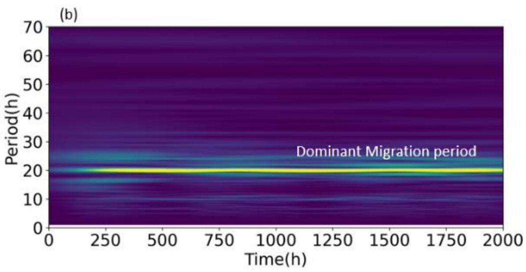

(a). 300-700 m^3/s, 10 hours

(b). 300-700 m^3/s, 20 hours

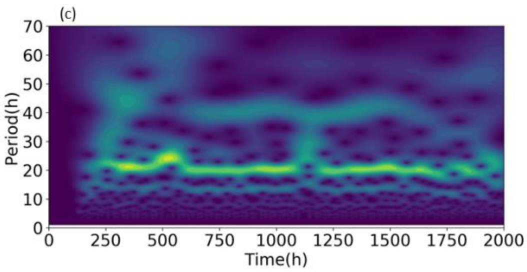

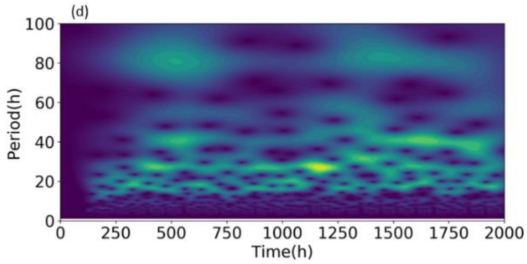

(c). 300-700 m^3/s, 40 hours

(d). 300-700 m^3/s, 80 hours

Figure C15. (a)-(d) Wavelet analysis of dominant migration periods in cases 300-700 m^3/s, cycles of 10, 20, 40 and 80 hours.

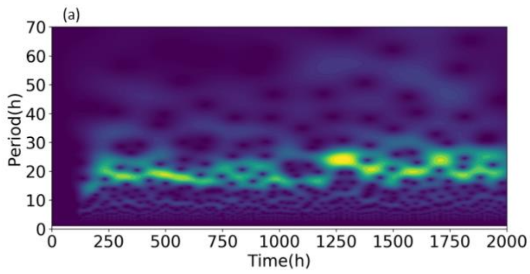

(a). 400-700 m^3/s, 10 hours

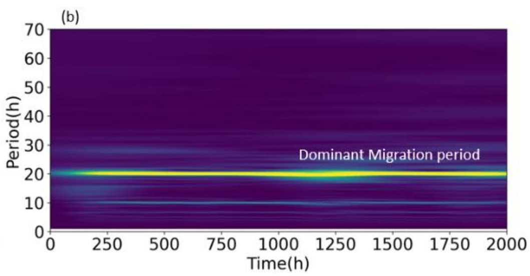

(b). 400-700 m^3/s, 20 hours

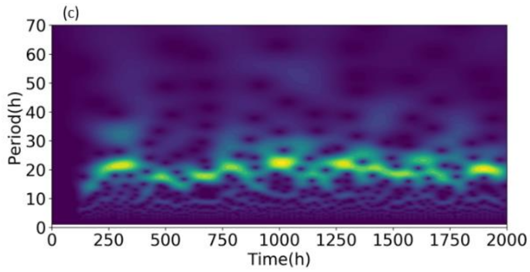

(c). 400-700 m^3/s, 40 hours

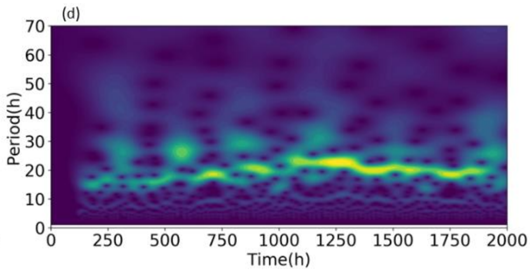

(d). 400-700 m^3/s, 80 hours

Figure C16. (a)-(d) Wavelet analysis of dominant migration periods in cases 400-700 m^3/s, cycles of 10, 20, 40 and 80 hours.

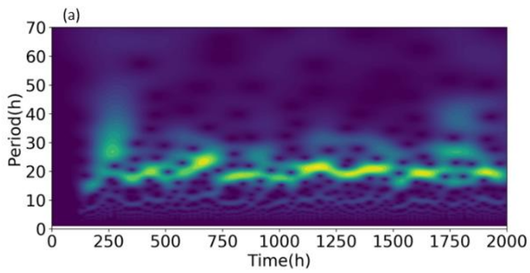

(a). 400-600 m^3/s, 10 hours

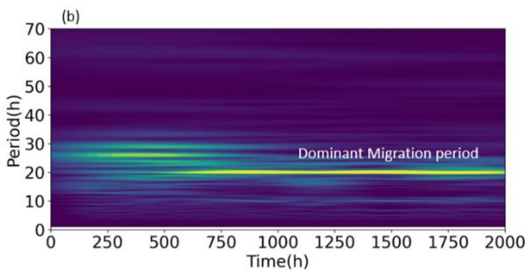

(b). 400-600 m^3/s, 20 hours

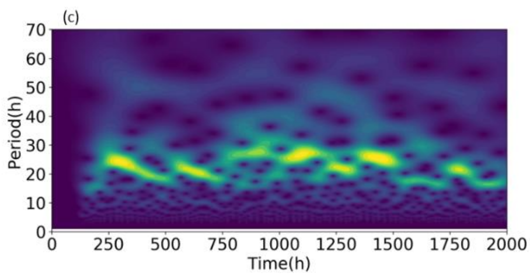

(c). 400-600 m^3/s, 40 hours

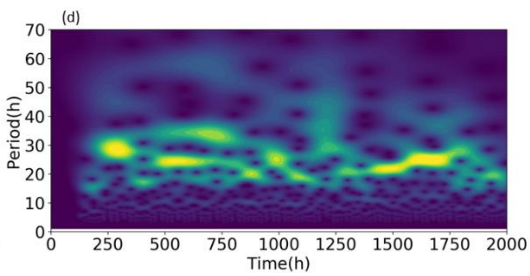

(d). 400-600 m^3/s, 80 hours

Figure C17. (a)-(d) Wavelet analysis of dominant migration periods in cases 400-600 m^3/s, cycles of 10, 20, 40 and 80 hours.

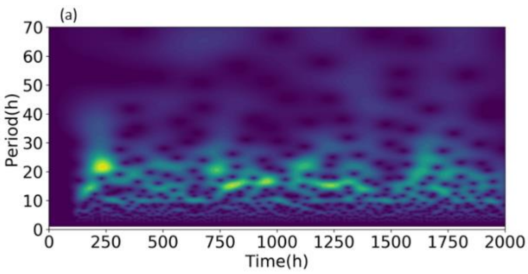

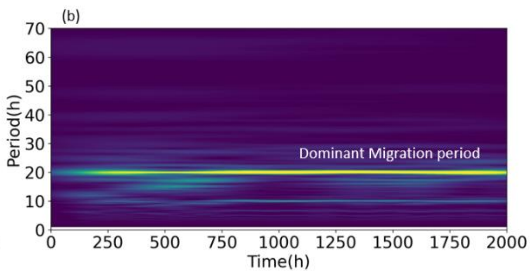

(a). 400-800 m^3/s, 10 hours (b). 400-800 m^3/s, 20 hours

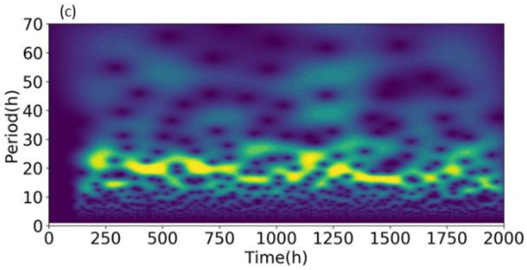

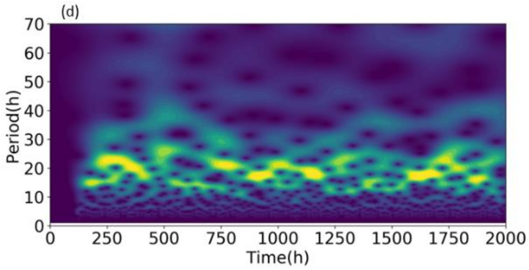

(c). 400-800 m^3/s, 40 hours (d). 400-800 m^3/s, 80 hours

Figure C18. (a)-(d) Wavelet analysis of dominant migration periods in cases 400-800 m^3/s, cycles of 10, 20, 40 and 80 hours.

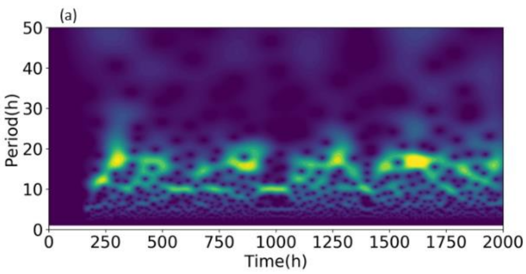

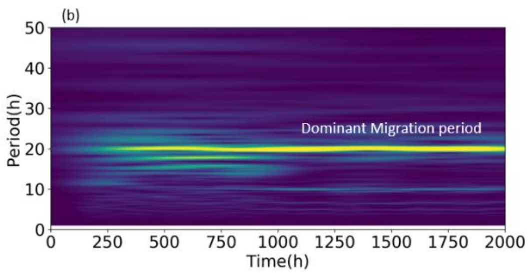

(a). 400-900 m^3/s, 10 hours (b). 400-900 m^3/s, 20 hours

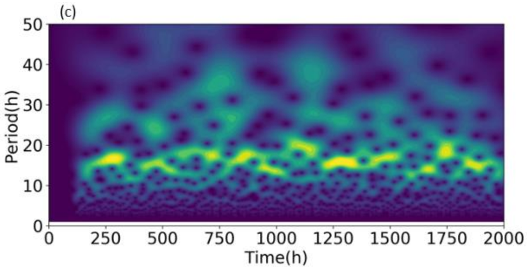

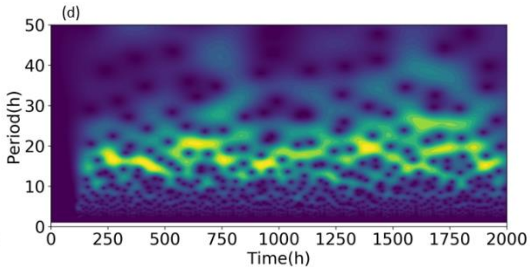

(c). 400-900 m^3/s, 40 hours (d). 400-900 m^3/s, 80 hours

Figure C19. (a)-(d) FFT analysis of dominant wavelength in cases 400-900 m^3/s, cycles of 10, 20, 40 and 80 hours.

Chapter 4

Conclusion

4.1 Sediment supply and river morphology

We investigated the effect of sediment supply on the morphodynamics of free alternate bars in gravel-bed rivers in terms of the HBL concept proposed by Wong and Parker, using a 2D morphodynamic numerical model, iRIC-Nays2DH. Confirmed that the morphodynamic features of the HBL reach are identical even if the condition is extended to 2D cases, including complex bedforms such as alternate bars.

In the present condition, the simulated alternate bars develop outside the HBL, and characteristics of the alternate bars such as wavelength, bar height and migration speed are almost identical in both sediment feed conditions. This result suggests that the HBL concept is still valid for 2D cases, where the upstream sediment disturbance is difficult to propagate beyond the HBL, and eventually, has a negligible effect on the downstream morphological characteristics. We also changed the hydrograph characteristics, that is, the hydrograph duration and peak discharge were increased by a factor of 2, to understand the sensitivity of this result to the extreme change in the hydrograph from a practical perspective. The larger and longer hydrographs extend the length of the HBL, but the upstream sediment boundary condition does not affect the general characteristics of the downstream alternate bars. In summary, the findings regarding HBL [49] are almost valid for the dynamics of alternate bars developed beyond the HBL, that is, sediment disturbance at the upstream end has a negligible effect on the mobile-bed dynamic processes, including alternate bar formation and development downstream of the HBL.

4.2 Unsteady flow and river morphology

Inspired by the special phenomenon in Chapter 2, hydrograph processes with different discharges & hydrograph cycles are given, aiming to discover the familiar morphodynamics equilibrium state, in which the wavelength and migration period of alternate bars remained constant, and the migration period was the same as the hydrograph cycle.

We found that the morphodynamics of alternate bars under a specific combination of discharge variation and hydrograph cycle reached an equilibrium state. This might be a unique morphodynamic feature of alternate bars under unsteady conditions because the steady discharge counterparts demonstrated a dynamic equilibrium state with slightly time-dependent features of the wavelength and migration period but did not exhibit non-time-dependent features.

To find out the reason of the formation of the morphodynamics equilibrium, we give the discharge process an abrupt change to observe the reaction of the alternate bars. The results show that the responses of the change in migration speed and elevation are different. The migration speed always varies quickly within several hours, but the elevation takes much longer time to reach equilibrium. The results indicate that, under a short hydrograph, the bar growth occurred much slower than the discharge changes, implying the bars cannot respond to the discharge variation. Meanwhile, the long hydrograph provided sufficient time for the deformation and development of alternate bars, causing a significant change in bar characteristics (e.g., wavelength) within one hydrograph, which is a similar process obtained under the steady discharge condition. The hydrograph cycle that achieves this equilibrium state must be moderately long so that the timescale of the hydrograph is similar but slightly smaller than the bar growth timescale, but not too small to allow equilibrium bar behaviors caused by steady discharge conditions.

Meanwhile, it is also found that the erosion & deposition patterns of the alternate bars in the morphodynamics equilibrium state are different. As the alternate bars are no longer migrating translationally like the steady flow case, some places of the riverbank might experience more serious and unfair erosion, which might be significant in the river morphology study.

4.3 Recommendation and future work

In the studies of both chapters, all the simulation is done under a straight channel with a single grain size of the sediment and a continuous triangle-shape hydrograph. The results are obtained under an ideal condition, regardless of the suspended sediment transport, mixed graded sediment supply, change of the channel width or curvature and the real hydrograph process. In fact, all the factors mentioned above are possible or have been proved to be effective to the HBL concept or morphodynamics equilibrium state as we have explained in the end of each chapter.

For the future study of imbalance sediment supply and HBL concept, consideration of the complexity of sediment transport should be very necessary, especially some factors that could spread their influence to further downstream out of HBL region including the mixed graded sediment supply and suspended sediment transport.

For the future study of morphodynamics equilibrium and unsteady flow conditions. Since the hydrograph condition to form morphodynamics equilibrium state is harsh and rarely exist in the real river channel. Therefore, experiment should be necessary to provided validation and mechanical analysis to find unclear reason behind this kind of equilibrium state of migrating alternate bars under repeated hydrograph conditions.

This study has its own limitations as a pure theoretical numerical simulation. But as a study about river engineering, it will be more worth if it can be put into reality and play a role. However, the extended application of HBL concept into 2-D simulation and discovery of morphodynamics equilibrium state can still be regarded as a small contribution that might provide useful knowledge in this field.

Reference

1. Y. Fujita, Y. Muramoto. Studies on the process of development of alternate bars. Bulletin of the disaster prevention research institute, 1985, 35.3: 55-86.

2. M. Dynesius, C. Nilsson. Fragmentation and flow regulation of river systems in the northern third of the world. Science, 1994, 266.5186: 753-762.

3. F. Molle. River-basin planning and management: The social life of a concept. Geoforum, 2009, 40.3: 484-494.

4. Nilsson, C., Reidy, C. A., Dynesius, M., & Revenga, C. Fragmentation and flow regulation of the world's large river systems. science, 2005, 308.5720: 405-408.

5. M. Colombini, G. Seminara, M. Tubino. Finite-amplitude alternate bars. Journal of Fluid Mechanics, 1987, 181: 213-232.

6. S. Ikeda. Prediction of alternate bar wavelength and height. Journal of Hydraulic Engineering, 1984, 110.4: 371-386.

7. Qian, H., Cao, Z., Liu, H., & Pender, G. Numerical modelling of alternate bar formation, development and sediment sorting in straight channels. Earth Surface Processes and Landforms, 2017, 42(4), 555-574.

8. A. Mendoza, J.D. Abad, E.J. Langendoen, et al. Effect of sediment transport boundary conditions on the numerical modeling of bed morphodynamics. Journal of Hydraulic Engineering, 2017, 143(4): 04016099.

9. F. Schuurman, Y. Shimizu, T. Iwasaki, & M. G. Kleinhans. Dynamic meandering in response to upstream perturbations and floodplain formation. Geomorphology, 2016, 253, 94-109..

10. S. Rodrigues, E. Mosselman, N. Claude, et al. Alternate bars in a sandy gravel bed river: generation, migration and interactions with superimposed dunes. Earth Surface Processes and Landforms, 2015, 40(5): 610-628.

11. Whiting P.J, Dietrich W.E. Experimental constraints on bar migration through bends: Implications for meander wavelength selection[J]. Water Resources Research, 1993, 29(4): 1091-1102.

12. Redolfi M, Welber M, Carlin M, et al. Morphometric properties of alternate bars

and water discharge: a laboratory investigation[J]. Earth Surface Dynamics, 2020, 8(3): 789-808.

13. Carlin M, Redolfi M, Tubino M. The Long-Term Response of Alternate Bars to the Hydrological Regime. Water Resources Research, 2021, 57(7): e2020WR029314.
14. Shi Q, Zhang X, Xu Q. Evolution of Alternate Bars in Straight Channel under Different Discharge and Sediment Conditions[J]. Journal of Yangtze River Scientific Research Institute, 2020, 37(4): 7.
15. Inoue T, Iwasaki T, Parker G, et al. Numerical simulation of effects of sediment supply on bedrock channel morphology[J]. Journal of Hydraulic Engineering, 2016, 142(7): 04016014.
16. Lisle T E, Iseya F, Ikeda H. Response of a channel with alternate bars to a decrease in supply of mixed-size bed load: A flume experiment[J]. Water Resources Research, 1993, 29(11): 3623-3629.
17. Jourdain C, Claude N, Tassi P, et al. Morphodynamics of alternate bars in the presence of riparian vegetation[J]. Earth Surface Processes and Landforms, 2020, 45(5): 1100-1122.
18. Iwasaki T, Shimizu Y, Kimura I. Numerical simulation of bar and bank erosion in a vegetated floodplain: A case study in the Otofuke River[J]. Advances in water resources, 2016, 93: 118-134.
19. Constantine J A, Dunne T, Ahmed J, et al. Sediment supply as a driver of river meandering and floodplain evolution in the Amazon Basin[J]. Nature Geoscience, 2014, 7(12): 899-903.
20. Stähly S, Franca M J, Robinson C T, et al. Sediment replenishment combined with an artificial flood improves river habitats downstream of a dam[J]. Scientific Reports, 2019, 9(1): 1-8.
21. Blum M D, Roberts H H. Drowning of the Mississippi Delta due to insufficient sediment supply and global sea-level rise[J]. Nature geoscience, 2009, 2(7): 488-491.
22. Nittrouer J A, Viparelli E. Sand as a stable and sustainable resource for nourishing

the Mississippi River delta[J]. Nature Geoscience, 2014, 7(5): 350-354.
23. Gaeuman D, Schmidt J C, Wilcock P R. Complex channel responses to changes in stream flow and sediment supply on the lower Duchesne River, Utah[J]. Geomorphology, 2005, 64(3-4): 185-206.
24. Morgan J A, Nelson P A. Experimental investigation of the morphodynamic response of riffles and pools to unsteady flow and increased sediment supply[J]. Earth Surface Processes and Landforms, 2021, 46(4): 869-886.
25. Tubino M. Growth of alternate bars in unsteady flow[J]. Water resources research, 1991, 27(1): 37-52.
26. Watanabe Y, Tubino M, Zolezzi G, et al. Behavior of alternate bars under unsteady flow conditions[C]//2nd IAHR Symposium On River, Coastal and Estuary Morphodynamics, Obihiro, Japan. Sapporo, Japan: Hokkaido Univ. Press, 2001: 673-682.
27. Izumi N, Takatsu M, Kawamura S. Effects of the Variation of Discharge on the Growth of Fluvial Bars[J]. Journal of Japan Society of Civil Engineers, Ser. A2 (Applied Mechanics (AM)), 2021, 77(2): I_451-I_456.
28. Hall P. Alternating bar instabilities in unsteady channel flows over erodible beds[J]. Journal of Fluid mechanics, 2004, 499: 49-73.
29. Kyuka T, Okabe K, Shimizu Y, et al. Dominating factors influencing rapid meander shift and levee breaches caused by a record-breaking flood in the Otofuke River, Japan[J]. Journal of Hydro-environment Research, 2020, 31: 76-89.
30. Nagata T, Watanabe Y, Yasuda H, et al. Development of a meandering channel caused by the planform shape of the river bank[J]. Earth Surface Dynamics, 2014, 2(1): 255-270.
31. Y. Shimizu, H. Takebayashi, T. Inoue, et al, iRIC-Software: Nays2DH solver manual. (2014), Available online: https://i-ric.org/en/ (accessed on 25 October 2021).
32. J.M. Nelson, Y. Shimizu, T. Abe, et al, The international river interface cooperative: Public domain flow and morphodynamics software for education and applications,

J. Advances in Water Resources, (2016), 93: 62–74.
33. T. Kang, I. Kimura, Y. Shimizu, Numerical simulation of large wood deposition patterns and responses of bed morphology in a braided river using large wood dynamics model, J. Earth Surface Processes and Landforms, (2020), 45(4): 962–977.
34. P. Rahman, M.S. Ali, Change in transverse slope of water surface at river bend: A numerical study, J. Journal of Engineering Science, (2021), 12(2): 93–101.
35. A.D. Tamminga, B.C. Eaton, C.H. Hugenholtz, UAS-based remote sensing of fluvial change following an extreme flood event, J. Earth Surface Processes and Landforms, (2015), 40(11): 1464–1476.
36. H. Dai, T. Iwasaki, Y. Shimizu, Effect of sediment supply on morphodynamics of free alternate bars: Insights from hydrograph boundary layer, J. Water, (2021), 13(23): 3437.
37. L.G. MacKenzie, B.C. Eaton, Large grains matter: contrasting bed stability and morphodynamics during two nearly identical experiments, J. Earth Surface Processes and Landforms, (2017), 42(8): 1287–1295.
38. Padawangi, R.; Douglass, M. Water, water everywhere: Toward participatory solutions to chronic urban flooding in Jakarta. Pac. Aff. 2015, 88, 517–550.
39. Yousefi, S.; Mirzaee, S.; Keesstra, S.; Surian, N.; Pourghasemi, H.R.; Zakizadeh, H.R.; Tabibian, S. Effects of an extreme flood on river morphology (case study: Karoon River, Iran). Geomorphology. 2018, 304, 30–39.
40. Kazama, M.; Yamakawa, Y.; Yamaguchi, A.; Yamada, S.; Kamura, A.; Hino, T.; Moriguchi, S. Disaster report on geotechnical damage in Miyagi Prefecture, Japan caused by Typhoon Hagibis in 2019. Soils Found. 2021, 61, 549–565.
41. Viero, D.P.; D'Alpaos, A.; Carniello, L.; Defina, A. Mathematical modeling of flooding due to river bank failure. Adv. Water Resour. 2013, 59, 82–94.
42. Inoue, T.; Mishra, J.; Kato, K.; Sumner, T.; Shimizu, Y. Supplied sediment tracking for bridge collapse with large-scale channel migration. Water 2020, 12, 1881.
43. Ohtsuka, S.; Sato, Y.; Yoshikawa, T.; Sugii, T.; Kodaka, T.; Maeda, K. Levee

damage and revetment erosion by the 2019 Typhoon Hagibis in the Chikuma River, Japan. Soils Found. 2021, 61, 1172–1188.

44. Visconti, F.; Camporeale, C.; Ridolfi, L. Role of discharge variability on pseudomeandering channel morphodynamics: Results from laboratory experiments. J. Geophys. Res. Earth Surf. 2010, 115 page.
45. Church, M. Channel morphology and typology. River Handb. 1994 , volume 126–143.
46. Parker, G.; Wilcock, P.R.; Paola, C.; Dietrich, W.E.; Pitlick, J. Physical basis for quasi-univeral relations describing bankfull hy-draulic geometry of single-thread gravel bed rivers. J. Geophys. Res. Earth Surf. 2007, 112, F04005.
47. Best, J. Anthropogenic stresses on the world's big rivers. Nat. Geosci. 2019, 12, 7–21.
48. Nelson, P.A.; Brew, A.K.; Morgan, J.A. Morphodynamic response of a variable-width channel to changes in sediment supply. Water Resour. Res. 2015, 51, 5717–5734.
49. Wong, M.; Parker, G. One-dimensional modeling of bed evolution in a gravel bed river subject to a cycled flood hydrograph. J. Geophys. Res. Earth Surf. 2006, 111, F03018.
50. An, C.; Cui, Y.; Fu, X.; Parker, G. Gravel-bed river evolution in earthquake-prone regions subject to cycled hydrographs and repeated sediment pulses. Earth Surf. Process. Landforms 2017, 42, 2426–2438.
51. An, C.; Fu, X.; Wang, G.; Parker, G. Effect of grain sorting on gravel bed river evolution subject to cycled hydrographs: Bed load sheets and breakdown of the hydrograph boundary layer. J. Geophys. Res. Earth Surf. 2017, 122, 1513–1533.
52. Nelson, P.A.; Morgan, J.A. Flume experiments on flow and sediment supply controls on gravel bedform dynamics. Geomorphology 2018, 323, 98–105.
53. Venditti, J.G.; Nittrouer, J.A.; Allison, M.A.; Humphries, R.P.; Shurch, M. Supply-limited bedform patterns and scaling downstream of a gravel-sand transition. Sedimentology 2019, 66, 2538–2556.

54. Shimizu, Y.; Nelson, J.; Arnez, K.F.; Asahi, K.; Giri, S.; Inoue, T.; Iwasaki, T.; Jang, C.L.; Kang, T.; Kimura, I.; et al. Advances in computational morphodynamics using the International River Interface Cooperative (iRIC) software. Earth Surf. Process. Land. 2019, 45, 11–37.
55. Iwasaki, T.; Nelson, J.; Shimizu, Y.; Parker, G. Numerical simulation of large-scale bed load particle tracer advection-dispersion in rivers with free bars. J. Geophys. Res. Earth Surf. 2017, 122, 847–874.
56. Okitsu, T.; Iwasaki, T.; Kyuka, T.; Shimizu, Y. The Role of Large-Scale Bedforms in Driftwood Storage Mechanics in Rivers. Water 2021, 13, 811.
57. Yamada, T.J. Adaptation measures for extreme floods using huge ensemble of high-resolution climate model simulation in Japan. Summ. Rep. Elev. Meet. Res. Dialogue 2019, volume 28–30 .
58. Hoshino, T.; Yamada, T.J.; Kawase, H. Evaluation for Characteristics of Tropical Cyclone Induced Heavy Rainfall over the Sub-basins in The Central Hokkaido, Northern Japan by 5-km Large Ensemble Experiments. Atmosphere 2020, 11, 435.
59. Yamada, T.J.; Hoshino, T.; Suzuki, A. Using a massive high-resolution ensemble climate data set to examine dynamic and thermodynamic aspects of heavy precipitation change. At. Sci. Lett. 2021, volume e1065.
60. Francalanci, S.; Solari, L.; Toffolon, M.; Parker, G. Do alternate bars affect sediment transport and flow resistance in gravel-bed rivers? Earth Surf. Process. Land. 2012, 37, 866–875.
61. East, A.E.; Logan, J.B.; Mastin, M.C.; Ritchie, A.C.; Bountry, J.A.; Magirl, C.S.; Sankey, J.B. Geomorphic evolution of a gravel-bed river under sediment-starved versus sediment-rich conditions: River response to the world's largest dam removal. J. Geophys. Res. Earth Surf. 2018, 123, 3338–3369.
62. Ahammad, M.; Czuba, J.A.; Pfeiffer, A.M.; Murphy, B.P.; Belmont, P. Simulated dynamics of mixed versus uniform grain size sediment pulses in a gravel-bedded river. J. Geophys. Res. Earth Surf. 2021, 126, e2021JF006194.
63. Sutherland, D.G.; Ball, M.H.; Hilton, S.J.; Lisle, T.E. Evolution of a landslide-

induced sediment wave in the Navarro River, California. GSA Bull. 2002, 114, 1036–1048.

64. Facchini, M.; Bertoldi, W.; Boes, R.; Vetsch, D.A.; Siviglia, A. Effects of natural and anthropogenic repeated water and sediment inputs to gravel-bed rivers: A numerial study. AGU Fall Meet. Abstr. 2018, 2018, EP31A–05.
65. Rachelly, C.; Friedl, F.; Boes, R.M.; Weitbrecht, V. Morphological response of channelized, sinuous gravel-bed rivers to sediment replenishment. Water Resour. Res. 2021, 57, e2020WR029178.
66. Schmidt, J.C.; Wilcock, P.R. Metrics for assessing the downstream effects of dams. Water Resour. Res. 2008, 44, W04404.
67. Morgan, J.A.; Nelson, P.A. Morphodynamic modeling of sediment pulse dynamics. Water Resour. Res. 2019, 55, 8691–8707.
68. Lisle, T.E.; Cui, Y.; Parker, G.; Pizzuto, J.E.; Dodd, A.M. The dominance of dispersion in the evolution of bed material waves in gravel-bed rivers. Earth Surf. Proc. Land. 2001, 26, 1409–1420.
69. Lanzoni, S.; Tubino, M. Grain sorting and bar instability. J. Fluid Mech. 1999. 393, 149-174.
70. Blom, A.; Parker, G. Vertical sorting and the morphodynamics of bed form-dominated rivers: A modeling framework. J. Geophys. Res. Earth Surf. 2004, 109, F02007.
71. Takebayashi, H.; Egashira, S. Non-equilibrium characteristics of bar geometry on bed with non-uniform sediment. J. Hydrosci. Hydraul. Eng. 2008, 26, 1–14.
72. An, C.; Moodie, A.; Ma, H.; Fu, X.; Zhang, Y.; Naito, K.; Parker, G. Morphodynamic model of the lower Yellow River: Flux or entrainment form for sediment mass conservation? Earth Surf. Dynam. 2018, 6, 989–1010.
73. Chen, Y.; Nakatsugawa, M.; Ohashi, H. Research of Impacts of the 2018 Hokkaido Eastern Iburi Earthquake on Sediment Trasnport in the Atsuma River Basin Using the SWAT Model. Water 2021, 13, 356.
74. Zolezzi, G.; Luchi, R.; Tubino, M. Modeling morphodynamic processes in

meandering rivers with spatial width variations. Rev. Geophys. 2012, 50, 1–24.

75. Kleinhans, M.; Wilbers, A.W.E.; de Swaaf, A.; Van den Berg, J.H. Sediment supply-limited bedforms in sand-gravel bed rivers. J. Sediment. Res. 2002, 72, 629.
76. A. Crosato, A. Grissetti-Vázquez, F. Bregoli, et al, Adaptation of river channels to a wetter or drier climate: Insights from the Lower Pilcomayo River, South America, J. Journal of Hydrology, (2022), 128254.
77. G. Duró, A. Crosato, P. Tassi, Numerical study on river bar response to spatial variations of channel width, J. Advances in Water Resources, (2016), 93: 21–38.
78. F. Amoako Johnson, C.W. Hutton, Dependence on agriculture and ecosystem services for livelihood in Northeast India and Bhutan: vulnerability to climate change in the Tropical River Basins of the Upper Brahmaputra, J. Climatic Change, (2014), 127(1): 107–121.
79. M. Jaballah, B. Camenen, L. Pénard, et al, Alternate bar development in an alpine river following engineering works, J. Advances in Water Resources, (2015), 81: 103–113.
80. T.E. Lisle, H. Ikeda, F. Iseya, Formation of stationary alternate bars in a steep channel with mixed‐size sediment: A flume experiment, J. Earth Surface Processes and Landforms, (1991), 16(5): 463‐469.
81. S. Ikeda, Prediction of alternate bar wavelength and height, J. Journal of Hydraulic Engineering, (1984), 110(4): 371–386.
82. A. Defina, Numerical experiments on bar growth, J. Water Resources Research, (2003), 39(4).
83. A. Crosato, F.B. Desta, J. Cornelisse, et al, Experimental and numerical findings on the long-term evolution of migrating alternate bars in alluvial channels, J. Water Resources Research, (2012), 48: W06524.
84. M. Colombini, A. Stocchino, Three-dimensional river bed forms, J. Journal of Fluid Mechanics, (2012), 695: 63–80.
85. D.J. Furbish, Irregular bed forms in steep, rough channels: 1. Stability analysis, J. Water Resources Research, (1998), 34: 3635–3648.

86. Y. Shimizu, S. Giri, S. Yamaguchi, et al, Numerical simulation of dune-flat bed transition and stage-discharge relationship with hysteresis effect, J. Water Resources Research, (2009), 45(4): W04429.
87. A. Grossmann, J. Morlet, Decomposition of hardy functions into square integrable wavelets of constant shape, J. SIAM Journal on Mathematical Analysis, (1984), 15(4): 723–736.
88. Y.A. Cataño-Lopera, J.D. Abad, M.H. García, Characterization of bedform morphology generated under combined flows and currents using wavelet analysis, J. Ocean Engineering, (2009), 36(9–10): 617–632.
89. M. Mahdade, N. Le Moine, R. Moussa, et al, Automatic identification of alternating morphological units in river channels using wavelet analysis and ridge extraction, J. Hydrology and Earth System Sciences, (2020), 24(7): 3513–3537.
90. M. Kuroki, T. Kishi, Regime criteria on bars and braids in alluvial straight channels, J. Proc. of JSCE, (1984), 342: 87–96. (in Japanese)
91. J.M. Nelson, J.D. Smith, Evolution and stability of erodible channel beds, J. River Meandering: AGU Water Resources Monograph, (1989), 321–377.
92. Y. Watanabe, K. Sato, F. Oyama, Experimental study on bar formation under unsteady flow conditions, J. Proceeding of hydraulic engineering, (2002), 46: 725–730.
93. L. Adami, W. Bertoldi, G. Zolezzi, Multidecadal dynamics of alternate bars in the Alpine Rhine River, J. Water Resources Research, (2016), 52: 8938–8955.
94. J.P.C. Eekhout, A.J.F. Hoitink, E. Mosselman, Field experiment on alternate bar development in a straight sand-bed stream, J. Water Resources Research, (2013), 49: 8357–8369.
95. M.B. Bertagni, C. Camporeale, Finite amplitude of free alternate bars with suspended load, J. Water Resources Research, (2018), 54: 9759–9773.
96. K. Kobayashi, Y. Shimizu, Y. Watanabe, Morphodynamic modeling of sandbar evolution under unsteady flow, J. Journal of applied mechanics, (2006), 9, 1031-1038. https://doi.org/10.2208/journalam.9.1031. (in Japanese)

97. Y. Watanabe, and K. Kawamura, Mode-decrease process of double-row bars, Proc. Int. Conf. Riv. Coast. Morph. Dyn., Illinois, USA, (2005), 445-453.
98. A. J. Serlet, A. M. Gurnell, G. Zolezzi, G. Wharton, P. Belleudy, & C. Jourdain, Biomorphodynamics of alternate bars in a channelized, regulated river: An integrated historical and modelling analysis. Earth Surface Processes and Landforms, (2018), 43(9), 1739-1756.
99. M. S. Horritt, P. D. Bates, & M. J. Mattinson, Effects of mesh resolution and topographic representation in 2D finite volume models of shallow water fluvial flow. Journal of Hydrology, 2006, 329(1-2), 306-314.
100. B, E. Oran. The fast Fourier transform and its applications. Prentice-Hall, Inc., 1988.
101. G. Heinzel, A. Rüdiger, & R. Schilling, Spectrum and spectral density estimation by the Discrete Fourier transform (DFT), including a comprehensive list of window functions and some new at-top windows. 2002.